STAR (1+2)

JPL PUBLICATION 82-37

DOE/ET-11326-1
Distribution Category UC-90c

Conversion of Hydrocarbons for Fuel Cell Applications

Part I: Autothermal Reforming of Sulfur-Free and Sulfur-Containing Hydrocarbon Liquids

Part II: Steam Reforming of n-Hexane on Pellet and Monolithic Catalyst Beds

Maria Flytzani-Stephanopoulos
Gerald E. Voecks

Final Report,
October 1981

Prepared for
U.S. Department of Energy
Fuel Cell Division
Through an agreement with
National Aeronautics and Space Administration
by
Jet Propulsion Laboratory
California Institute of Technology
Pasadena, California

JPL PUBLICATION 82-37

DOE/ET-11326-1
Distribution Category UC-90c

Conversion of Hydrocarbons for Fuel Cell Applications

Part I: Autothermal Reforming of Sulfur-Free and Sulfur-Containing Hydrocarbon Liquids

Part II: Steam Reforming of n-Hexane on Pellet and Monolithic Catalyst Beds

Maria Flytzani-Stephanopoulos
Gerald E. Voecks

Final Report,
October 1981

Prepared for

U.S. Department of Energy
Fuel Cell Division

Through an agreement with

National Aeronautics and Space Administration

by

Jet Propulsion Laboratory
California Institute of Technology
Pasadena, California

Prepared by the Jet Propulsion Laboratory, California Institute of Technology, for the U.S. Department of Energy through an agreement with the National Aeronautics and Space Administration.

ABSTRACT

In support of the Department of Energy (DOE) Fuel Cell Program, aimed at operating fuel cells on middle distillate petroleum liquids in the near term and coal-derived hydrocarbon liquids in the near future, experimental work has been conducted on improving the autothermal and steam reforming processes. Autothermal reforming (ATR) tasks have been directed toward understanding the different mechanisms by which various fuel component hydrocarbons (related to both heavy petroleum and coal-derived liquids) are converted to hydrogen without forming carbon. Steam reforming tasks have been directed toward examination of monolithic catalysts with higher available active surface area and better thermal conductivity than conventional pellet beds, making it possible to steam reform fuels heavier than naphtha without sacrificing efficiency.

Experimental ATR results obtained in the previous phase of this work with sulfur-free pure hydrocarbon liquids are summarized here. Catalyst types and configuration used were the same as in earlier tests with No. 2 fuel oil to facilitate comparisons. Fuel oil has been found to form carbon in ATR at conditions much milder than those predicted by equilibrium. Reactive differences between paraffins and aromatics in ATR, and thus the formation of different carbon precusors, have been shown to be responsible for the observed carbon formation characteristics (fuel-specific). The types of carbon formed in the reformer were identified by SEM and XRD analyses of catalyst samples and carbon deposits. From tests with both light and heavy paraffins and aromatics, it is concluded that high boiling point hydrocarbons and polynuclear aromatics enhance the propensity for carbon formation in ATR.

Effects of olefin (propylene) addition on the ATR performance of benzene are described in this report. The amount of propylene that can be added at the inlet of the reformer before carbon begins to be formed is higher than what can be added at locations within the steam reforming region of the bed.

In ATR tests with mixtures of paraffins and aromatics (n-tetradecane and benzene) synergistic effects on conversion characteristics were identified. Thus, the mixtures' propensity for carbon formation was intermediate between that of the pure hydrocarbon component fuels under similar operating conditions.

Comparisons of the No. 2 fuel oil data with the experimental results from this work with pure (and mixed) sulfur-free hydrocarbons indicate that the sulfur content of the fuel may be the limiting factor for efficient ATR operation, i.e., low oxygen-to-carbon ratios and low preheat temperature. Exploratory tests with sulfur-containing paraffins and aromatics are described here in which the conversion and degradation effects of the sulfur additive (thiophene) in ATR were examined. At the low preheat temperatures and steam-to-carbon ratios used here, the front part of the catalyst was deactivated by sulfur-catalyst interaction, while the propensity for carbon formation was enhanced.

Steam reforming of hydrocarbons in conventional reformers is heat transfer limited. Steam reforming tasks performed in this work have included performance comparisons between conventional pellet beds and honeycomb monolith catalysts. The same fuel, n-hexane, was used in all cases. Metal-supported

monoliths were examined in this phase of the work. These offer higher structural stability than ceramic supports, which were found to disintegrate under the steam reforming conditions used in previous work in this laboratory. Moreover, metal monoliths offer the advantage of higher thermal conductivity.

Data from two metal monoliths of different catalyst (nickel) loading have been compared to pellets under same operating conditions. Improved heat transfer and better conversion efficiencies than for the pellets were obtained with the metal monolith of the higher catalyst loading. Experimental results are indicative of surface-gas interaction throughout the length of the monoliths.

ACKNOWLEDGMENT

The authors gratefully acknowledge the contribution of Glen D. Smith and Clarence L. Tuttle in carrying out the tests described in this work. We also wish to thank Stephen F. Dawson and Kuo-Hung Chen for their assistance.

This work was conducted at the Jet Propulsion Laboratory through NASA Task RD-152, Amendment 183, and was sponsored by the U.S. Department of Energy under Interagency Agreement DE-AI03-79ET11326-1.

TABLE OF CONTENTS

TABLE OF CONTENTS (Cont'd)

D1

PART I

AUTOTHERMAL REFORMING OF SULFUR-FREE AND SULFUR-CONTAINING HYDROCARBON LIQUIDS

INTRODUCTION

Autothermal reforming (ATR) offers an advantageous alternative to steam reforming for hydrogen production for fuel cells because of the wider range of fuels that can be converted. This process involves the combination of partial oxidation and steam reforming of a hydrocarbon fuel to produce principally hydrogen and carbon monoxide as described in the following reactions:

$$C_nH_m + n/2\ O_2 \rightarrow nCO + m/2\ H_2 \quad (1)$$

$$C_nH_m + n\ H_2O \rightarrow nCO + (n + m/2)\ H_2 \quad (2)$$

These reactions are followed by establishment of the equilibria:

$$CO + H_2O \rightleftarrows CO_2 + H_2 \quad (3)$$

$$CO + 3H_2 \rightleftarrows CH_4 + H_2O \quad (4)$$

Other than reactants' preheat, no external heat source is required since the exothermic reaction 1 plus the preheat sustain the endothermic reaction 2.

In this work, the autothermal reforming of hydrocarbon liquids has been considered as a viable route for hydrogen generation for fuel cell power plants. The particular advantage that this process offers is to expand the range of applicable fuels to heavier petroleum-based and coal-derived liquids. In comparison, light naphtha is the heaviest fuel that can be converted to hydrogen without carbon deposition by conventional steam reforming, which is the process to

be used initially for fuel cells. The applications considered here demand a process with high thermal efficiency, carbon-free operation, and high hydrocarbon conversion efficiency as dictated by equilibrium. Partial oxidation alone has lower thermal efficiency than steam reforming. Carbon formation in this process can be prevented either by increasing the air/fuel ratio (i.e.. decreasing thermal efficiency) or by adding steam (1-3), which also increases the hydrogen yield because of simultaneous steam reforming.

The prevention of carbon formation in the catalyst bed is one of the most important aspects of reformer operation. The following carbon producing reactions are possible:

$$2CO \rightarrow C + CO_2 \quad (5)$$

$$CO + H_2 \rightarrow C + H_2O \quad (6)$$

$$CH_4 \rightarrow C + 2\,H_2 \quad (7)$$

$$(-CH_2-)_n \rightarrow nC + n\,H_2 \quad (8)$$

Under certain conditions in the mixture of CO, CO_2, H_2, CH_4 and H_2O, free carbon is thermodynamically possible. This carbon, produced according to reactions 5 and 6, is usually referred to as thermodynamic carbon or Boudouard carbon. Carbon can also be formed as a result of thermocracking of the fuel hydrocarbon used; the olefinic compounds formed degrade to carbon very easily giving an overall reaction as set out in reaction 8.

Using the principle of thermodynamic equilibrium, it is possible to specify which chemical species will be present in the product gases of the autothermal reformer at equilibrium. The computer program used here (4) is based on the minimization of the Gibb's free energy of the system (using graphite data for carbon), and is run under constant system enthalpy, H, and pressure, P, i.e.,

truly adiabatic conditions. In all calculations, a pressure of 1 atm was considered, as this was approximately the pressure in the reactor system in our tests. Also, in the well insulated experimental reactor, a nearly adiabatic operation was achieved.

The autothermal reformer is envisioned as a fuel processor that may have to operate with sulfur in the process stream, because the sulfur compounds (principally thiophenic) in distillate fuel oils are not readily removed by the commonly used desulfurization methods for natural gas and naphtha. By combusting a portion of fuel inside the catalyst bed, higher catalyst temperatures (1200°-1400°K) can be reached than in conventional steam reformers. At these higher temperatures, the supported nickel catalysts commercially used for steam hydrocarbon reforming are anticipated to be less susceptible to sulfur poisoning because of reduced stability of the nickel sulfides (as predicted by thermodynamics (5)). The sulfur content of a fuel may also change the conditions for carbon formation on a given steam reforming catalyst. Hence, particular emphasis was necessary in delineating this possible sulfur-carbon formation relation by well planned experiments.

In a recent JPL report to EPRI (6) on autothermal reforming of No.2 fuel oil, the conditions under which carbon formation started were shown to be much milder than those predicted by the equilibrium theory. Experimental results by other workers (7-9) are in agreement with the JPL data. Follow-on autothermal reforming work at JPL has focused on identifying the causes for the observed behavior of No.2 fuel oil. During this work, tasks have been directed toward delineating the conversion characteristics of individual fuel components

(paraffins, aromatics, olefins, and sulfur compounds) in the autothermal reformer. Since heavy distillate fuels are comprised of a mixture of different hydrocarbons covering a range of boiling points from about 350 to 650°K, the autothermal reforming of both light and heavy compounds was studied. The same catalyst types and configuration as in earlier tests with No.2 fuel oil were used in these tests. Experimental results have been published (10-12) on the ATR of model light and heavy paraffins (n-hexane, n-tetradecane) and aromatics (benzene, naphthalene). These results have demonstrated that differences in chemical reactivity and carbon-forming tendency in ATR are related to the type of fuel hydrocarbon used. Locations and types of carbon in the autothermal reformer have been correlated with intermediate reaction species for each hydrocarbon type. In addition, the effects of the operating parameters on reaction temperature and products, and carbon-forming tendency have been established.

In this report, the previously obtained information on carbon formation from individual paraffins and aromatics is summarized to facilitate comparisons with data collected in the present phase of the experimental ATR work. New experimental results reported herein are from three recent tasks:

(a) Addition of Propylene to Benzene.

In these experiments, the influence of an olefin (propylene) on the ATR characteristics (conversion, carbon formation) of benzene was studied by injecting propylene at different catalyst bed locations.

(b) ATR of Mixtures of Paraffins and Aromatics.

These tests were performed with different mixtures of n-tetradecane and benzene. Using similar operating conditions to those used for the pure mixture components, data were collected on the carbon formation characteristics of these mixtures.

(c) ATR of Sulfur-containing Paraffins and Aromatics.

Thiophene, a good model sulfur compound for heavy distillate fuels was used in these tests in mixtures with either n-tetradecane or benzene to study the conversion and degradation effects of fuel sulfur on the catalyst. Reaction temperatures and products from the ATR of thiophene-contaminated n-tetradecane, and benzene are compared to those pertaining to each pure hydrocarbon. Possible relation between the sulfur content of a fuel and propensity for carbon formation is discussed in view of the experimental data.

EXPERIMENTAL

Apparatus

The design of the autothermal reforming system used in this work has been developed from previous tests with No.2 fuel oil (6) and pure hydrocarbons (10, 11). Figure 1 shows a schematic of the autothermal reformer. During operation, preheated air and steam are mixed first, followed by the injection of vaporized fuel downstream of the mixer. The three components are further mixed in a helical swirler just prior to the reactor entrance. By minimizing the residence time of the fuel inside the mixing tubes in this manner, the extent to which carbon-forming, gas phase reactions proceed is limited and were held to zero in this system. The reactor inlet is made of refractory insulation and has a conical shape to avoid stagnation areas and to provide uniform inlet conditions. Externally, the reactor and all feed lines are insulated to minimize heat losses.

The reactor (3.75 in. I.D.), made from Inconel, was filled to the top flange with catalyst pellets. The catalyst bed configuration is depicted in Figure 1. Off-center, axial bed temperatures were recorded by a chromel-alumel thermocouple probe which traversed inside an Inconel thermowell. A traversing Inconel gas probe was used to sample gaseous reaction products throughout the catalyst bed length. This probe was freely moving inside an Inconel tube which was closed at the end and perforated at 2 in. intervals. Gas samples were analyzed by on-line gas analyzers for H_2, CO, and CO_2, and with two gas chromatographs, one with a Flame Ionization Detector (FID) for hydrocarbons, and one with a Flame Photometric Detector (FPD) for sulfur compounds. Pressures and pressure differentials were monitored by pressure transducers, gauges, and manometers.

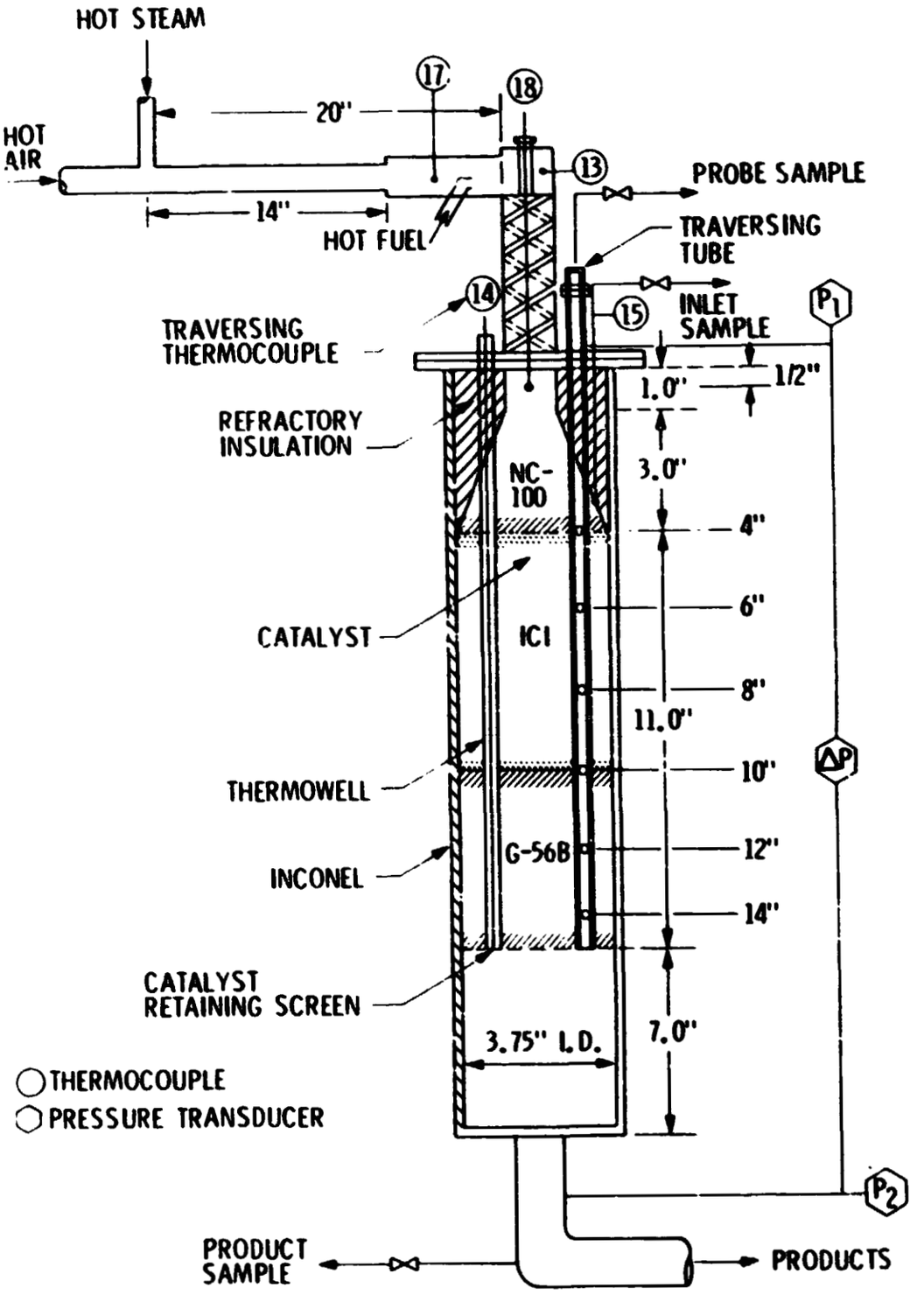

Figure 1. Schematic of the Autothermal Reformer.

Materials

(a) Fuels. Technical grade n-tetradecane, and pure grade benzene liquids were used in these tests. The technical grade n-tetradecane (Humphrey Chem. Co.) consisted of 100% paraffins, with n-dodecane, branched hexadecane, and branched tetradecane as the only trace impurities. The pure grade benzene (Phillips Chem. Co.) consisted of 99.5 vol.% benzene, and 0.4% other aromatics. The propylene gas (99% +) used as a fuel additive was purchased from Matheson Co. High purity (99% +) liquid thiophene was purchased from Eastman Kodak Co.

(b) Catalysts. The autothermal reactor was packed with three layers of supported nickel catalysts as shown in Figure 1. In all tests, the top and bottom zones consisted of Norton NC-100 spheres and cylindrical G-56B tablets, respectively. The middle zone was packed either with ICI 46-1 or ICI 46-4 Raschig rings. The physical and chemical characteristics of these catalysts, commercially used in steam reformers, are given in Table I.

The catalyst types and configuration used here were those found to be most effective in previous ATR tests with No. 2 fuel oil (6). The choice of catalyst was dictated by the requirements for enhancing ATR operation, and commercial availability. Thus, in the first zone a low activity catalyst was used to effect a gradual increase in the reactants' temperature to the level of subsequent main reaction temperature, and inhibit carbon formation. The mechanism of heat transfer in this segment is mainly radiation and conduction aided by some exothermal reaction. The Norton NC-100 catalyst spheres were selected to mediate the initial

TABLE I

PHYSICAL AND CHEMICAL CHARACTERISTICS OF TEST CATALYSTS

TRADE NAME	NORTON NC-100	ICI 46-1	ICI 46-4	GIRDLER G-56B
Particle Size, inches	1/2 spheres	11/16 OD x 1/4 ID x 5/16 length	11/16 OD x 1/4 ID x 5/16 length	1/8 x 1/8 cylinders
Bulk (packing) Density, lb/cu ft.	65	72	62	90
Chemical Analysis, wt.%*				
NiO	6.4 - 7.6	21.0	11.0	30.8
SiO_2	-	14.0	-	0.9
Al_2O_3	-	29.0	77.0	59.9
ZrO_2	~93.0	-	0.3	-
K_2O	-	7.0	-	-
MgO	-	13.0	-	7.0
$CaCO_3$	-	-	-	-
CaO	-	13.0	12.0	-
Fe_2O_3	-	3.0	-	-
Fusion Temperature, °F	2650	>2000	>2000	2500
Surface Area, m^2/g	1.0	11.0	14.0	13.0

*Composition as provided by manufacturer

oxidation reaction and help to inhibit precombustion as well as to act as a reactant distributor. These highly porous spheres fill the conical inlet portion of the bed to the top flange as shown in Figure 1, eliminating voids that enhance the probability of precombustion. In the middle zone, an active catalyst capable of oxidizing the hydrocarbons must be used. In this section the oxygen is completely reacted and limited steam reforming is also maintained. The ICI 46-1 catalyst, which contains potassium as a soot-suppressant, was chosen initially in order to reduce carbon formation during steam reforming. This catalyst is in the form of Raschig rings with a high void-to-surface ratio that allows for gas expansion in this region where the initial rapid reaction and temperature rise take place. In experiments with aromatics, the middle zone was filled with ICI 46-4 Raschig rings that have geometry identical to 46-1 but lower nickel loading. This catalyst was used to mediate the high heat release from the aromatic ring oxidation reaction. Finally, the bottom layer of the catalyst bed should contain a highly active, steam reforming catalyst to convert the residual hydrocarbons and methane. In this zone, the Girdler G-56B catalyst was used in the form of small cylindrical pellets. As shown in Table I, these pellets had the highest nickel loading.

RESULTS AND DISCUSSION

All autothermal reforming tests were run at atmospheric pressure and at moderately high reactant preheat temperature, T_p, within the range of 1000-1150°F (800-900°K). This is the temperature recorded by thermocouple No.13 of Figure 1. At each condition, the gas hourly space velocity (G.H.S.V. or S.V. for brevity) was specified. This quantity is defined here as the volumetric flow rate of reactants (NTP) divided by the volume of catalyst corrected for void fraction.

For each fuel, the carbon formation limit was sought as a function of the steam-to-carbon, $(S/C)_m$, and oxygen-to-carbon,* $(O_2/C)_m$, molar ratios at constant pressure and preheat temperature, and over a narrow range of space velocities. The $(O_2/C)_m$, $(S/C)_m$ ratios are defined here as ratios of moles of oxygen and steam respectively to atoms of carbon in fuel based on hourly flow rates. At each $(O_2/C)_m$ ratio, the $(S/C)_m$ ratio was reduced stepwise until carbon began to form with each condition maintained at a steady state for 4 to 6 hours. The determination of carbon formation was detected by a continuous rise in the bed differential pressure and (or) carbonaceous deposits (soot) on the filter in the exhaust product sample line. These "accelerated" carbon formation tests may not describe the precise conditions necessary to completely inhibit carbon for extended periods of reaction. Thus, "carbon formation" is defined here as carbon forming at a rate significant enough to be measured in the time frame during which these tests were conducted.

---

* To be consistent with the majority of the reported fuel cell work, the oxygen-to-carbon ratio is used here instead of the previously used air-to-carbon, $(A/C)_m$, molar ratio. To convert from $(O_2/C)_m$ to $(A/C)_m$ multiply the former by 4.773.

(A) Summary Of Previous ATR Work With Pure Paraffinic And Aromatic Hydrocarbons

Carbon Formation in ATR

Experimental results from autothermal reforming tests with several paraffinic and aromatic hydrocarbon liquids have recently been reported (10-12). These have shown clearly that reactive differences exist between these two types of hydrocarbons which affect their carbon formation characteristics in the autothermal reformer.

Carbon formation lines were determined experimentally for each fuel at similar operating conditions. These lines separate the carbon-free from the carbon-forming region in the $(O_2/C)_m$ - $(S/C)_m$ plane, i.e., they are the loci of the minimum $(S/C)_m$ ratio before carbon formation begins for a given set of the other operating parameters. In each case, the experimental carbon line was compared to the theoretical one predicted by thermodynamic equilibrium (graphite free energies). The shape of the experimental carbon formation curves was found to be similar for light and heavy hydrocarbons of the same type. However, the heavy homologs of each series formed carbon in ATR at milder conditions than the light ones.

Unique carbon formation characteristics pertaining to each hydrocarbon type were identified indicating different sensitivity to the operating parameters, and possibly different carbon formation mechanisms. Typical carbon formation lines for paraffins and aromatics are shown in Figures 2 and 3, respectively. For n-tetradecane, Figure 2, the experimental carbon formation line converges to the equilibrium line at high $(O_2/C)_m$ ratios, but diverges from it for

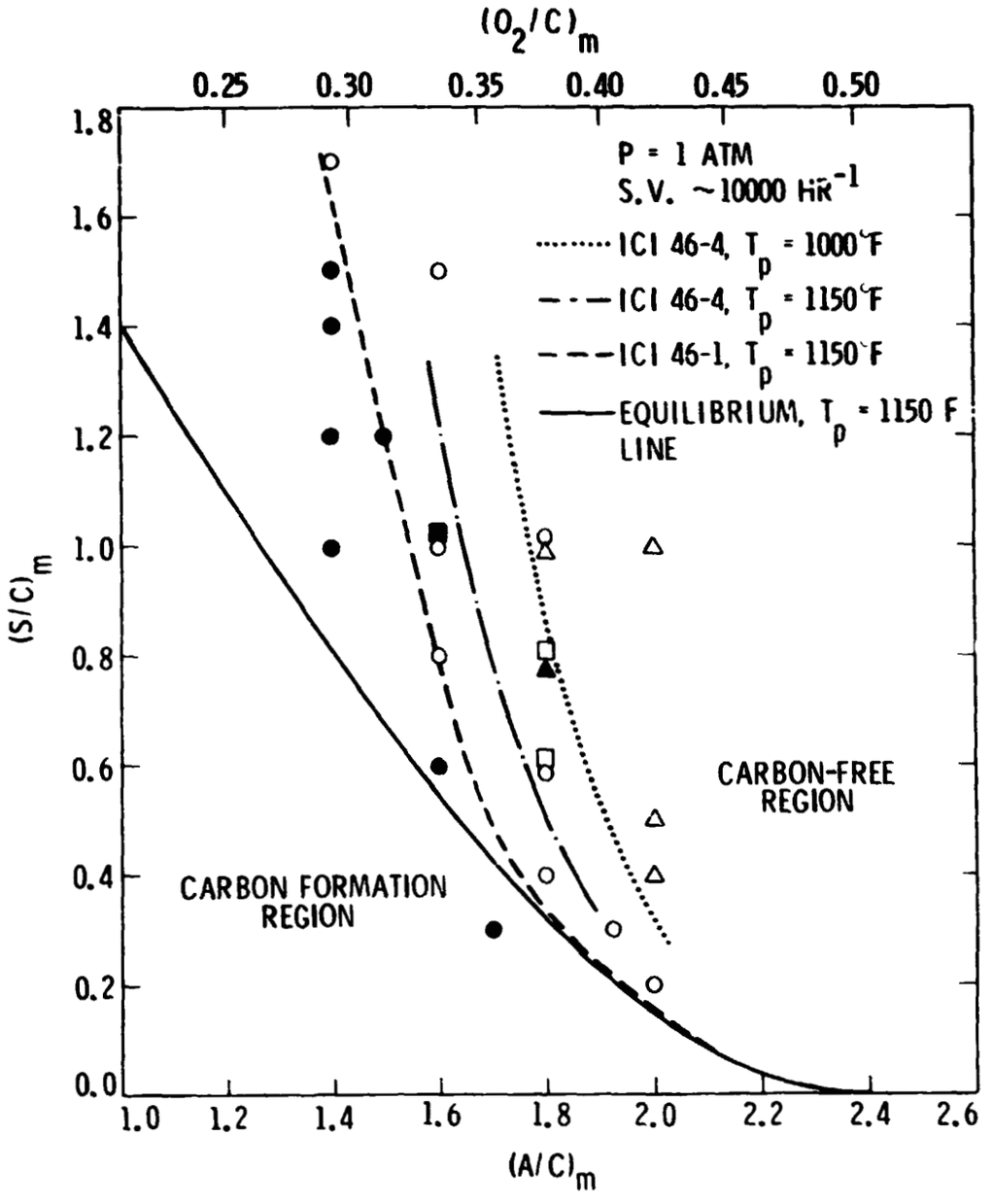

Figure 2. Autothermal Reforming of n-Tetradecane. Carbon Formation Lines.
△▲: ICI 46-4 at T_p = 1000°F.
□■: ICI 46-4 at T_p = 1150°F.
○●: ICI 46-1 at T_p = 1150°F.
Open Symbols: Carbon-Free
Closed Symbols: Carbon Formation

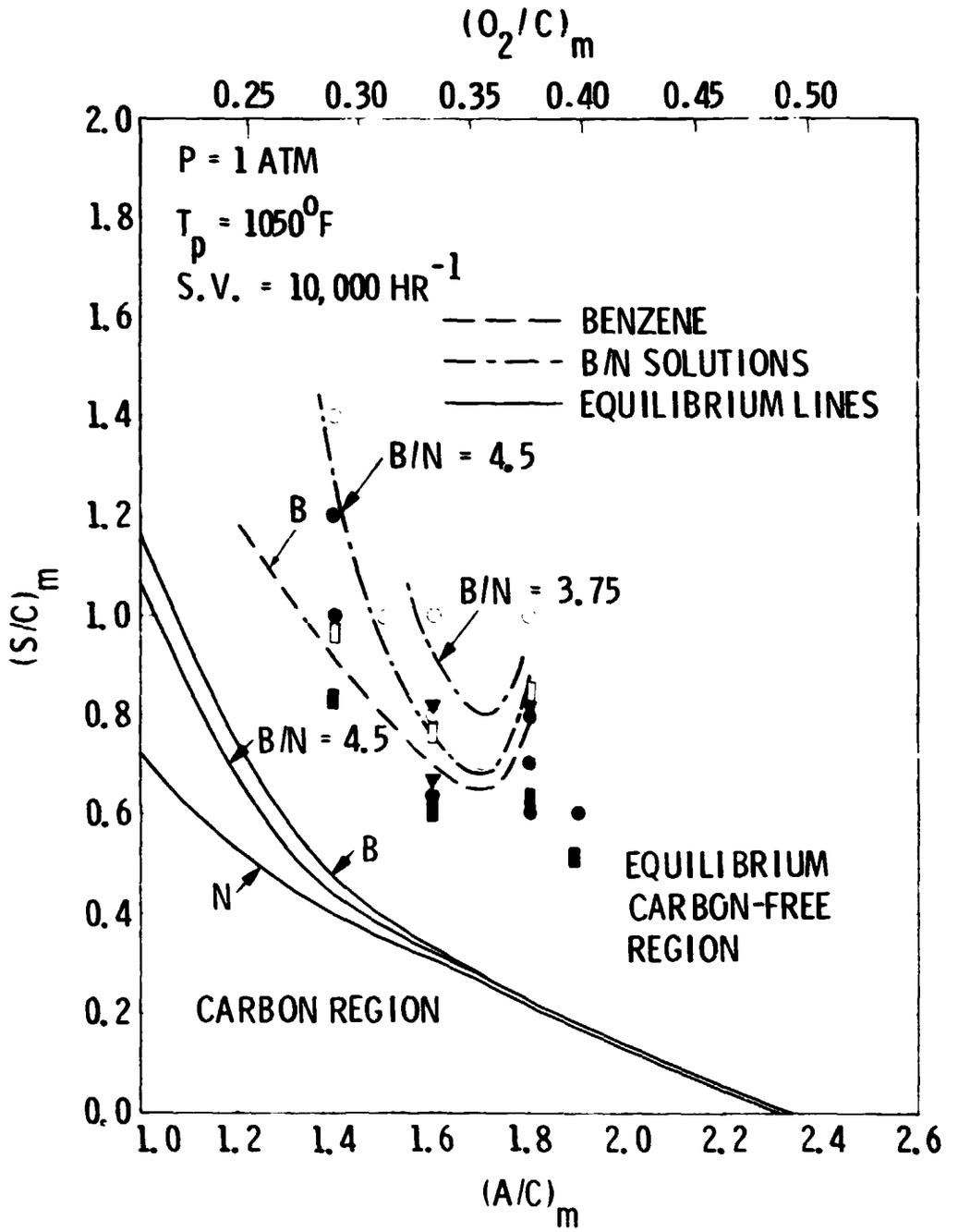

Figure 3. Autothermal Reforming of Benzene and Benzene Solutions of Naphthalene. Carbon Formation Lines.
▯▮: Benzene neat
◌●: Benzene/Naphthalene Solution, $(B/N)_m$ = 4.5
▽▼: Benzene/Naphthalene Solution, $(B/N)_m$ = 3.75
Open Symbols: Carbon-Free
Closed Symbols: Carbon Formation

$(O_2/C)_m$ values lower than about 0.33. On the other hand, the carbon formation lines for benzene, and benzene solutions of naphthalene, Figure 3, diverge from equilibrium at high $(O_2/C)_m$ ratios, and are almost parallel to the theoretical lines at low $(O_2/C)_m$ ratios, thus exhibiting a minimum. This minimum $(S/C)_m$ value occurs at $(O_2/C)_m$ of about 0.36, and is a unique characteristic of the behavior of aromatics in ATR.

The effect of different reactant preheat temperatures on carbon formation is depicted in Figure 2 for the ATR of n-tetradecane. The dotted and hatched curves in this figure were determined on the same catalyst (with ICI 46-4 in the middle zone) for T_p = 1000°F (811°K) and 1150°F (894°K), respectively. The carbon forming tendency was higher at lower reactant preheat temperatures. The effect of different catalyst types in the middle reactor zone is shown for n-tetradecane by the hatched and dashed curves of Figure 2. For the same preheat temperature of 1150°F (894°K), the experimental carbon line corresponding to ICI 46-1 catalyst is located closer to the equilibrium line than for ICI 46-4, which does not contain potassium oxide as a soot-suppressant.

Potential carbon precursors for each hydrocarbon type in ATR were sought in comparative studies of axial bed temperature and reaction profiles. Both carbon-free and carbon-forming conditions were examined. Figures 4 and 5 show typical plots of axial bed temperatures and gas compositions, respectively, for benzene and n-tetradecane run under the same autothermal reforming operating conditions (carbon-forming). Bed temperature profiles are very different for the two hydrocarbons, while reaction intermediates throughout the bed differ in amounts only, not in type. The experimental results plotted in Figures 4 and 5 indicate the following:

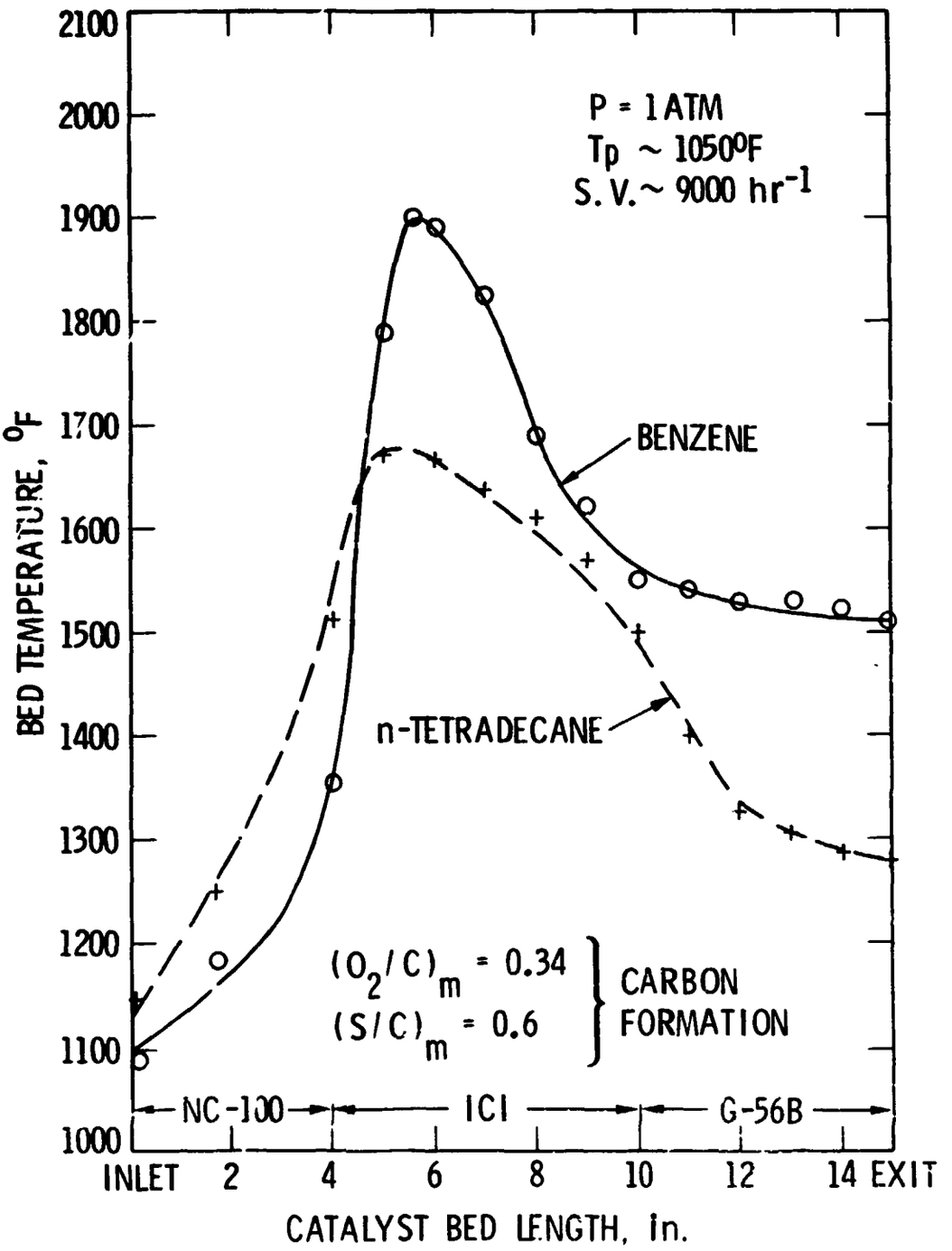

Figure 4. Axial Bed Temperature Profiles.
— — ATR of n-Tetradecane, ICI 46-1
——— ATR of Benzene, ICI 46-4.

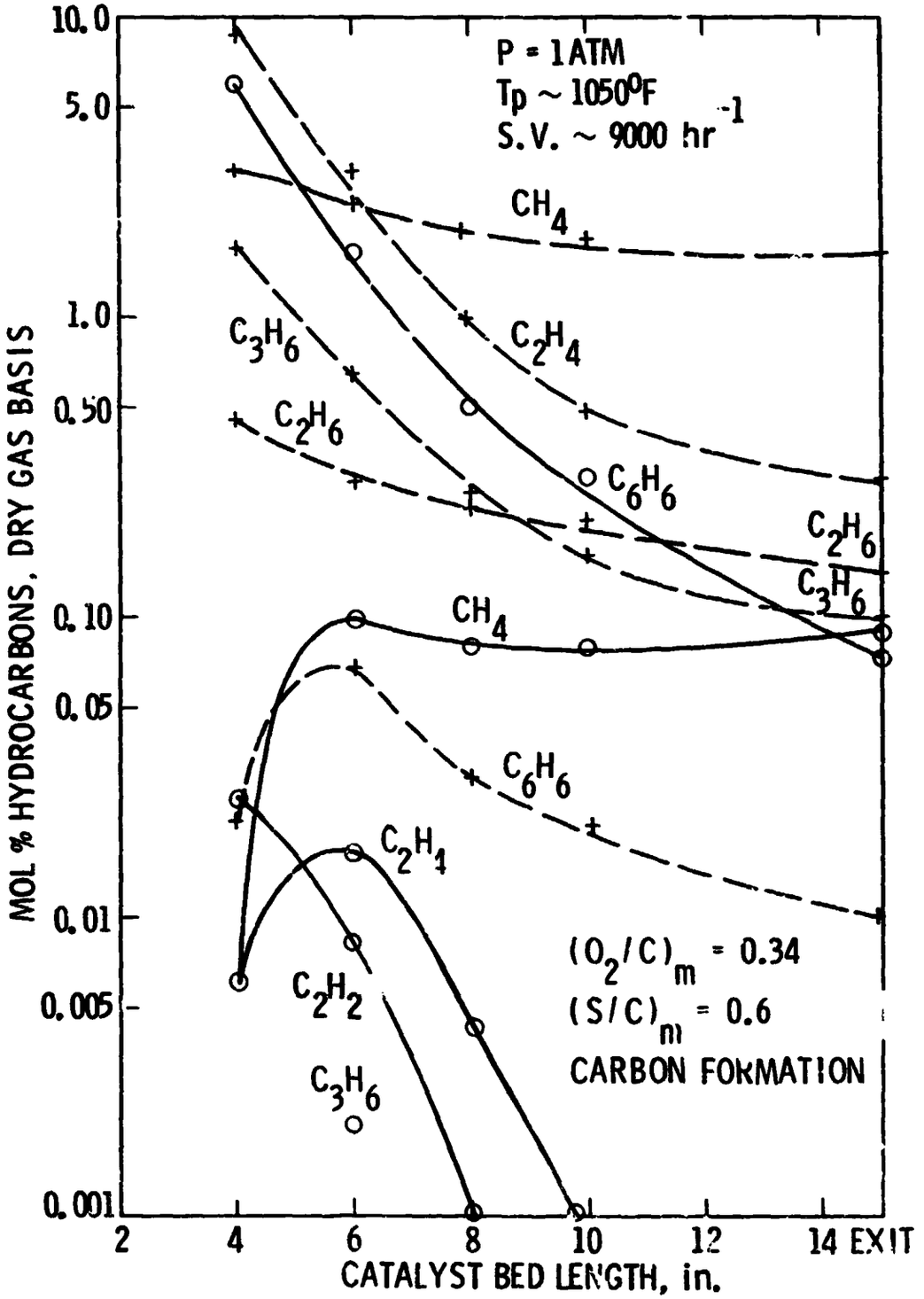

Figure 5. Axial Bed Composition Profiles.
— — ATR of n-Tedradecane, ICI 46-1
——— ATR of Benzene, ICI 46-4

(a) Two main reaction zones exist for aromatics. The first, partial oxidation of the fuel, takes place in a very narrow region well downstream of the reactor inlet. This is depicted by sharp-peaked axial bed temperature profiles with zero initial slope. A complete absence of benzene cracking (to olefins and acetylenes) at the inlet, and very limited reaction in the top catalyst zone account for the slopes of the ascending portion of the temperature profile, and the higher bed temperatures compared to n-tetradecane. In the immediate vicinity of the temperature peak, hydrocarbons such as ethylene, acetylene and methane are rapidly produced and reach a peak. The first two of these intermediate species are indicative of benzene cracking, which however is very limited, as was found by mass balance calculations.

The second reaction zone for aromatics involves the steam reforming reaction, which mainly begins upon completion of the first reaction (partial oxidation), initially at high temperatures, and then at lower temperatures in the lower half of the catalyst bed. The slopes of the descending (past the temperature peak) portion of the temperature profile for benzene in Figure 4 indicate that steam reforming occurs at a fast rate close to the temperature peak (large slope), but it is limited in the last catalyst zone, where the temperature profile levels off. From Figure 5, we can see that the profiles of unconverted benzene and produced methane are commensurate with temperature changes in this catalyst zone. Thus, the slope of the unconverted benzene profile is decreasing through the length of the bed downstream of the temperature peak, while that of methane is almost constant in this region, and slightly increasing towards the reformer exit. On the other hand, cracking products

disappear rapidly and are no longer detected in gas samples taken from the lower end of the bed. Since carbon is being formed throughout the steam reforming region of the bed (see below), and because the olefins and acetylene are negligible in the gas phase throughout the bed, the main carbon precursor appears to be the aromatic molecule (benzene) itself. Benzene may form carbon through dehydrogenation in the gas phase at the high temperatures prevailing in the vicinity of the temperature peak. The rate of carbon formation by this mechanism may exceed the rate of carbon removal by gasification for a given range of temperature and limited steam availability. Further down the bed, at lower temperature, surface-bound carbon may be produced from benzene-nickel interaction. The fact that the methane concentration did not decrease through the lower part of the bed seemed to be unrelated to carbon formation, since it was also observed under carbon-free conditions.

(b) In the case of paraffins, the same two reaction zones were identified as for the aromatics, i.e., partial oxidation and steam reforming. However, a third zone, cracking to low molecular weight olefins and paraffins, was very pronounced in the top part of the catalyst bed. This is portrayed by the temperature and reaction profiles of Figures 4 and 5. These intermediate cracking products were already detectable at the bed inlet (up to 25 vol.% of the incoming n-tetradecane cracks at the inlet (10)), and peaked just upstream of the temperature peak location. In addition, a small amount of benzene was produced in the upper part of the bed indicative of cyclization reactions. The benzene profile also peaked just prior to the temperature peak. Because of the endothermic cracking reactions, bed temperatures were lower for n-tetradecane than for benzene.

Partial oxidation was taking place throughout the front end of the bed in the case of n-tetradecane (paraffins being much less refractory than aromatics), as indicated by larger initial slope of the n-tetradecane temperature profile.

Similar to the aromatics, the continuous drop in bed temperature begins immediately past the temperature peak, due to steam reforming of the paraffins and olefins just produced. In the vicinity of the temperature peak, at the prevailing high temperatures, both gas phase and surface carbon formation may take place principally from the olefins abundant in this region of the bed since the benzene intermediate is present in negligible amounts. Figure 5 shows that the profiles of the olefins (and not the paraffins) have the largest slope (highest rate of conversion) in the bed. Close to the bed exit, all species' profiles level off, indicating low steam reforming reaction rates. At the low temperatures of this region, the rate of carbon formation by olefin degradation on the catalyst surface may exceed the rate of carbon removal if there is not enough steam available.

It should be noted that the same reaction intermediates have been detected in ATR either under carbon-free or carbon-forming conditions. The extent of cracking, however, was much higher under carbon-forming conditions, and resulted in lower steam-to-carbon ratios in the region of the bed downstream of the temperature peak. As we have discussed in a previous report (11), the rates of carbon formation are greatly affected by changing the $(S/C)_m$ ratio, more so than by temperature changes. In the following section, the locations for carbon formation in ATR are

shown to be within the steam reforming region of the bed at the operating conditions considered in this work.

Locations and Types of Carbon in ATR

Information about the locations of carbon deposition and types of carbon formed in the catalyst bed was obtained by examination of the bed after carbon-forming conditions, and analyses of catalyst samples by Scanning Electron Microscopy (SEM), Thermal Gravimetric Analysis (TGA) and X-ray Diffraction (XRD).

For both paraffinic and aromatic hydrocarbons, catalyst from the front end of the bed always appeared free of carbon deposits and retained its structural integrity. No surface grown carbon was found on the catalyst in this region where partial oxidation of the fuel mainly occurs. On the other hand, catalyst from the lower half of the bed had an eroded appearance, and broken pieces and fines were collected from this region of the bed where steam reforming takes place. This physical breakdown of the catalyst material can be attributed to carbon formation inside the pores followed by carbon removal (13) during the desooting process. Figures 6a and b show SEM photomicrographs of the upper and lower half, respectively, of ICI 46-1 catalyst used in the ATR of n-tetradecane. Needle-like carbon growths from all directions inside the pores are seen in Figure 6b, while no carbon is seen in Figure 6a at the same magnification. The same catalyst samples were also checked for carbon by TGA, and the results are in agreement with SEM.

Surface grown carbon was identified by SEM on samples from the lower part of the catalyst bed. Figure 7 shows a typical SEM photomicrograph of the surface of the lower end of ICI 46-1 catalyst bed used in ATR of n-tetradecane under

ORIGINAL PAGE
BLACK AND WHITE PHOTOGRAPH

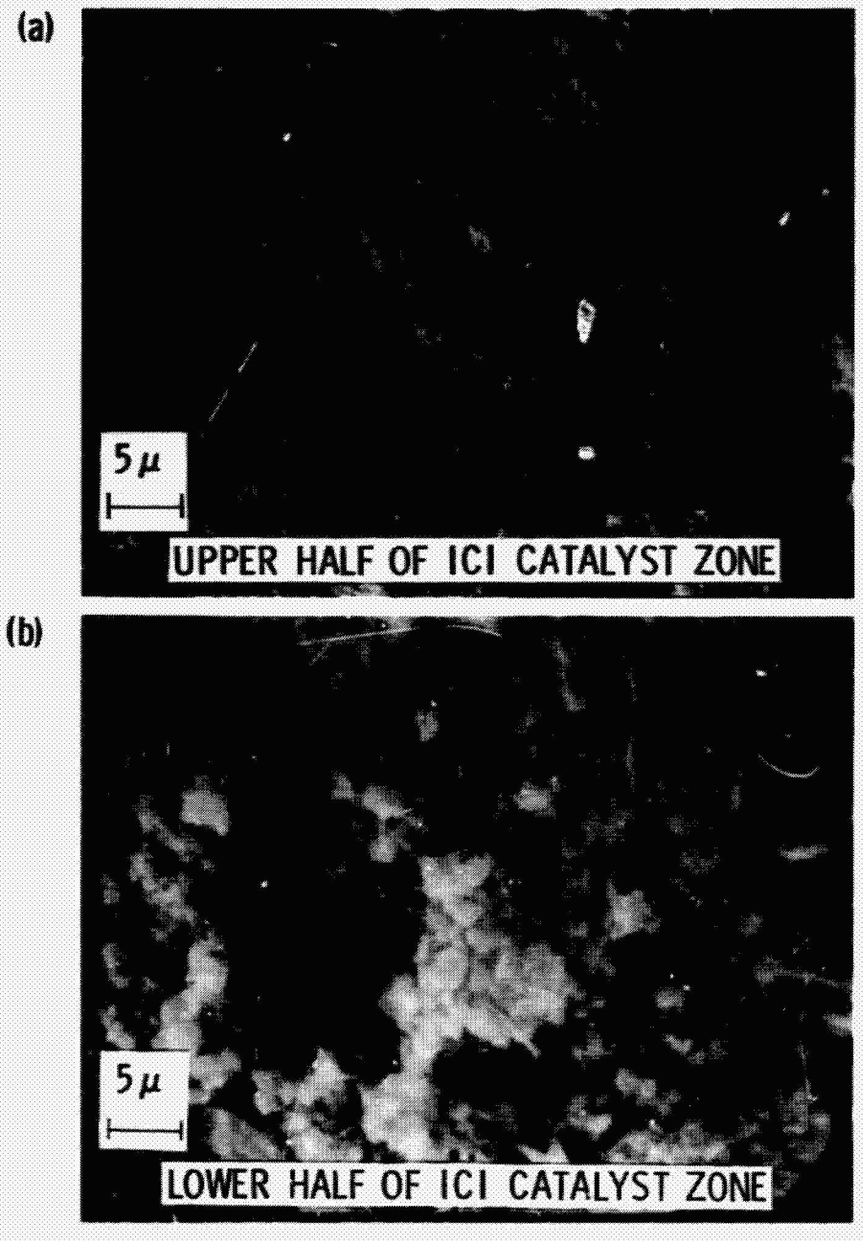

Figure 6. SEM photomicrographs of the surface of ICI 46-1 catalyst used in ATR of n-Tetradecane under carbon-forming conditions: P = 1 atm, T_p = 1150°F, $(O_2/C)_m$ = 0.34, $(S/C)_m$ = 0.6, and S.V. = 10,000 hr^{-1}.

ORIGINAL PAGE
BLACK AND WHITE PHOTOGRAPH

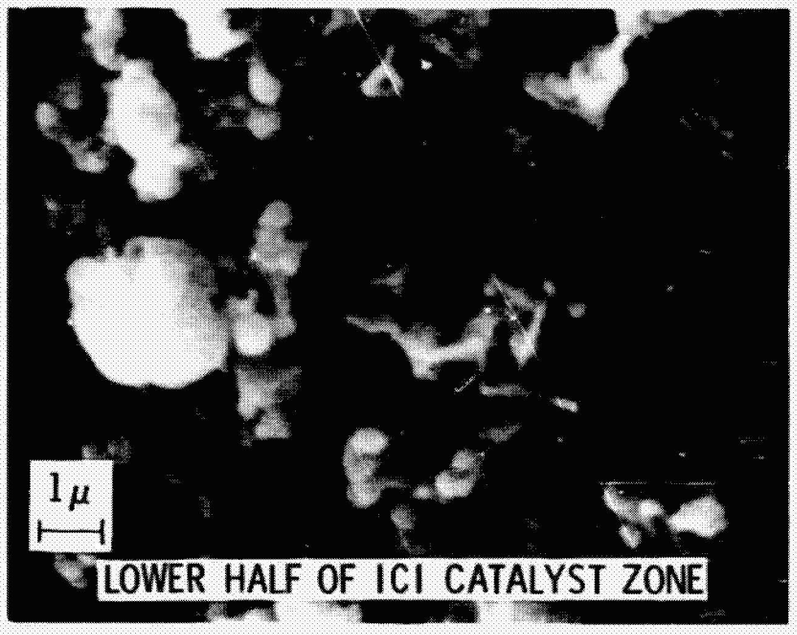

Figure 7. SEM photomicrograph of the surface of ICI 46-1 catalyst used in ATR of n-cetradecane under carbon-forming conditions: P = 1 atm, T_p 1150°F, $(O_2/C)_m$ = 0.38, $(S/C)_m$ = 0.25, and S.V. = 10,000 hr^{-1}.

carbon-forming conditions. Tubular carbon whiskers are observed that appear to have a nickel crystallite located at the end. The diameter of the whisker is very close to that of the nickel crystallite. These observations are in agreement with earlier reports by Rostrup-Nielsen (14) on coking studies under steam reforming conditions. Further XRD analysis of the catalyst samples that showed evidence of surface grown carbon indicated that graphite carbon was present.

In addition to surface grown carbon, evidence of gas phase carbon formation was obtained from large amounts of soot (carbon fines) collected from the interstices between catalyst particles throughout the lower two thirds of the catalyst bed. Heavy deposits of this type of carbon were found on the catalyst surfaces, but they did not appear to be surface-bound. The gas phase carbon, as found by XRD, consisted of a mixture of amorphous (non-crystalline) and graphitic carbon forms. The locations of gas phase carbon formation cannot be defined with certainty, because carbon fines found in the lower half of the bed could have originated either there or upstream, and transferred down by the flowing gases. It appears that the most probable location for this type of carbon formation is around the temperature peak, where thermocracking of paraffins to olefins, which can easily degrade to carbon, or degradation of aromatics to carbon proceed at the fastest rates.

Differences between the types of carbon produced during the ATR of paraffinic and aromatic hydrocarbons have not been quantified. However, from several examinations of the catalyst bed after operation at carbon-forming conditions, gas phase carbon formation in the middle catalyst zone appeared to be more extensive for aromatics than for paraffins. Limited surface-bound carbon was

detected in the middle catalyst zone in the case of aromatics. Further downstream, in the lower catalyst zone, surface grown carbon was detected with either hydrocarbon type.

These results indicate possible differences in the mechanisms of carbon formation between paraffins and aromatics. As discussed in the previous section, at the high temperatures prevailing in the middle catalyst zone, immediately past the location of complete oxygen consumption (temperature peak), paraffins crack to olefins. These can then degrade to carbon either in the gas phase or on the catalyst/support surface at a rate exceeding that of carbon removal (depending on the conditions). Thus, both types of carbon observed may have olefinic precursors. Aromatics, on the other hand, may form gas phase carbon at these high temperatures by fission of the C-H bonds rather than the C-C bonds. This hypothesis is supported by (a) negligible amounts of reaction intermediates (olefins, acetylenes) from aromatics as compared to considerable amounts of intermediates from cracking of paraffins and (b) the characteristic "minimum" in the experimental carbon formation line for aromatics, whereby an increase in the $(O_2/C)_m$ ratio (i.e., a temperature increase) has an adverse effect on carbon formation, possibly indicating the onset of gas phase benzene dehydrogenation to form carbon at a faster rate than the surface reaction (with steam). Finally, in the lower catalyst zone, where steam reforming takes place at continuously decreasing temperatures, the rates of surface carbon formation from either hydrocarbon type may exceed the steam reforming rates depending on the excess steam and temperature available in this part of the bed. A concise performance comparison of the autothermal reforming paraffins and aromatics is given in Table II. The main characteristics of each hydrocarbon type in ATR, as discussed above, are listed in this table.

TABLE II

ATR PERFORMANCE COMPARISON OF PARAFFINIC AND AROMATIC HYDROCARBONS

ATR VARIABLES	PARAFFINS	AROMATICS
Inlet Reactions	Extensive cracking	No cracking
Exit Reactions	Steam reforming	Steam reforming slower than paraffins; methanation
Bed Temperature Profiles	Broad-peaked; slow rise and fall	Sharp-peaked; zero slope at inlet and exit of bed
Peak Temperatures	Low	Higher than paraffins
Intermediate Hydrocarbon Species	Predominantly olefinic; low aromatic	Predominantly unconverted aromatic; low olefins, acetylene
Carbon Formation Conditions	Low O_2/C, low S/C; High molecular weight	High O_2/C, low S/C; polynuclear aromatics
Carbon Types	Surface carbon growths (whiskers)	Limited surface carbon growths
	Gas phase carbon (fines in voids)	Extensive gas phase carbon formation
Location of Carbon Deposits	Surface carbon } Throughout steam reforming zone	Surface carbon } Throughout steam reforming zone
	Gas phase carbon } Vicinity of temperature peak?	Gas phase carbon } Vicinity of temperature peak?
Catalyst Erosion	Considerable	Less extensive

(B) Addition Of Propylene To Benzene

In this work, a new series of tests with benzene were run in the autothermal reformer in which the effects of olefin addition on reaction products and carbon formation were studied. Propylene, one of the main reaction intermediates in the autothermal reforming of paraffins (10-12) was the olefin used in these tests. The baseline operating conditions with pure benzene were chosen in the carbon-free region. The amount and location of propylene injection into the reformer were varied, thereby permitting the identification of the reaction zone most prone to carbon formation under the chosen operating conditions.

Tests CP-183 through 190 were run in the ATR reactor on the same catalyst bed. This was composed of the usual upper and lower zone catalysts, NC-100 and G-56B, respectively, while in the middle zone the ICI 46-4 catalyst was used. The reactants' preheat temperature, T_p, was kept at 1050°F, and the $(O_2/C)_m$ and $(S/C)_m$ ratios, based on benzene only, were 0.33 and 0.80, respectively. Carbon-free operation for benzene neat was expected for these conditions based on previous data (10), and this was verified in tests CP-183, 184. As can be seen in Figure 3, however, this data point lies close to the experimentally determined carbon formation line for benzene, so that with rather small perturbations on the operating conditions, carbon deposition may take place. Propylene gas was added at various bed locations at flowrates of 0.02, 0.045, 0.20 and 0.40 lb/hr. Because of the low flowrates of propylene added, the space velocity in all runs remained approximately the same at 9500 hr^{-1}.

Table III summarizes the data collected from these runs, and Table III-a shows longitudinal bed temperatures for each test run. Also shown in Table III are baseline data from tests CP-183, 184, which were run with pure benzene without carbon formation. The dry gas product analysis from the pure benzene tests showed a total of 900 ppm hydrocarbons, of which 700 ppm were CH_4 and 200 ppm were unconverted benzene. In tests CP-185 through 187, and in CP-189-1, propylene was injected through the access tube of TC-18 (located 1/2 inch below the reactor inlet, Figure 1) in progressively higher amounts from 0.02 to 0.40 lb/hr. The total hydrocarbon content of the product gases in CP-189-1 (with 0.4 lb/hr propylene addition) was increased to 4500 ppm, of which 4200 ppm was CH_4 and 300 ppm benzene. In all cases, no unconverted propylene was detected in the product gases, and the operation remained carbon-free. As can be seen from Table III-a, bed temperatures were lower when propylene was injected at the inlet of the catalyst bed, mainly because the propylene was added at room temperature, but in part because of changes in the $(O_2/C)_m$ and $(S/C)_m$ ratios effected by the propylene addition. Thus, $(O_2/C)_m$ and $(S/C)_m$ ratios of 0.33 and 0.80 respectively for 6 lb/hr flow of benzene, became 0.31 and 0.76 respectively upon addition of 0.4 lb/hr propylene.

Following these tests, propylene was injected at eight inches below the reactor inlet using the gas probe access tube. With 0.20 lb/hr propylene addition, test CP-188-1, unconverted propylene was detected in the exhaust gases, but the reactor could still be operated in the carbon-free region. However, when the flowrate of propylene was raised to 0.40 lb/hr, injection at this level led to carbon formation in the bed (tests CP-188-3, 189-2). Carbon was detected by a sooty deposit in the sample line filter. The recorded temperatures in this

TABLE III

AUTOTHERMAL REFORMING OF BENZENE

Effects of Propylene Addition on Conversion

TEST	FUEL	$(O_2/C)_m$	$(S/C)_m$	(1) T_P	(2) MAX. BED TEMPERATURE		(3) $\dot{m}_f$	(4) S.V.	CARBON	(5) GAS PROBE	DRY GAS COMPOSITION, MOL %												
					T_{MAX}	AT				AT													
				°F	°F	IN.	LB/HR	HR^{-1}	N	INCHES	H_2	CO_2	CO	HC_T	CH_4	C_2H_4	C_2H_6	C_3H_6	C_3H_8	C_4	C_5	C_6	C_6H_6
183, 184	Benzene	0.33	0.80	1050	1730	6.4	6.0	9500	NO	6	19.20	6.83	19.49	3.10	0.05	0.01	0.02	0.002	-	0.01	-	-	2.92
		"	"	"	1720	6.8	"	"	"	8	28.43	6.64	23.95	0.53	0.03	-	-	-	-	-	-	-	0.50
		"	"	"	1714	6.8	"	"	"	10	30.75	6.46	23.38	0.21	0.03	-	-	-	-	-	-	-	0.18
		"	"	"	1744	7.0	"	"	"	EXIT	31.32	6.16	24.43	0.09	0.07	-	-	-	-	-	-	-	0.02
185*	Benzene	0.33	0.80	1050	1716	6.8	6.02	9500	NO	4	0.99	0.59	1.90	7.03	0.01	-	-	0.06	-	-	-	-	6.96
	+0.02 lb/hr	"	"	"	1730	6.8	"	"	"	6	21.54	7.32	20.19	2.91	0.06	0.04	-	-	-	0.02	0.03	-	2.76
	Propylene	"	"	"	1715	6.8	"	"	"	8	29.22	6.57	23.55	1.07	0.03	0.01	-	-	-	-	-	-	1.03
		"	"	"	1718	6.8	"	"	"	10	30.95	6.34	24.62	0.57	0.02	-	-	-	-	-	-	-	0.55
186*	Benzene	0.33	0.80	1050	1693	7.0	6.045	9500	NO	4	0.99	0.67	1.70	6.74	0.01	0.01	-	0.18	-	-	-	-	6.54
	+0.045 lb/hr	"	"	"	1703	7.0	"	"	"	6	21.60	8.09	19.60	2.37	0.07	0.05	-	0.02	-	0.01	0.03	-	2.19
	Propylene	"	"	"	1695	7.0	"	"	"	8	30.21	6.92	23.36	0.76	0.05	0.01	-	-	-	-	-	-	0.70
187*	Benzene	0.33	0.78	1050	1663	7.0	6.20	9540	NO	4	1.24	0.68	2.41	7.27	0.03	0.01	-	0.73	-	-	-	-	6.50
	+0.2 lb/hr	"	"	"	1666	7.0	"	"	"	6	22.05	7.59	25.90	2.83	0.12	0.07	-	0.08	-	0.01	0.02	-	2.53
	Propylene	"	"	"	1668	7.0	"	"	"	EXIT	32.98	5.68	25.95	0.30	0.27	-	-	-	-	-	-	-	0.03

TABLE III (Cont'd)

TEST CP	FUEL	$(O_2/C)_{in}$	$(S/C)_m$	(1) T_P °F	(2) MAX. BED TEMPERATURE T_{MAX} °F	AT IN.	(3) $\dot{m}_f$ LB/HR	(4) S.V. HR^{-1}	CARBON	(5) GAS PROBE AT INCHES	DRY GAS COMPOSITION, MOL % H_2	CO_2	CO	HC_T	CH_4	C_2H_4	C_2H_6	C_3H_6	C_3H_8	C_4	C_5	C_6	C_6H_6
189-1+	Benzene	0.31	0.76	1050	1645	7.8	6.40	9580	NO	0	-	-	-	7 41	0.01	-	-	1.06	-	-	-	-	6.34
	+0.4 lb/hr	"	"	"	1644	7.8	"	"	"	4	0.99	0.97	1.92	7.25	0.01	-	0.01	1.20	-	-	-	-	6.03
	Propylene	"	"	"	1648	7.8	"	"	"	6	28.15	6.57	22.71	1.34	0.07	0.02	-	0.09	-	-	-	-	1.16
		"	"	"	1645	7.8	"	"	"	8	32.57	6.36	23.59	C.60	0.09	-	-	0.02	-	-	-	-	0.49
		"	"	"	1661	7.8	"	"	"	EXIT	33.35	5.35	25.39	(.45	0.42	-	-	-	-	-	-	-	0.03
188-1++	Benzene	0.33*	0.80*	"	1734	6.8	6.0*	9500*	NO	EXIT	32.25	6.06	25.19	0 43	0.14	0.01	-	0.23	-	-	-	-	0.05
	+0.2 lb/hr																						
	Propylene																						
188-2	Benzene	0.33	0.80	1050	1715	6.8	6.0	9500	NO	EXIT	32. 8	6.43	23.82	0.09	0.07	-	-	-	-	-	-	-	0.02
188-3++	Benzene	0.33*	0.80*	1050	1725	6.8	6.0*	9500*	YES	EXIT	33.17	5.84	24.31	0.58	0.29	-	-	0.21	-	-	-	-	0.08
	+0.4 lb/hr																						
	Propylene																						

(1) Preheat temperature, T.C. No. 13 (Fig. 1)
(2) Maximum bed temperature and location with reference point at the reactor inlet
(3) Mass flowrate of fuel
(4) Space velocity based on reactants' flowrates (NTP)
(5) Gas sample probe location with reference point at the reactor inlet

TABLE III-a

AUTOTHERMAL REFORMING OF BENZENE

Effects of Propylene Addition on Bed Temperatures

TEST CP -	$(O_2/C)_m$	$(S/C)_m$	(1) T_p °F	S.V. hr^{-1}	BED TEMPERATURE, °F At (in. from Reactor Inlet)													
					0.5	3	4	5	6	7	8	9	10	11	12	13	14	15
184	0.33	0.8	1070	19447	1068	1283	1282	1651	1731	1744	1719	1659	1596	1542	1482	1451	1443	1451
186	0.33	0.8	1061	9447	1060	1277	1270	1632	1750	1757	1743	1688	1624	1572	1520	1496	1498	1487
188-1	0.33	0.8	1062	9447	1060	1230	1267	1607	1711	1733	1711	1649	1592	1554	1498	1470	1453	1448
-2	"	"	"	"	1064	1222	1275	1630	1742	1764	1763	1692	1630	1581	1529	1489	1476	1465
-3	"	"	"	"	1065	1217	1247	1574	1694	1723	1708	1657	1601	1557	1486	1453	1428	1420
189-1	0.33	0.8	1050	9447	1049	1195	1194	1523	1626	1646	1659	1601	1540	1494	1421	1387	1362	1350

(1) Preheat Temperature, T.C. No. 13 (Figure 1)

case were higher than those corresponding to injection at the inlet (see Table III-a). However, this did not prevent carbon formation.

These results indicate that olefin (in this case, propylene) addition to the reacting gas mixture in ATR can cause carbon formation, only after a "critical" amount of the olefin has been reached. The important finding of this study is that this "critical" amount of propylene is higher if the injection is made at the reactor inlet rather than at a level 8 inches downstream of the inlet. In other words, higher amounts of propylene can be "tolerated" at the reactor inlet. This means that the relative competition of benzene and propylene for the available oxygen at the front end of the reactor does not produce a carbon formation situation. This was also observed for injection of propylene at other points upstream of the main oxygen depletion zone, which corresponds to the bed temperature peak region. The extent of propylene/benzene-oxygen reaction in this region is sufficient to convert an adequate amount of propylene and generate enough heat to steam reform the ensuing "carbon precursor" hydrocarbon species. The 8 inch injection level, on the other hand, located about 1 inch downstream of the temperature peak for these runs, is in the region where steam reforming, unaided by oxygen, takes place. A reduction in the overall value of the steam-to-carbon ratio at this level can be crucial for carbon formation (11).

Figure 8 shows axial dry gas hydrocarbon profiles for the conditions of tests CP-183, 189-1, and 188-3 corresponding to neat benzene, and benzene + 0.4 lb/hr propylene injected at the inlet and the 8 inch level of the bed, respectively. The propylene content of the mixtures at the 8 inch level was calculated by solving the mass balance equations, which were also used to calculate the

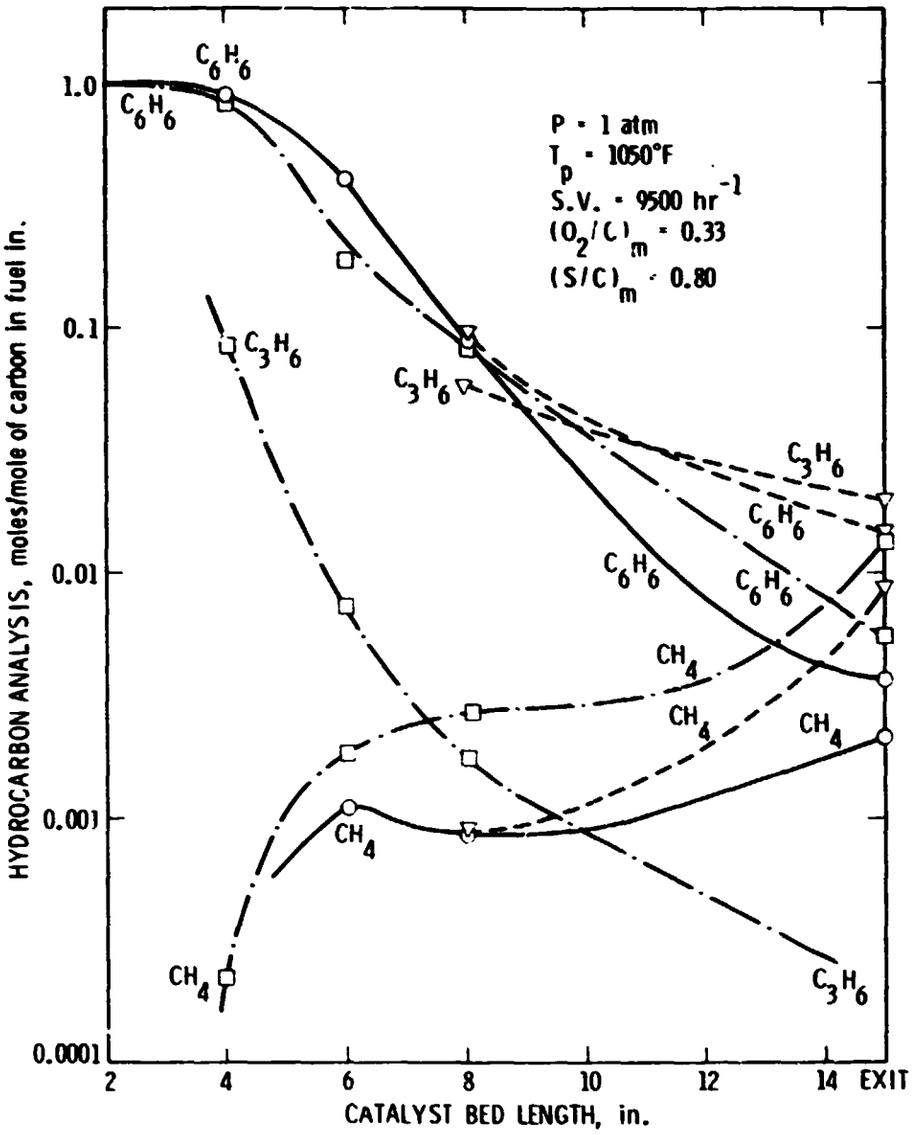

$(S/C)_m$ RATIOS AT THE 8" LEVEL				
TEST	$(S/C)_{m,B}$	$(S/C)_{m,D}$	$(S/C)_{m,M}$	$(S/C)_{m,T}$
○ CP-183	3.66	-	368	3.62
□ CP-189-1	2.64	132	85	2.50
▽ CP-188-3	3.66	5.41	368	2.17

Figure 8. Addition of Propylene to Benzene. Effect of injection location on axial bed hydrocarbon profiles.
——— ATR of C_6H_6 neat, test CP-183.
— . — ATR of C_6H_6 w/C_3H_6 (inlet injection), test CP-189-1.
— — — ATR of C_6H_6 w/C_3H_6 (8" level injection), test CP-188-3.

$(S/C)_{m,i}$ ratios (where i = Benzene (B), Propylene (P), Methane (M), or Total Hydrocarbons (T) at this level). The ordinate in Figure 8 gives moles of each species per carbon atom in the fuel at the inlet. The change of slope of the curves of Figure 8 (indicating rate changes) illustrates the effect of propylene addition on benzene conversion and carbon formation. With 0.4 lb/hr propylene injection at the inlet, the benzene conversion is somewhat inhibited, and methane goes up, while propylene disappears faster than benzene. As shown in the bottom of Figure 8, the overall $(S/C)_{m,T}$ ratio at the 8 inch level is 2.5 in this case, lower than the 3.6 value corresponding to the data for neat benzene. However, this ratio is still adequate to steam reform "carbon precursors" that might result from either propylene or benzene, and no carbon is detected either at this level or at the bed exit. With 0.4 lb/hr propylene injection at the 8 inch level, however, the amount of unconverted benzene at the exit is further increased, the rate of propylene conversion is low, and the methane content of the exhaust gases is lower than that required for complete carbon balance. Carbon detected in this case had been formed presumably in the part of the bed downstream of the 8 inch level. The overall $(S/C)_{m,T}$ ratio at this level was calculated to be 2.2, a value not adequate to steam off the carbon formed.

In Figure 9, a comparison similar to that of Figure 8 is depicted for tests CP-183, 188-1, and 188-3 corresponding to neat benzene, and benzene plus 0.2 lb/hr and 0.4 lb/hr, respectively, of propylene. The propylene gas was injected at the 8 inch level in both CP-188-1 and 188-3. No carbon was observed in test CP-188-1 (0.2 lb/hr propylene addition). As can be seen from Figure 9, in the remaining 7 inches of the bed downstream of the injection point the rate of benzene conversion decreases, and the rate of methane formation increases,

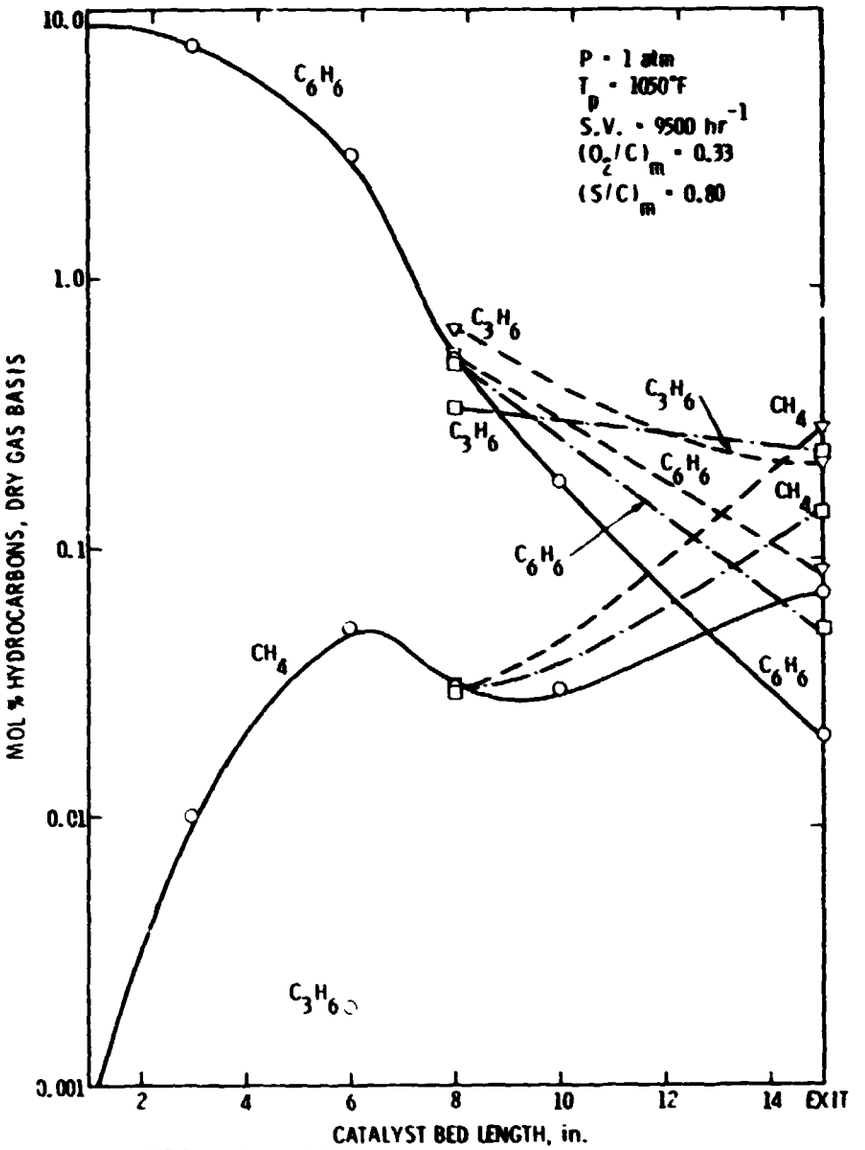

$(S/C)_m$ RATIOS AT THE 8" LEVEL				
TEST	$(S/C)_{m,B}$	$(S/C)_{m,P}$	$(S/C)_{m,M}$	$(S/C)_{m,T}$
○ CP-183	3.66	-	368	3.62
□ CP-188-1	3.66	10.82	368	2.72
▽ CP-188-3	3.66	5.41	368	2.17

Figure 9. Addition of Propylene to Benzene. Effect of propylene flowrate on axial bed hydrocarbon profiles.

——— ATR of C_6H_6 neat, test CP-183.

— · — ATR of C_6H_6 w/C_3H_6 (0.2 lb/hr), 8" level injection, test CP-188-1.

— — — ATR of C_6H_6 w/C_3H_6 (0.4 lb/hr), 8" level injection, test CP-188-3.

while propylene itself disappears very slowly. The overall $(S/C)_{m,T}$ ratio at the 8 inch level was calculated to be 2.7, as shown in the bottom of Figure 9. This $(S/C)_{m,T}$ value appears to be high enough to steam reform any carbon formed from either propylene or benzene. However, the $(S/C)_{m,T}$ ratio at the 8 inch level was 2.2 for the case of 0.4 lb/hr propylene injection, which was carbon-forming. As discussed above, this $(S/C)_{m,T}$ value must be lower than the "critical" one for carbon-free operation at these conditions.

While this data does not produce information about the mechanism of carbon formation in the bed, it definitely shows that the steam reforming region of the bed is the most prone to carbon formation. In support of this is the above presented evidence that a reduced $(S/C)_m$ ratio at the ATR inlet, created here by olefin addition, has less effect on carbon formation than a similar $(S/C)_m$ reduction in the steam reforming part of the bed. Scanning electron microscope (SEM) examinations of catalyst samples used under carbon-forming conditions with pure benzene or n-tetradecane fuels also support this. As discussed in the previous section, surface carbon growths (mainly in the form of whiskers) were found on catalyst samples taken from the steam reforming region of the reformer, while no surface carbon was found on the NC-100 or the top ICI catalysts, where oxygen is present.

(C) ATR Of Mixtures Of Benzene And n-Tetradecane

Concluding the experimental studies of the autothermal reforming of sulfur-free hydrocarbon liquids, a series of tests with mixtures of paraffins and aromatics were run in the reformer. The purpose was to determine what effects aromatic and paraffinic hydrocarbon combinations have on catalyst bed temperatures, intermediate reaction products, and carbon formation, as compared to the pure component hydrocarbon data.

Mixtures of benzene and n-tetradecane were used because of the previous tests on them, individually, and the ease of following the hydrocarbon intermediates. Two mixtures were prepared in which the molar ratio of n-tetradecane to benzene, $(T/B)_m$, was set equal to 2.0 and 0.5, respectively. Tests were run at similar operating conditions as earlier tests with each of the component fuels. Fresh catalysts were loaded in the reformer prior to the first test of this series. In the middle catalyst zone, the ICI 46-1 catalyst was used to better control carbon formation. Tests CP-212 through 216 were run with the $(T/B)_m$ = 2.0 mixture, while in tests CP-217 through 221, the $(T/B)_m$ = 0.5 mixture was used. Table IV shows the operating conditions and summarizes the results from these tests. Corresponding axial bed temperatures are shown in Table IV-a.

Carbon-forming conditions for each mixture tested were determined and compared to those for the pure component hydrocarbons. These are depicted in Figure 10, in which the carbon formation lines determined for the mixtures are plotted along with carbon lines for neat benzene and n-tetradecane (see Figures 2 and 3). Similar inlet conditions, and the same catalyst types were used with all

TABLE IV

AUTOTHERMAL REFORMING OF MIXTURES
OF BENZENE AND N-TETRADECANE

TEST CP -	FUEL	$(O_2/C)_m$	$(S/C)_m$	(1) T_P °F	(2) MAX. BED TEMPERATURE T_{MAX} °F	AT IN.	(3) $\dot{m}_f$ LB/HR	(4) S.V. HR^{-1}	CARBON	(5) GAS PROBE AT INCHES	DRY GAS COMPOSITION, MOL % H_2	CO_2	CO	HC_T	CH_4	C_2H_4	C_2H_6	C_3H_6	C_3H_8	C_4	C_5	C_6	C_6H_6
212	$(T/B)_m$ = 2.0	0.38	0.6	1050	1798	6.3	7.0	9941	NO	4	8.50	5.63	13.50	8.16*	1.43	3.78	0.30	0.91	0.02	0.60	0.18	0.10	0.84
		"	"	1052	1789	6.3	"	"	"	6	24.73	5.86	20.47	4.44*	1.72	1.88	0.18	0.21	0.02	0.06	0.01	-	0.36
		"	"	1048	1777	6.3	"	"	"	8	32.73	4.30	23.52	1.70	1.02	0.42	0.09	0.06	-	0.01	-	-	0.10
		"	"	1049	1776	6.3	"	"	"	10	33.50	4.24	23.57	1.55	1.01	0.30	0.09	0.06	-	0.01	-	-	0.08
		"	"	1050	1805	6.3	"	"	"	EXIT	34.92	3.81	24.01	0.52	0.44	0.04	0.02	0.01	-	-	-	-	0.01
213	$(T/B)_m$ = 2.0	0.31	1.2	1146	1593	6.3	6.0	9549	NO	4	9.76	5.15	11.75	6.53*	0.94	2.60	0.21	0.79	0.01	0.51	0.23	0.20	1.04
		"	"	1154	1603	6.3	"	"	"	6	23.57	8.75	14.20	6.13*	1.39	2.56	0.26	0.77	0.01	0.39	0.09	0.05	0.61
		"	"	1150	1596	6.3	"	"	"	8	36.89	8.34	19.41	2.27	0.98	0.66	0.15	0.22	-	0.06	0.01	0.01	0.18
		"	"	1145	1593	6.3	"	"	"	10	37.14	8.86	18.96	2.53	1.08	0.73	0.17	0.26	-	0.07	0.02	0.01	0.19
		"	"	1150	1587	6.3	"	"	"	12	39.16	8.20	19.92	1.67	0.93	0.34	0.14	0.13	-	0.01	0.01	0.01	0.10
		"	"	1148	1612	6.3	"	"	"	EXIT	39.28	8.47	19.77	1.30	0.87	0.19	0.08	0.07	-	0.02	0.01	-	0.06
214	$(T/B)_m$ = 2.0	0.38	0.4	1055	1897	6.0	7.8	10183	YES	4	20.17	5.02	20.19	4.13*	1.41	1.77	0.19	0.30	0.01	0.10	0.02	-	0.33
		"	"	1051	1890	6.0	"	"	"	6	27.82	3.03	24.29	2.69*	1.24	0.64	0.09	0.57	-	0.01	-	-	0.14
		"	"	1058	1896	6.0	"	"	"	8	31.07	2.14	25.03	1.48	1.08	0.25	0.06	0.02	-	-	-	-	0.07
		"	"	1060	1901	6.0	"	"	"	EXIT	31.96	2.12	25.20	0.71	0.58	0.07	0.03	0.01	-	-	-	-	0.02
215	$(T/B)_m$ = 2.0	0.34	0.8	1048	1631	5.9	6.5	9456	NO	4	16.80	8.25	14.50	5.90*	1.06	2.43	0.23	0.76	0.01	0.46	0.16	0.10	0.69
		"	"	1055	1630	5.9	"	"	"	6	32.99	6.01	21.15	2.43*	0.95	0.73	0.15	0.25	-	0.09	0.02	0.02	0.22
		"	"	1045	1617	5.9	"	"	"	8	34.56	6.10	21.67	2.27	1.03	0.62	0.15	0.21	-	0.07	0.01	0.01	0.17
		"	"	1050	1613	5.9	"	"	"	10	36.70	5.52	22.45	1.56	0.91	0.28	0.13	0.11	-	0.03	0.01	-	0.09
		"	"	1052	1607	5.9	"	"	"	EXIT	37.51	5.90	22.18	1.11	0.83	0.09	0.09	0.05	-	0.01	-	-	0.04

TABLE IV (Cont'd)

TEST OP -	FUEL	$(O_2/C)_m$	$(S/C)_m$	(1) T_p °F	(2) MAX. BED TEMPERATURE T_{MAX} °F	AT IN.	(3) $\dot{m}_f$ LB/HR	(4) S.V. HR^{-1}	CARBON	(5) GAS PROBE AT INCHES	DRY GAS COMPOSITION, MOL % H_2	CO_2	CO	HC_T	CH_4	C_2H_4	C_2H_6	C_3H_6	C_3H_8	C_4	C_5	C_6	C_6H_6
216	$(T/B)_m$ = 2.0	0.29	1.5	1159	1525	6.0	5.5	9378	NO	INLET	0.06	0.37	0.54	2.36*	0.72	0.02	-	0.01	-	0.01	0.01	0.01	1.58
		"	"	1148	1531	6.0	"	"	"	4	8.50	4.63	10.13	4.97*	0.63	1.69	0.13	0.54	-	0.36	0.21	0.21	1.20
		"	"	1156	1531	6.0	"	"	"	6	30.63	9.09	15.71	4.00*	0.95	1.46	0.18	0.51	-	0.25	0.09	0.07	0.49
		"	"	1142	1528	6.0	"	"	"	8	35.05	9.38	16.24	3.01	0.95	0.97	0.16	0.36	-	0.15	0.05	0.04	0.33
		"	"	1153	1523	6.0	"	"	"	10	39.34	9.24	17.60	2.00	0.83	0.50	0.14	0.21	-	0.07	0.03	0.02	0.20
		"	"	1161	1528	6.0	"	"	"	12	40.54	9.26	18.13	1.61	0.77	0.34	0.12	0.15	-	0.04	0.02	0.02	0.15
		"	"	1158	1537	6.0	"	"	"	EXIT	41.12	9.81	17.51	1.29	0.74	0.20	0.11	0.09	-	0.03	0.01	0.01	0.10
217	$(T/B)_m$ = 0.5	0.38	0.6	1151	2011	5.8	6.5	9553	NO	4	23.90	4.34	22.78	2.93*	1.49	0.83	0.05	0.03	0.01	0.02	0.02	-	0.48
		"	"	1150	2017	5.8	"	"	"	6	29.22	3.76	24.43	1.46*	1.03	0.22	0.02	0.01	-	-	-	-	0.18
		"	"	1152	2014	5.8	"	"	"	8	30.38	3.59	24.84	1.01	0.83	0.08	0.01	-	-	-	-	-	0.09
		"	"	1152	2010	5.8	"	"	"	10	31.72	3.42	24.97	0.73	0.65	0.03	0.01	-	-	-	-	-	0.04
		"	"	1148	2005	5.8	"	"	"	EXIT	32.20	3.12	25.12	0.25	0.25	-	-	-	-	-	-	-	-
218	$(T/B)_m$ = 0.5	0.29	1.2	1148	1558	6.0	6.0	9520	YES	4	14.40	8.00	14.10	6.28*	0.78	1.97	0.16	0.61	0.01	0.37	0.14	0.11	2.13
		"	"	1152	1571	6.0	"	"	"	6	33.49	9.11	18.67	2.55*	0.66	0.69	0.11	0.24	-	0.09	0.03	0.02	0.71
		"	"	1152	1560	6.0	"	"	"	8	38.21	8.84	20.13	1.77	0.66	0.37	0.10	0.14	-	0.04	0.01	0.01	0.44
		"	"	1150	1557	6.0	"	"	"	10	39.82	8.62	21.13	1.23	0.60	0.17	0.09	0.08	-	0.02	0.01	0.01	0.24
		"	"	1153	1555	6.0	"	"	"	EXIT	39.95	8.74	19.97	1.04	0.58	0.12	0.07	0.05	-	0.02	0.01	0.01	0.18
219	$(T/B)_m$ = 0.5	0.36	0.7	1148	1854	5.8	6.5	9554	NO	4	20.80	5.15	21.44	3.95*	1.20	1.40	0.13	0.18	0.02	0.07	0.02	-	0.93
		"	"	1146	1874	5.8	"	"	"	6	29.61	4.87	23.66	1.93*	1.12	0.35	0.05	0.02	-	0.01	0.01	-	0.33
		"	"	1144	1870	5.8	"	"	"	8	32.62	4.22	24.42	1.04	0.77	0.11	0.03	0.01	-	-	-	-	0.12
		"	"	1150	1872	5.8	"	"	"	10	33.23	4.35	24.37	0.83	0.71	0.04	0.02	-	-	-	-	-	0.06
		"	"	1150	1851	5.8	"	"	"	EXIT	33.59	4.06	27.70	0.45	0.39	0.02	0.01	-	-	-	-	-	0.03

TABLE IV (Cont'd)

TEST OP -	FUEL	$(O_2/C)_m$	$(S/C)_m$	(1) T_P °F	(2) MAX. BED TEMPERATURE T_{MAX} °F	AT IN.	(3) $\dot{m}_f$ LB/HR	(4) S.V. HR^{-1}	CARBON	(5) GAS PROBE AT INCHES	DRY GAS COMPOSITION, MOL % H_2	CO_2	CO	HC_T	CH_4	C_2H_4	C_2H_6	C_3H_6	C_3H_8	C_4	C_5	C_6	C_6H_6
220	$(T/B)_m$ = 0.5	0.40	0.6	1051	1953	6.5	6.25	9553	NO	4	15.15	5.65	19.13	4.56*	1.18	1.69	0.16	0.26	0.01	0.10	0.03	-	1.13
		"	"	1046	1987	6.5	"	"	"	EXIT	31.48	3.42	24.55	0.31*	0.28	0.01	0.01	-	-	-	-	-	0.01
		0.40	0.5	1062	2007	6.0	6.25	9190	NO	4	23.44	3.93	23.19	2.76*	1.54	0.70	0.05	0.02	0.01	0.02	0.02	-	0.40
		"	"	1052	2001	6.0	"	"	"	6	27.84	3.40	24.56	1.76*	1.20	0.28	0.03	0.01	-	0.01	0.01	-	0.22
		"	"	1051	1998	6.0	"	"	"	8	29.77	3.11	25.09	1.03	0.83	0.08	0.02	-	-	-	-	-	0.10
		"	"	1057	1997	6.0	"	"	"	EXIT	30.69	2.83	25.16	0.34	0.29	0.01	0.01	-	-	-	-	-	0.03
221	$(T/B)_m$ = 0.5	0.34	0.6	1145	1855	5.6	7.0	9473	YES	4	23.07	5.21	21.98	4.54*	1.47	1.59	0.14	0.18	0.02	0.07	0.02	-	1.05
		"	"	1151	1861	5.6	"	"	"	EXIT	34.86	3.82	25.20	0.83*	0.74	0.02	0.03	0.01	-	-	-	-	0.03
		0.34	0.4	1150	1889	5.0	7.0	8654	YES	4	20.25	3.59	23.60	5.26*	1.79	2.01	0.10	0.10	0.03	0.05	0.03	-	1.15
		"	"	1160	1885	5.0	"	"	"	6	29.18	2.25	25.61	2.85	1.32	0.86	0.10	0.10	0.01	0.03	0.01	-	0.62
		"	"	1149	1887	5.0	"	"	"	8	31.33	1.10	26.88	1.59	1.08	0.21	0.06	0.03	-	-	-	-	0.21
		"	"	1148	1877	5.0	"	"	"	EXIT	32.60	1.94	26.66	1.12	0.94	0.06	0.03	0.01	-	-	-	-	0.08

(1) - (5) See Table III

* Gaseous hydrocarbons not including n-tetradecane

TABLE IV-a

AUTOTHERMAL REFORMING OF MIXTURES OF BENZENE AND N-TETRADECANE

Longitudinal Bed Temperatures

TEST CP -	$(O_2/C)_m$	$(S/C)_m$	(1) T_p °F	S.V. hr^{-1}	BED TEMPERATURE, °F At (in. from Reactor Inlet)													
					0.5	3	4	5	6	7	8	9	10	11	12	13	14	15
212	0.38	0.6	1050	9941	1145	1350	1451	1690	1792	1802	1751	1697	1680	1682	1594	1536	1502	1467
213	0.31	1.2	1150	9549	1200	1320	1418	1540	1602	1611	1571	1523	1493	1502	1425	1365	1331	1308
214	0.38	0.4	1055	10183	1200	1450	1520	1809	1901	1879	1841	1820	1817	1792	1711	1675	1640	1612
215	0.34	0.8	1055	9456	1120	1275	1400	1597	1629	1587	1541	1524	1530	1466	1396	1363	1328	1314
216	0.29	1.5	1155	9378	1190	1250	1329	1491	1537	1515	1466	1442	1453	1421	1339	1276	1241	1214
217	0.38	0.6	1150	9553	1275	1560	1635	1958	2015	1949	1868	1832	1819	1790	1734	1700	1676	1665
218	0.29	1.2	1152	9520	1196	1250	1325	1488	1575	1533	1472	1456	1469	1461	1409	1351	1301	1275
219	0.36	0.7	1150	9554	1255	1410	1460	1762	1848	1785	1699	1670	1668	1661	1629	1596	1562	1539
220-1	0.40	0.6	1050	9553	1134	1350	1392	1770	1965	1915	1814	1779	1770	1771	1747	1709	1674	1650
220-3	0.40	0.5	1055	9190	1175	1530	1680	1886	2003	1909	1798	1768	1748	1714	1681	1676	1659	1635
221-1	0.34	0.6	1150	9473	1350	1540	1589	1828	1852	1741	1644	1576	1513	1469	1434	1401	1385	1380
221-4	0.34	0.4	1150	8654	1375	1650	1703	1889	1812	1675	1587	1515	1466	1449	1413	1392	1383	1379

(1) Preheat Temperature, T.C. No. 13 (Figure 1)

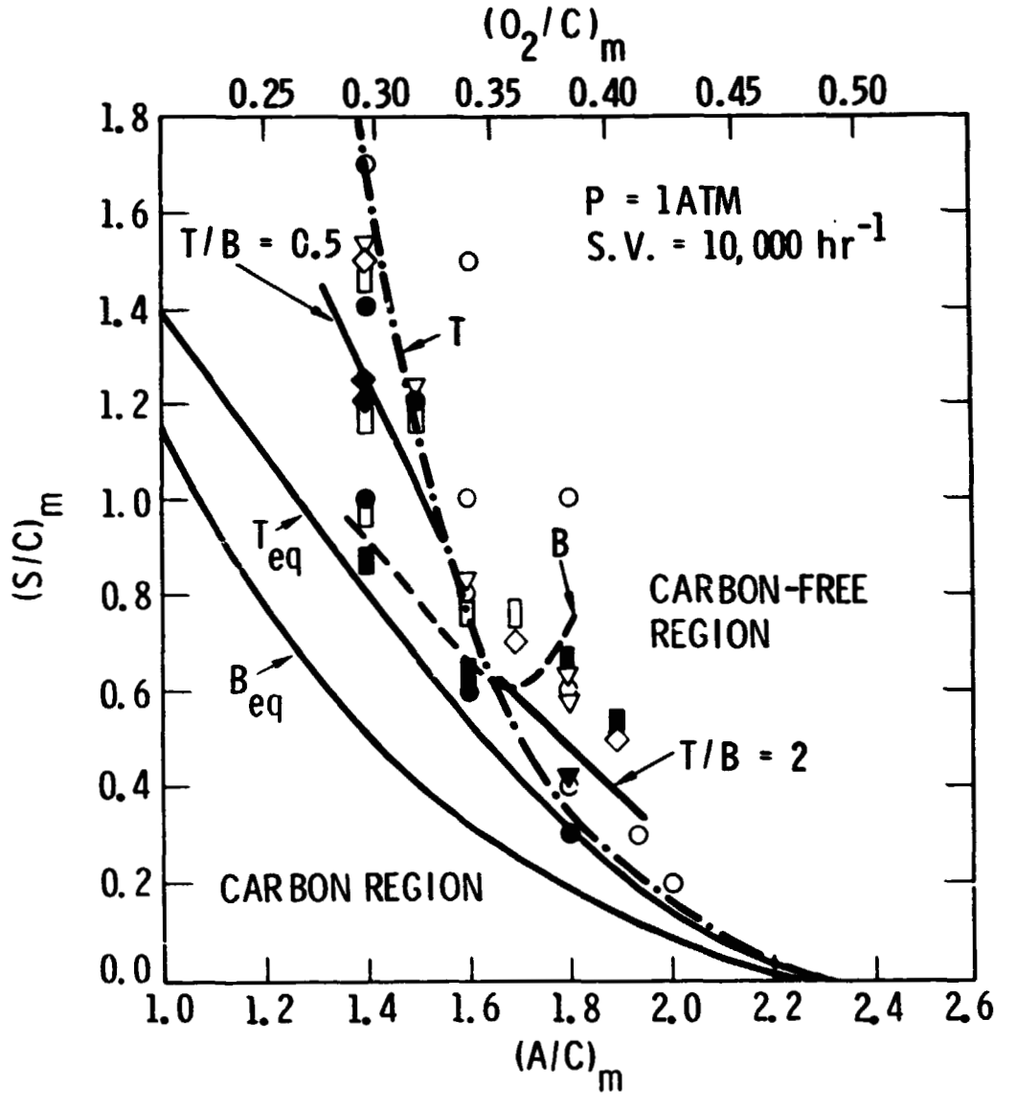

Figure 10. Autothermal Reforming of n-Tetradecane/Benzene Mixtures. Carbon Formation Lines.
○ ●: n-Tetradecane ($C_{14}H_{30}$), neat
▽ ▼: Benzene solution ($C_{14}H_{30}/C_6H_6$ = 2, molar basis)
◇ ◆: Benzene solution ($C_{14}H_{30}/C_6H_6$ = 0.5, molar basis)
▯ ▮: Benzene (C_6H_6), neat
Open Symbols: Carbon-Free
Closed Symbols: Carbon Formation

fuels with the exception of neat benzene, which had been tested with ICI 46-4 catalyst in the middle ATR zone.

The plots in Figure 10 clearly demonstrate that a synergistic effect exists in mixtures of benzene/n-tetradecane, whereby the carbon-formation line of the mixture lies between those of the component hydrocarbons. In the case of the mixture $(T/B)_m$ = 2.0, the paraffinic character is prevailing; the carbon line diverges from equilibrium at low $(O_2/C)_m$ ratios, but not as much as the line for pure n-tetradecane. The reverse is true for the $(T/B)_m$ = 0.5 mixture, which has more of the aromatic character. This line diverges from equilibrium at high $(O_2/C)_m$ ratios, but not as pronouncedly as the pure benzene line.

To further understand the causes of the observed synergism in benzene/n-tetradecane mixtures, reaction bed products and temperatures during ATR of mixtures were compared to these for the pure hydrocarbon components. Tables V and V-a show dry gas analyses and temperatures, respectively, from tests run at similar operating conditions with the mixtures and each pure hydrocarbon component. These data comparisons have revealed the following:

(a) Bed temperatures for the mixtures were intermediate, i.e., they were lower than respective temperatures for neat benzene and higher than those for neat n-tetradecane.

(b) The presence of benzene in the benzene/n-tetradecane mixtures appeared to limit the amount of intermediate hydrocarbons (primarily low molecular weight olefins) produced by cracking of n-tetradecane. As a result of

this, carbon formation was suppressed at low $(O_2/C)_m$ ratios where the deviation of the experimental from the theoretical carbon formation line was the largest for pure n-tetradecane (see Figure 2). The fact that the benzene/n-tetradecane mixtures had lower propensity for carbon formation than pure n-tetradecane at low $(O_2/C)_m$ ratios may be explained by the higher bed temperatures during ATR of the mixtures. The rate of carbon removal by steam reforming may exceed the rate of carbon formation (via paraffin cracking) at these temperatures, resulting in no carbon deposition in the bed.

(c) The presence of n-tetradecane in the benzene/n-tetradecane mixtures appeared to control carbon formation from benzene at high $(O_2/C)_m$ ratios, where the deviation of the experimental from the theoretical carbon formation line was the largest for pure benzene (see Figure 3). This can be explained by the lower bed temperatures during ATR of the mixtures, which were caused by the endothermic cracking reactions of n-tetradecane. The rate of carbon formation via dehydrogenation of the benzene molecule would then be decreased because of lower temperatures. However, these temperatures are still high enough for steam reforming, so that the overall effect for paraffinic/aromatic mixtures in ATR is a carbon removal rate that is faster than in the case of the pure aromatic fuel at high $(O_2/C)_m$ ratios.

TABLE V

ATR COMPARISON OF BENZENE/N-TETRADECANE MIXTURES AND
THEIR PURE HYDROCARBON COMPONENTS

TEST CP -	FUEL	$(O_2/C)_m$	$(S/C)_n$	(1) T_P °F	(2) MAX. BED TEMPERATURE T_{MAX} °F	AT IN.	(3) $\dot{m}_f$ LB/HR	(4) S.V. HR^{-1}	CARBON	(5) GAS PROBE AT INCHES	DRY GAS COMPOSITION, MOL % H_2	CO_2	CO	HC_T	CH_4	C_2H_4	C_2H_6	C_3H_6	C_3H_8	C_4	C_5	C_6	C_6H_6
136	n-Tetradecane	0.38	0.6	1006	1742	5.0	7.19	10,000	NO	4	7.33	6.93	6.40	9.04*	1.62	4.57	0.26	1.31	0.01	0.78	0.29	-	0.20
		"	"	1005	1744	5.0	"	"	"	6	28.11	6.21	17.11	4.43*	1.89	1.75	0.17	0.36	-	0.11	0.14	-	0.01
		"	"	1005	1746	5.0	"	"	"	8	32.49	4.82	20.17	2.30	1.50	0.50	0.12	0.11	-	0.02	0.03	-	0.01
		"	"	1017	1776	5.0	"	"	"	EXIT	35.40	4.48	21.13	1.08	0.87	0.03	0.06	0.01	0.01	-	0.04	-	0.01
212	$(T/B)_m = 2.0$	0.38	0.6	1050	1798	6.3	7.0	9941	NO	4	8.50	5.63	13.50	8.16*	1.43	3.78	0.30	0.91	0.02	0.60	0.18	0.10	0.84
		"	"	1052	1789	6.3	"	"	"	6	24.73	5.86	20.47	4.44*	1.72	1.88	0.18	0.21	0.02	0.06	0.01	-	0.36
		"	"	1048	1777	6.3	"	"	"	8	32.73	4.30	23.52	1.70	1.02	0.42	0.09	0.06	-	0.01	-	-	0.10
		"	"	1050	1805	6.3	"	"	"	EXIT	34.92	3.81	24.01	0.54	0.44	0.04	0.02	0.01	-	0.02	-	-	0.01
217	$(T/B)_m = 0.5$	0.38	0.6	1151	2011	5.8	6.5	9553	NO	4	23.90	4.34	22.78	2.93*	1.49	0.83	0.05	0.03	0.01	0.02	0.02	-	0.48
		"	"	1150	2017	5.8	"	"	"	6	29.22	3.76	24.43	1.46*	1.03	0.22	0.02	0.01	-	-	-	-	0.18
		"	"	1152	2014	5.8	"	"	"	8	20.38	3.59	24.84	1.01	0.83	0.08	0.01	-	-	-	-	-	0.09
		"	"	1145	2005	5.8	"	"	"	EXIT	32.20	3.12	25.12	0.25	0.25	-	-	-	-	-	-	-	-
71-1	Benzene	0.38	0.6	1050	2010	4.8	7.0	10,000	YES	EXIT	27.82	3.18	27.12	0.03	0.02	-	-	-	-	-	-	-	0.01

TABLE V (Cont'd)

TEST OP -	FUEL	$(O_2/C)_m$	$(S/C)_f$	(1) T_p °F	(2) MAX. BED TEMPERATURE T_{MAX} °F	AT IN.	(3) $\dot{m}_f$ LB/HR	(4) S.V. HR^{-1}	CARBON	(5) GAS PROBE AT INCHES	DRY GAS COMPOSITION, MOL % H_2	CO_2	CO	HC_T	CH_4	C_2H_4	C_2H_6	C_3H_6	C_3H_8	C_4	C_5	C_6	C_6H_6
129	n-Tetradecane	0.34	0.8	1127	1664	5.7	6.43	8960	NO	4	12.68	6.55	12.50	13.10*	3. .	6.84	0.43	1.45	0.03	0.87	0.37	0.02	0.04
		"	"	1132	1658	5.6	"	"	"	6	31.34	6.99	16.40	5.13*	2.26	1.74	0.22	0.46	0.03	0.19	0.06	0.11	0.06
		"	"	1136	1658	5.7	"	"	"	8	35.12	6.18	18.90	3.45	1.95	0.72	0.21	0.27	0.01	0.13	0.15	-	0.01
		"	"	1136	1663	5.6	"	"	"	EXIT	37.36	6.45	18.96	1.71	1.40	0.11	0.10	0.04	0.01	0.04	0.01	-	-
215	(T/B) = 2.0	0.34	0.8	1048	1631	5.9	6.5	9456	NO	4	16.80	8.25	14.50	5.40*	1.06	2.43	0.23	0.76	0.01	0.46	0.16	0.10	0.69
		"	"	1055	1630	5.9	"	"	"	6	32.99	6.01	21.15	2.43*	0.95	0.73	0.15	0.25	-	0.09	0.02	0.02	0.22
		"	"	1045	1617	5.9	"	"	"	8	34.56	6.10	21.67	2.27	1.03	0.62	0.15	0.21	-	0.07	0.01	0.01	0.17
		"	"	1050	1613	5.9	"	"	"	10	36.70	5.52	22.45	1.56	0.91	0.28	0.13	0.11	-	0.03	0.01	-	0.09
		"	"	1052	1607	5.9	"	"	"	EXIT	37.51	5.90	22.18	1.11	0.83	0.09	0.09	0.05	-	0.01	-	-	0.04
203	Benzene	0.34	0.8	1050	1811	6.0	6.0	9300	NO	4	2.73	2.80	7.58	7.49	0.09	0.24	-	0.01	0.02	0.06	0.07	0.01	6.99
		"	"	1048	1807	6.0	"	"	"	6	26.35	6.62	22.93	1.01	0.08	0.02	-	-	-	0.01	0.02	-	0.88
		"	"	1043	1813	6.0	"	"	"	EXIT	30.06	5.31	24.40	0.04	0.03	-	-	-	-	-	-	-	0.01

(1) - (5) See Table III

* Gaseous hydrocarbons not including n-tetradecane

TABLE V-a

COMPARISON OF ATR TEMPERATURES OBTAINED WITH BENZENE/N-TETRADECANE MIXTURES AND THEIR PURE HYDROCARBON COMPONENTS

TEST CP -	$(O_2/C)_m$	$(S/C)_m$	(1) T_p °F	S.V. hr^{-1}	BED TEMPERATURE, °F At (in. from Reactor Inlet)													
					0.5	3	4	5	6	7	8	9	10	11	12	13	14	15
136	0.38	0.6	1020	10000	1180	1420	1600	1746	1678	1606	1553	1519	1476	1438	1421	1404	1390	1376
212	0.38	0.6	1050	9940	1145	1350	1451	1690	1792	1802	1751	1697	1680	1682	1594	1536	1502	1467
217	0.38	0.6	1150	9553	1275	1560	1635	1958	2015	1949	1868	1832	1819	1790	1734	1700	1676	1665
71	0.38	0.6	1033	11000	1200	1875	1900	1986	1925	1968	1825	1716	1743	1719	1718	1723	1723	1713
129	0.34	0.8	1130	8950	1155	1400	1511	1634	1657	1599	1545	1489	1458	1407	1365	1334	1304	1275
215	0.34	0.8	1050	9456	1120	1275	1400	1597	1629	1587	1541	1524	1530	1466	1396	1363	1328	1314
203	0.34	0.8	1054	9269	1041	1343	1310	1661	1813	1774	1730	1667	1615	1570	1528	1516	1509	1498

(1) Preheat Temperature, T.C. No. 13 (Figure 1)

(D) ATR Of Sulfur-Containing Paraffins And Aromatics

In an effort to delineate the previously observed (6) conversion characteristics and carbon-forming limitations of No. 2 fuel oil in ATR, experimental work up to this point has focused on identifying the behavior of individual fuel components in the autothermal reformer. Differences in the ATR reactivity of sulfur-free paraffins and aromatics have been found, and the effects of the operating parameters on reaction intermediates, bed temperatures, and carbon formation have been determined.

An overall picture of the carbon formation lines for the various sulfur-free hydrocarbons used under similar conditions in the autothermal reformer is shown in Figure 11. The effects of chemical character, and molecular weight (or boiling point) on carbon formation in ATR can be seen from this figure. Experimental data from the ATR of No. 2 fuel oil (6) are also shown in Figure 11. This data cannot be used for a quantitative comparison of the fuel oil and pure hydrocarbon requirements for carbon-free operation (since a different catalyst (6) had been used in the low preheat (~1150°F) tests with No. 2 fuel oil). However, from a qualitative comparison of the shape and location of these curves, it appears that the chemical character (e.g., aromatic content) and the boiling point effects are not enough to explain the extremely pronounced propensity of fuel oil for carbon formation in ATR.

The No. 2 fuel oil used in the earlier JPL work (6) consisted of a mixture of paraffins (71% vol.), aromatics (22% vol.), and olefins (7% vol.). The sulfur content of that oil was 0.35% wt. As discussed in the previous section, mixtures of paraffins and aromatics exhibit a synergism with respect to carbon

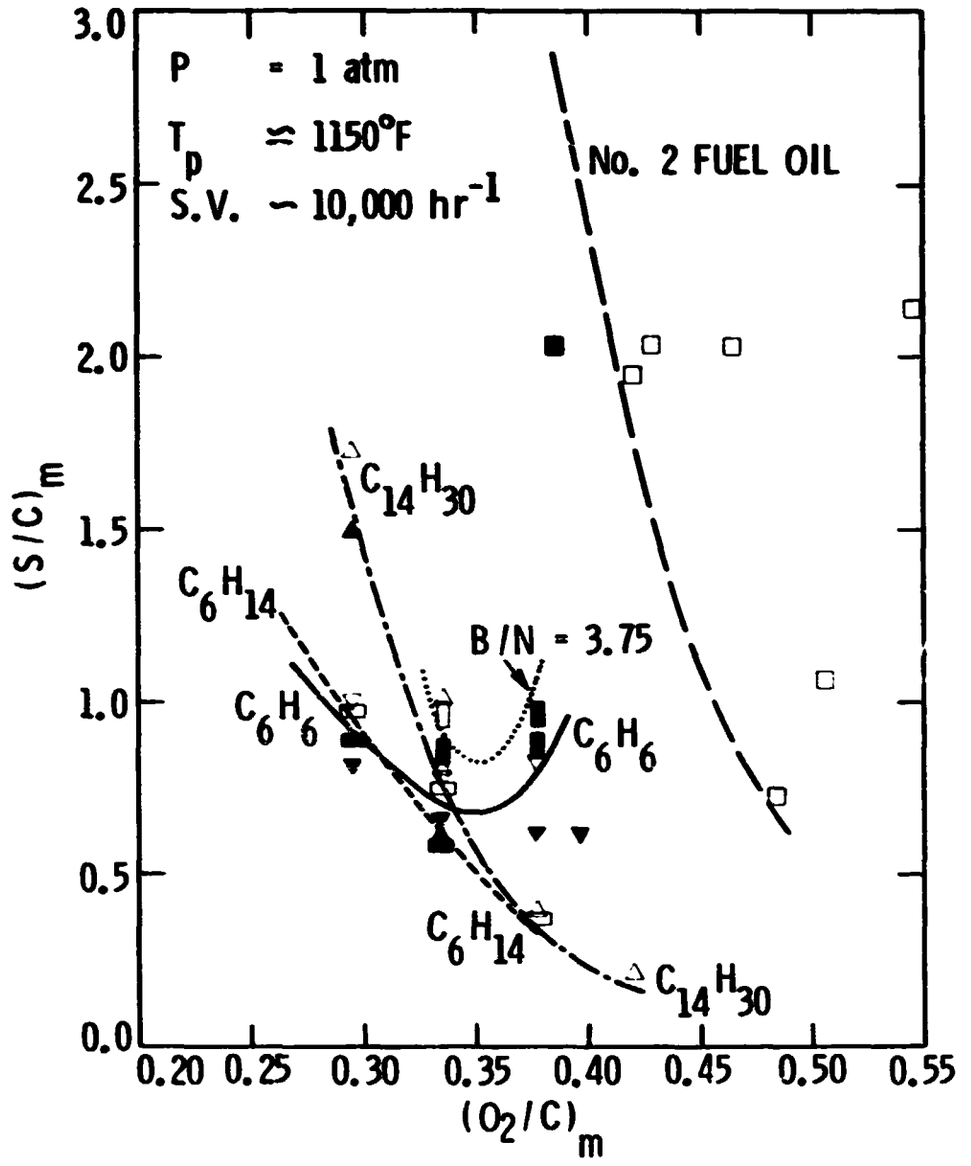

Figure 11. ATR of Various Hydrocarbon Liquids.
Experimental Carbon Formation Lines.
□ ■ : No. 2 Fuel Oil, Catalyst Configuration A (Ref. 6).
▽ ▼ : Benzene (C_6H_6)
▯ ▮ : Benzene/Naphthalene, $(B/N)_m$ = 3.75 } Catalyst Configuration B (Fig. 1)
▭ ▬ : n-Hexane (C_6H_{14})
△ ▲ : n-Tetradecane ($C_{14}H_{30}$)
Open Symbols: Carbon-Free
Closed Symbols: Carbon Formation

formation in ATR. Hence, the steam requirements for carbon-free operation with No. 2 fuel oil should be lower than those corresponding to its heaviest aromatic components (at high O_2/C ratios) or its heaviest paraffinic components (at low O_2/C ratios). Obviously, what remains unanswered at this point is the relative importance of the sulfur content of fuels with respect to carbon formation in ATR. In the following, results from preliminary tests with thiophene-contaminated n-tetradecane and benzene are presented. This work was undertaken in order to study the conversion and degradation effects of fuel sulfur on the catalyst. It has been found that No. 2 fuel oil can contain up to 90% thiophenic sulfur compounds (15). Thus, thiophene is a good model sulfur compound for heavy distillate fuels.

ATR of Thiophene-containing n-Tetradecane

The effect of sulfur in the ATR characteristics of paraffins was examined first by using n-tetradecane contaminated with thiophene, 2000 ppmw (by weight). This amount of thiophene is equivalent to 762 ppmw sulfur. Tests with this mixture were run at similar conditions as earlier ones for n-tetradecane alone. These tests were performed to determine what effect the conversion of sulfur compounds would have on the autothermal reformer temperatures, catalyst activity, intermediate reaction products, and carbon-forming tendency.

Table VI summarizes the experimental data collected from tests with the n-tetradecane/thiophene mixture at three sets of operating conditions, which were carbon-free for pure n-tetradecane (11). A fresh catalyst bed was loaded in the reactor prior to test CP-222, and again prior to test CP-229. As in tests with neat n-tetradecane, the ICI catalyst used in the second catalyst zone was of the 46-1 type, which contains potassium oxide as a soot-suppres-

TABLE VI

ATR PERFORMANCE COMPARISON OF THIOPHENE-CONTAINING
N-TETRADECANE AND PURE N-TETRADECANE

TEST OP -	FUEL	$(O_2/C)_m$	$(S/C)_m$	(1) T_p °F	(2) MAX. BED TEMPERATURE T_{MAX} °F	AT IN.	(3) $\dot{m}_f$ LB/HR	(4) S.V. HR^{-1}	CARBON	(5) GAS PROBE AT INCHES	DRY GAS COMPOSITION, MOL % H_2	CO_2	CO	HC_T	CH_4	C_2H_4	C_2H_6	C_3H_6	C_3H_8	C_4	C_5	C_6	C_6H_6
160	n-Tetradecane	0.36	0.6	1038	1719	5.3	7.50	10,000	NO	INLET	0.24	0.56	0.48	43.72	4.28	21.13	0.51	17.16	0.14	0.15	0.15	0.16	0.04
	"	"	"	1037	1707	"	"	"	"	4	7.87	8.52	11.59	10.01	2.00	4.75	0.32	1.31	0.02	0.98	0.37	0.26	0.09
	"	"	"	1040	1713	"	"	"	"	6	28.08	5.09	17.82	5.30	2.00	2.17	0.23	0.55	0.01	0.22	0.06	0.06	0.05
	"	"	"	1034	1725	"	"	"	"	EXIT	35.57	4.74	20.80	1.71	1.27	0.21	0.12	0.07	-	0.02	-	0.20	0.01
234	n-Tetradecane w/Thiophene	0.38	0.4	1102	2007	7.0	7.20	9208	NO	4	4.50	3.70	12.50	20.83	3.95	13.40	0.23	1.59	0.13	1.01	0.20	0.13	0.13
	"	"	"	1131	2002	"	"	"	"	6	20.25	3.40	21.00	10.95	4.89	5.66	-	0.13	0.05	0.08	0.01	-	0.13
	"	"	"	1124	1990	"	"	"	"	8	26.30	3.58	22.03	7.84	4.11	3.46	0.09	0.04	0.01	0.04	-	-	0.09
235	"	0.38	0.4	1130	2030	6.7	7.20	9208	NO	4	6.02	4.86	14.50	18.44	4.75	11.66	0.15	0.96	0.13	0.56	0.08	-	0.16
	"	"	"	1141	2025	"	"	"	"	6	22.78	4.11	20.97	9.24	4.53	4.43	-	0.06	0.04	0.06	0.01	-	0.11
	"	"	"	1134	2027	"	"	"	"	8	27.34	3.66	22.34	7.16	3.86	2.56	0.60	0.01	0.01	0.03	0.01	-	0.08
	"	"	"	1099	1970	"	"	"	"	EXIT	31.56	2.47	24.14	2.20									
146	n-Tetradecane	0.38	0.3	1056	1892	4.7	8.2	10000	YES	4	9.60	5.65	11.63	14.00	4.09	7.92	0.49	1.20	0.05	0.02	0.11	0.02	0.09
	"	"	"	1051	1916	"	"	"	"	6	29.49	2.01	22.86	3.52	2.45	0.82	0.13	0.09	-	0.02	-	-	0.01
	"	"	"	1053	1922	"	"	"	"	8	31.96	1.17	24.33	2.30	1.97	0.20	0.09	0.03	-	-	-	-	0.01
	"	"	"	1056	1880	"	"	"	"	EXIT	32.76	0.99	25.20	1.66	1.56	0.03	0.06	0.01	-	-	-	-	-

TABLE VI (Cont'd)

TEST OP -	FUEL	$(O_2/C)_m$	$(S/C)_m$	(1) T_p °F	(2) MAX. BED TEMPERATURE T_{MAX} °F	AT IN.	(3) $\dot{m}_f$ LB/HR	(4) S.V. HR^{-1}	CARBON	(5) GAS PROBE AT INCHES	DRY GAS COMPOSITION, MOL % H_2	CO_2	CO	HC_T	CH_4	C_2H_4	C_2H_6	C_3H_6	C_3H_8	C_4	C_5	C_6	C_6H_6
222	n-Tetradecane w/Thiophene	0.38	0.6	1021	2000	8.0	7.20	10000	NO	EXIT	32.24	4.36	22.05	4.38	2.36	1.75	0.14	0.08	-	0.02	-	-	0.03
226	"	0.38	0.6	1011	1959	8.9	7.20	10000	NO	INLET	-	-	-	0.96	0.06	0.21	0.01	0.16	-	0.14	0.13	0.16	0.09
224	"	0.38	0.6	1048	1985	8.5	7.20	10000	NO	4	0.22	2.45	2.19	4.70	0.58	2.03	0.09	0.64	-	0.34	0.32	0.44	0.26
	"	"	"	1051	1970	"	"	"	"	6	0.27	2.76	7.13	18.55	2.70	9.75	0.21	2.39	0.04	1.83	0.63	0.68	0.32
	"	"	"	1037	1968	"	"	"	"	8	1.49	4.49	19.75	13.73	5.00	7.78	0.06	0.36	0.11	0.20	0.04	0.17	0.02
225	"	0.38	0.6	1048	1995	9.0	7.20	10000	NO	10	23.97	4.54	20.98	10.10	4.70	4.97	0.04	0.15	0.03	0.09	0.01	0.11	-
226	"	"	"	1080	1989	8.9	7.20	10000	NO	12	28.89	4.51	21.31	4.25	3.10	1.09	0.02	-	-	-	-	0.04	-
	"	"	"	1078	1968	"	"	"	"	14	29.97	4.63	21.64	4.34	3.12	1.16	0.02	-	-	-	-	0.04	-
	"	"	"	1078	1957	"	"	"	"	EXIT	31.89	4.11	22.86	3.62	2.86	0.65	0.07	0.01	-	-	-	0.03	-
136	n-Tetradecane	0.38	0.6	1006	1762	5.0	7.19	10000	NO	4	7.33	6.93	6.40	9.04	1.62	4.57	0.26	1.31	0.01	0.78	0.29	-	0.20
	"	"	"	1005	1744	"	"	"	"	6	28.11	6.21	17.11	4.43	1.89	1.75	0.17	0.36	-	0.11	0.14	-	0.01
	"	"	"	1005	1746	"	"	"	"	8	32.49	4.82	20.17	2.30	1.50	0.50	0.12	0.11	-	0.02	0.03	-	0.01
	"	"	"	1017	1776	"	"	"	"	EXIT	35.40	4.48	21.13	1.08	0.87	0.30	0.06	0.01	0.01	-	0.04	-	0.01
233	n-Tetradecane	0.36	0.6	1111	1910	8.8	7.52	10000	NO	4	0.05	2.02	3.13	10.18	1.21	5.00	0.27	1.40	0.18	1.02	0.50	0.53	0.07
	w/Thiophene	"	"	1114	1915	"	"	"	"	6	0.72	5.01	14.50	20.45	4.53	13.45	0.27	1.26	0.11	0.63	0.03	0.01	0.19
	"	"	"	1109	1904	"	"	"	"	8	1.54	4.00	17.50	8.28	3.31	4.45	0.18	0.16	-	0.07	-	0.01	0.10
231	n-Tetradecane	0.36	0.6	1118	1964	8.5	7.52	10000	NO	10	27.10	4.39	21.68										
	w/Thiophene	"	"	1119	1961	"	"	"	"	12	30.80	4.59	21.88										
	"	"	"	1116	1949	"	"	"	"	14	31.72	4.57	21.89										
229	"	0.36	0.6	1057	1964	8.0	7.52	10000	NO	EXIT	33.57	4.41	22.64	4.83	3.29	1.27	0.15	0.06	-	0.01	-	0.05	-

(1) - (5) See Table III

* Gaseous hydrocarbons not including n-tetradecane

sant. Data from tests with neat n-tetradecane run earlier (11) at the same conditions are also shown in Table VI for comparison. The following observations were made during this series of autothermal reforming tests:

(a) Temperatures with the mixture of n-tetradecane and thiophene were lower in the upper half of the bed and higher in the lower half of the bed than respective temperatures with neat n-tetradecane. The peak temperature with the mixture was recorded at least 3 inches below that for n-tetradecane, indicating that the activity of the front-end catalyst was lower in the presence of sulfur. The value of the maximum temperature was higher by about 200°F in the case of the mixture, probably because fresh catalyst was used in both tests. Figure 12 shows axial bed temperature profiles for n-tetradecane, neat and with thiophene at $(O_2/C)_m = 0.36$, $(S/C)_m = 0.60$. The profile for the mixture corresponds to test CP-223 in which the maximum temperature was recorded at 9 inches below the reactor inlet. However, the initial location of the temperature peak for these conditions was at 8 inches from the inlet (test CP-229) indicating that the catalyst in the oxidation zone was rapidly being poisoned during exposure to the sulfur-containing fuel.

(b) While no carbon formation was detected with the n-tetradecane/thiophene mixtures at the conditions of Table VI, the amounts of intermediate reaction products formed via cracking reactions were higher with the mixtures than with n-tetradecane. This was true throughout the length of the bed except at the front 4 to 5 inches from the bed inlet. Figure 13 depicts axial composition profiles corresponding to the temperature profiles of

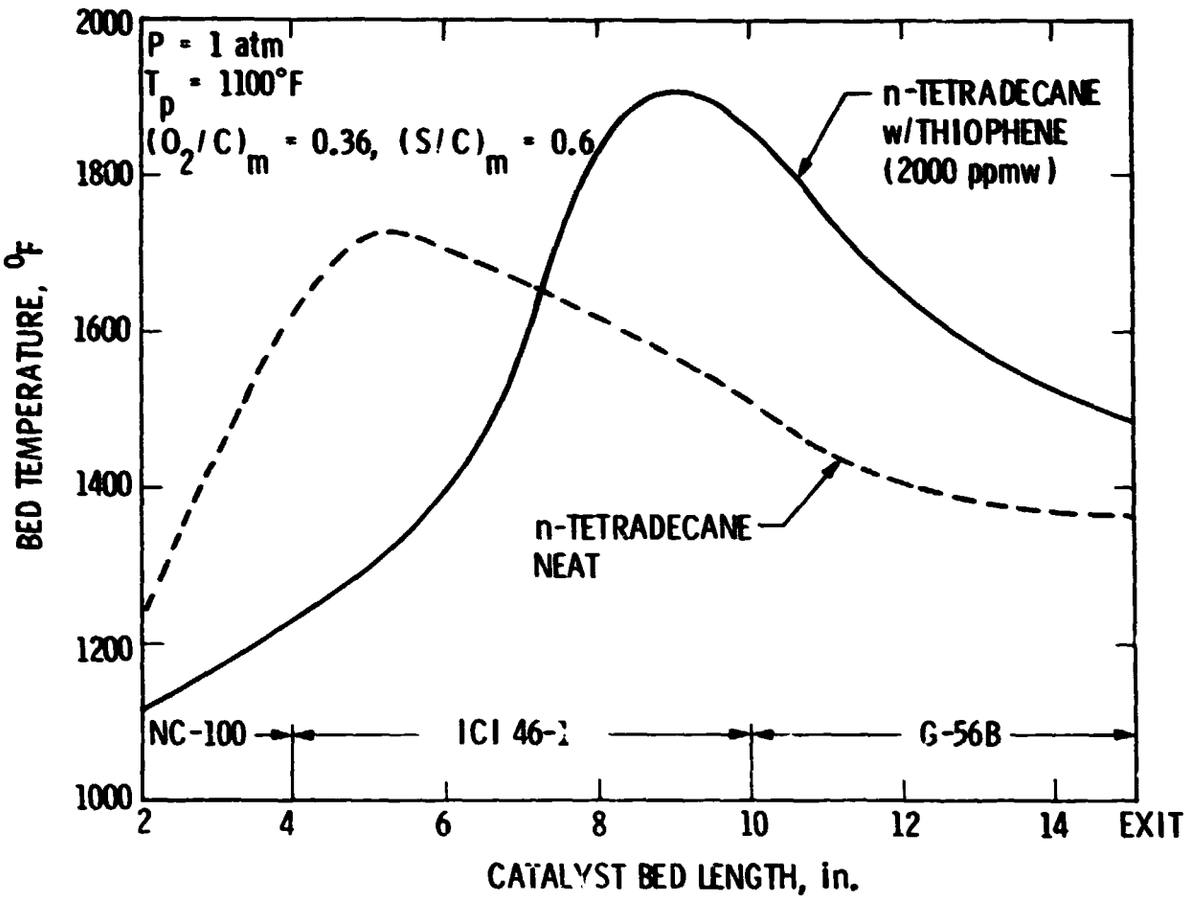

Figure 12. Autothermal Reforming of n-Tetradecane, neat with 2000 ppmw Thiophene.
Axial Bed Temperature Profiles.

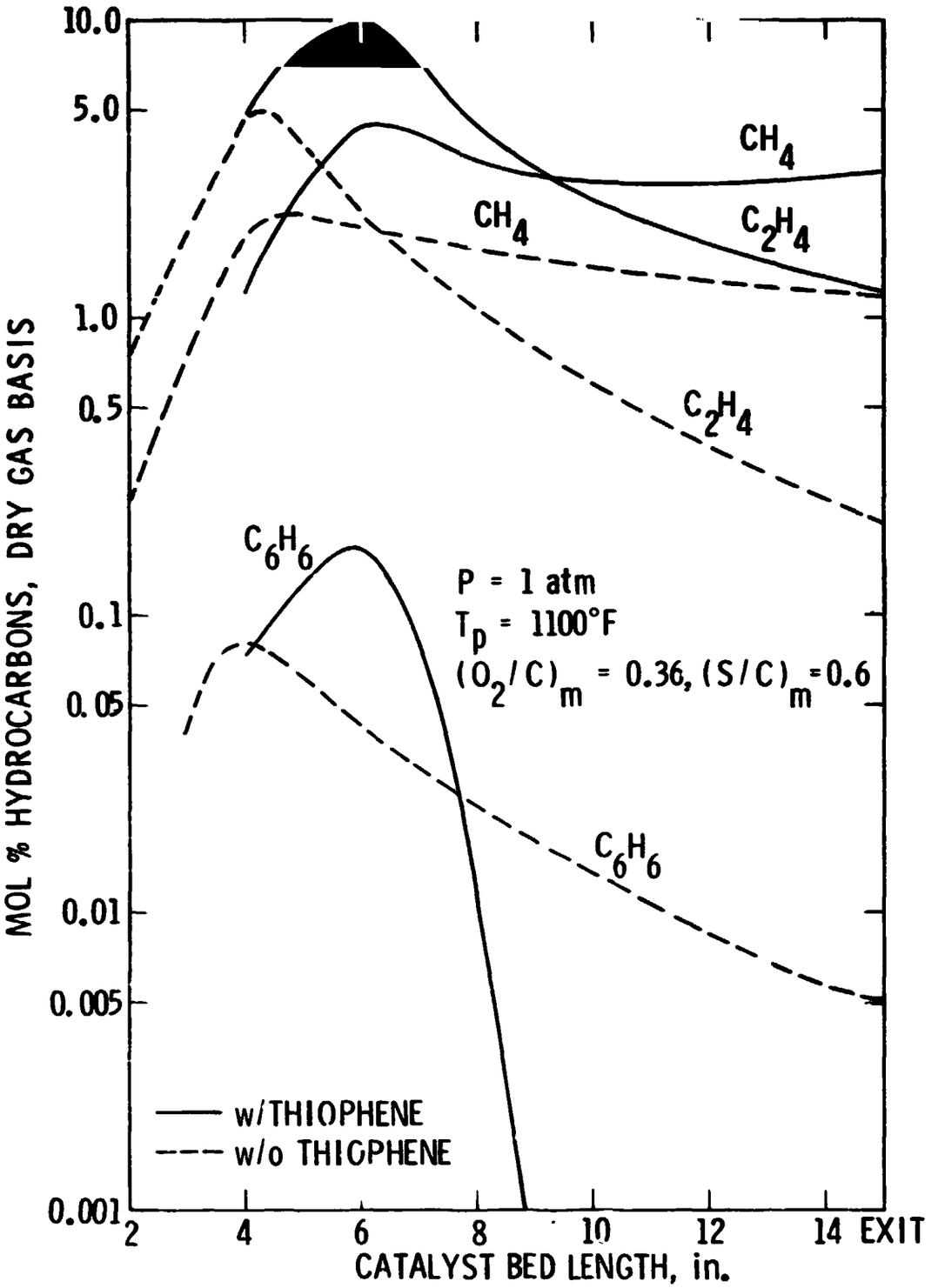

Figure 13. Autothermal Reforming of n-Tetradecane, neat and with 2000 ppmw Thiophene. Axial Bed Composition Profiles.

Figure 12. In both cases, i.e., n-tetradecane and the n-tetradecane/ thiophene mixture, the intermediate hydrocarbons peaked just upstream of the respective temperature peak. However, the concentrations of ethylene, methane, benzene etc., were much higher or the mixture. In addition, the methane conversion in the steam reforming region of the bed was limited, and a higher methane leakage was measured at the bed exit when the mixture was used in ATR.

(c) Along with hydrocarbon analysis, gas samples from different levels of the catalyst bed were analyzed for sulfur compounds by G.C. (FPD). In the partial oxidation region of the bed, uncoverted thiophene was the only sulfur-containing species found in the gas phase. However, the amount of thiophene detected in this region was lower than at the reactor inlet, indicating that sulfur had reacted with the catalyst/support and formed a stable compound on the solid surface. Around the location of the temperature peak, and further down the bed (in the steam reforming region), a higher rate of thiophene conversion was observed, and other sulfur products, namely H_2S, COS and traces of CS_2, appeared in the gas phase. Figure 14 shows axial profiles of H_2S, COS and thiophene in the bed. Since all sulfur species were not quantitatively analyzed, Figure 14 is intended as a qualitative plot only. Thus, an arbitrary logarithmic scale is used on the ordinate of Figure 14. The H_2S profile was found to be almost flat throughout the G-56B catalyst zone, and about two orders of magnitude higher than the COS, which peaked at the position of the temperature peak, gradually decreasing thereafter.

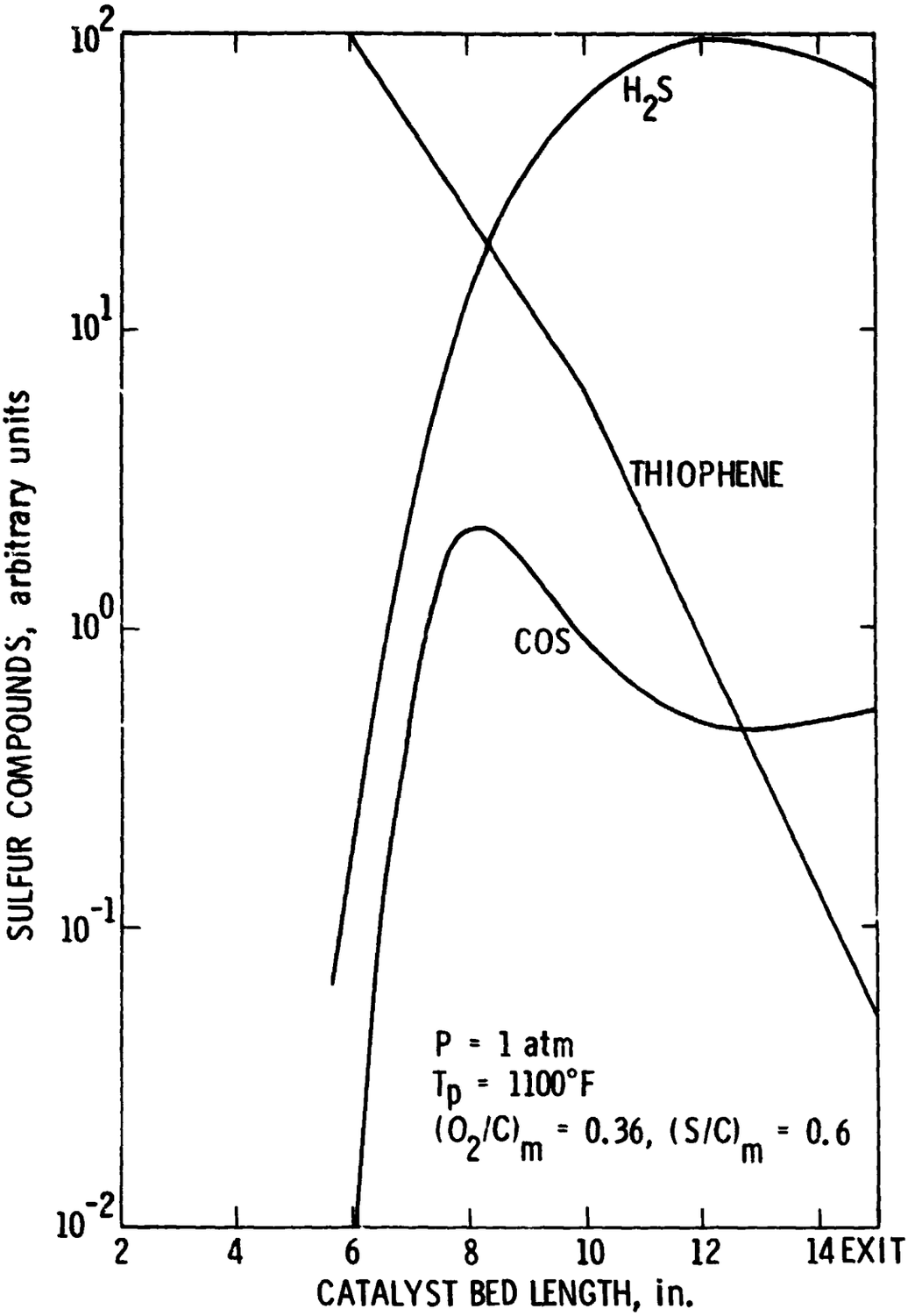

Figure 14. Autothermal Reforming of n-Tetradecane with 2000 ppmw Thiophene.
Gas Phase Axial Profiles of Sulfur Compounds.

(d) Catalyst samples from different bed locations were examined by SEM/EDAX. No surface carbon was detected in any of these samples. However, sulfur was found (by EDAX) on the surface of all three types of catalysts (NC-100, ICI 46-1, G-56B) throughout the bed. Figure 15 shows a SEM photomicrograph of the surface of ICI 46-1 catalyst taken from a location upstream of the maximum temperature region of the bed. A large part of this surface is comprised of a crystalline material, perhaps inorganic sulfate. Quantitative sulfur analysis was not made here since the total run times of these catalysts with the sulfur-containing fuel were not sufficiently long to make such an analysis conclusive at this point.

The above exploratory investigation of the effects of fuel sulfur in the ATR of paraffins has indicated the following:

(i) At the front end of the bed where partial oxidation of the fuel takes place, thiophene reacts with the catalyst/support surface and, presumably, forms some stable surface compound. Gases from this part of the bed contain no COS, indicating that any COS produced there is retained by the solid or rapidly reacted. During this process, catalyst sites active for the oxidation reaction of the hydrocarbon fuel are being depleted, temperatures are lower, and the location of the temperature maximum is shifted down the bed, indicating catalyst deactivation. It is interesting to note that it took less than 1 hour of run time for temperature profiles such as in Figure 12 to develop, indicating a more rapid loss in activity than when no sulfur is present in the fuel. However, temperatures in this part of the bed appear to be high enough for exten-

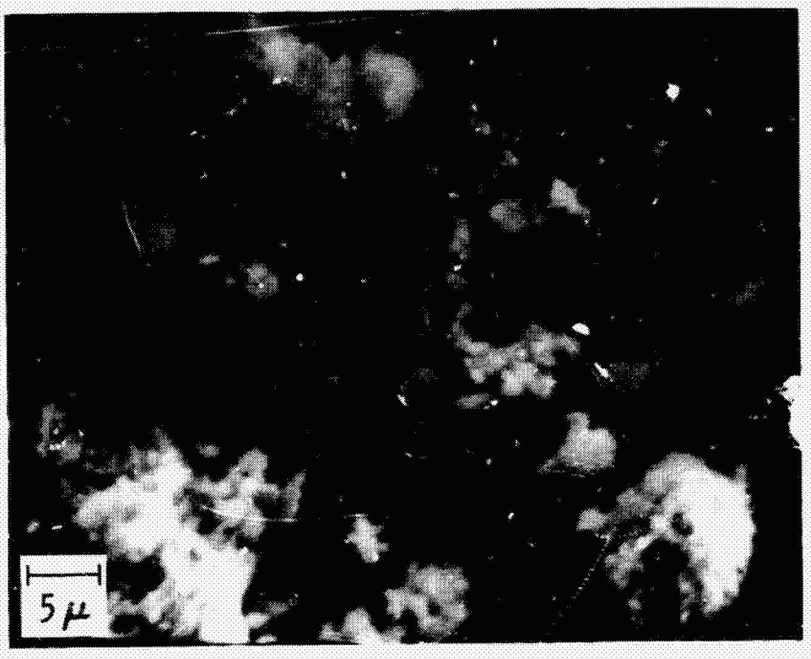

Figure 15. SEM photomicrograph of the surface of ICI 46-1 catalyst used in ATR of the n-tetradecane/thiophene mixture at P = 1 atm, T_p = 1150°F, $(O_2/C)_m$ = 0.38, $(S/C)_m$ = 0.6, and S.V. = 10,000 hr^{-1}.

sive steam cracking (in the gas phase) and thermocracking of the fuel on the catalyst/support surface (or in the gas phase) to take place, as was observed experimentally.

(ii) In the vicinity of the temperature peak, carbonyl sulfide becomes measurable in the gas phase (see Figure 14), and peaks upstream of the temperature peak. In the same region, H_2S is rapidly increasing to a peak in parallel with more hydrogen produced from the main reactions. Further down the bed, a lower amount of COS is observed in the gas phase, probably because it hydrolyzes to H_2S and/or reacts with the catalyst surface.

(iii) In the steam reforming region of the bed, in the absence of oxygen, the predominant sulfur species is H_2S. Temperatures in this region, though decreasing, are very high (see Figure 12), steam reforming can proceed at a fast rate, and there may be enough hydrogen available so that any potential surface sulfide of nickel becomes unstable (5). The flat H_2S profile in this part of the bed (see Figure 14) is indicative of no or very little H_2S/solid interaction. The sulfur laydown in the lower end of the catalyst bed identified by SEM/EDAX may be due to transients in the operating conditions. To prove this point, however, additional experiments under well controlled conditions are necessary.

(iv) While no carbon formation took place in the autothermal reformer at the conditions of Table VI, one may predict (based on the amounts of intermediate hydrocarbons in the gases) that carbon would be

formed in the case of the mixture by decreasing slightly the $(S/C)_m$ ratio at the inlet, while leaving all other parameters the same (11). The new conditions would still be carbon-free for the pure hydrocarbon, hence the propensity for carbon formation appears to be higher for the sulfur-containing hydrocarbon.

ATR of Thiophene-containing Benzene

Following tests with sulfur-containing paraffins, autothermal reforming tests were performed with benzene in which 1750 ppmw thiophene (or 667 ppmw sulfur) had been added in order to examine the effect of sulfur on the ATR characteristics of aromatic fuels.

Tests CP-237 through 239 were run at $(O_2/C)_m$ = 0.34, $(S/C)_m$ = 0.80. Fresh catalyst was loaded in the reactor prior to test CP-237. In the middle catalyst zone, the ICI 46-4 catalyst was used as in earlier tests with neat benzene (10). In tests CP-241 through 243, the same operating conditions were used on a fresh batch of the same catalyst types. Table VII summarizes the data collected from these tests, and also lists data from an earlier test, CP-203, run with benzene for comparison.

Sulfur conversion (and deposition) in the upper part of the catalyst bed affected bed temperatures in a similar way to the case of n-tetradecane/thiophene mixture. As shown in Figure 16, the axial temperature profile for benzene/thiophene was displaced by 4 inches down the bed from that corresponding to neat benzene. A higher peak temperature was observed with the mixture, probably due to its proximity with the G-56B catalyst which has a higher nickel loading than the ICI 46-4 catalyst. As with n-tetradecane, the sulfur poison-

TABLE VII

ATR PERFORMANCE COMPARISON OF THIOPHENE-CONTAINING BENZENE AND PURE BENZENE

TEST OP -	FUEL	$(O_2/C)_m$	$(S/C)_m$	(1) T_P °F	(2) MAX. BED TEMPERATURE T_{MAX} °F	(2) MAX. BED TEMPERATURE AT IN.	(3) $\dot{m}_f$ LB/HR	(4) S.V. HR^{-1}	CARBON	(5) GAS PROBE AT INCHES	DRY GAS COMPOSITION, MOL % H_2	CO_2	CO	HC_T	CH_4	C_2H_4	C_2H_6	C_3H_6	C_3H_8	C_4	C_5	C_6	C_6H_6
239	Benzene	0.34	0.8	1079	2074	9.0	6.01	9440	YES	INLET	-	0.07	0.38	7.68	-	-	-	-	-	-	-	0.01	7.67
238	w/Thiophene	"	"	1076	2049	9.8	"	"	"	6	10.07	5.82	21.30	7.09	0.49	0.62	0.01	0.04	-	0.12	0.14	-	5.67
	"	"	"	1085	2046	"	"	"	"	8	22.40	5.28	24.28	3.42	0.29	0.08	0.04	0.01	-	0.02	0.04	-	2.94
239	"	"	"	1079	2082	"	"	"	"	10	22.32	5.15	24.47	2.81	0.28	0.08	0.03	0.01	-	0.01	-	-	2.36
	"	"	"	1072	2073	"	"	"	"	12	28.77	5.25	25.53	2.17	0.16	0.02	-	-	-	-	-	-	1.99
	"	"	"	1073	2065	"	"	"	"	14	28.46	5.37	25.64	1.66	0.14	0.02	-	-	-	-	-	-	1.50
	"	"	"	1083	2056	"	"	"	"	EXIT	30.36	5.63	25.56	0.56	0.11	0.01	-	-	-	-	-	0.01	0.43
241	Benzene	0.34	0.8	1086	2009	8.7	6.01	9440	YES	4	0.05	3.06	11.50	11.33	0.12	4.07	-	0.03	0.01	0.10	0.04	0.07	6.89
	w/Thiophene	"	"	1069	2011	"	"	"	"	EXIT	30.66	5.39	25.60	0.37	0.10									0.27
243	Benzene w/Thiophene	0.34	0.8	1074	2074	9.8	6.01	9440	YES	EXIT	30.14	5.16	25.28	0.80	0.14	0.01	-	-	-	-	-	-	0.65
203	Benzene	0.34	0.8	1050	1811	6.0	6.00	9300	NO	4	2.73	2.80	7.58	7.49	0.09	0.24	-	0.01	0.02	0.06	0.07	0.01	6.99
	"	"	"	1048	1807	"	"	"	"	6	26.35	6.62	22.93	1.01	0.08	0.02	-	-	-	0.01	0.02	-	0.88
	"	"	"	1043	1813	"	"	"	"	EXIT	30.05	5.31	24.40	0.04	0.03	-	-	-	-	-	-	-	0.01
240	Benzene	0.29	1.0	1187	2043	9.8	7.01	11020	NO	6	-	7.80	1.25	7.87	0.03	0.01	0.01	-	-	-	-	-	7.82
242	w/Thiophene	"	"	1053	2000	10.2	7.01	"	"	EXIT	31.23	7.32	23.93	1.19	0.07	0.01	-	-	-	-	-	-	1.11
61	Benzene	0.29	1.0	1056	1700	5.8	7.00	11020	NO	EXIT	35.75	7.03	22.75	0.27	0.20		-	-	-	-	-	-	0.07

(1) - (5) See Table III

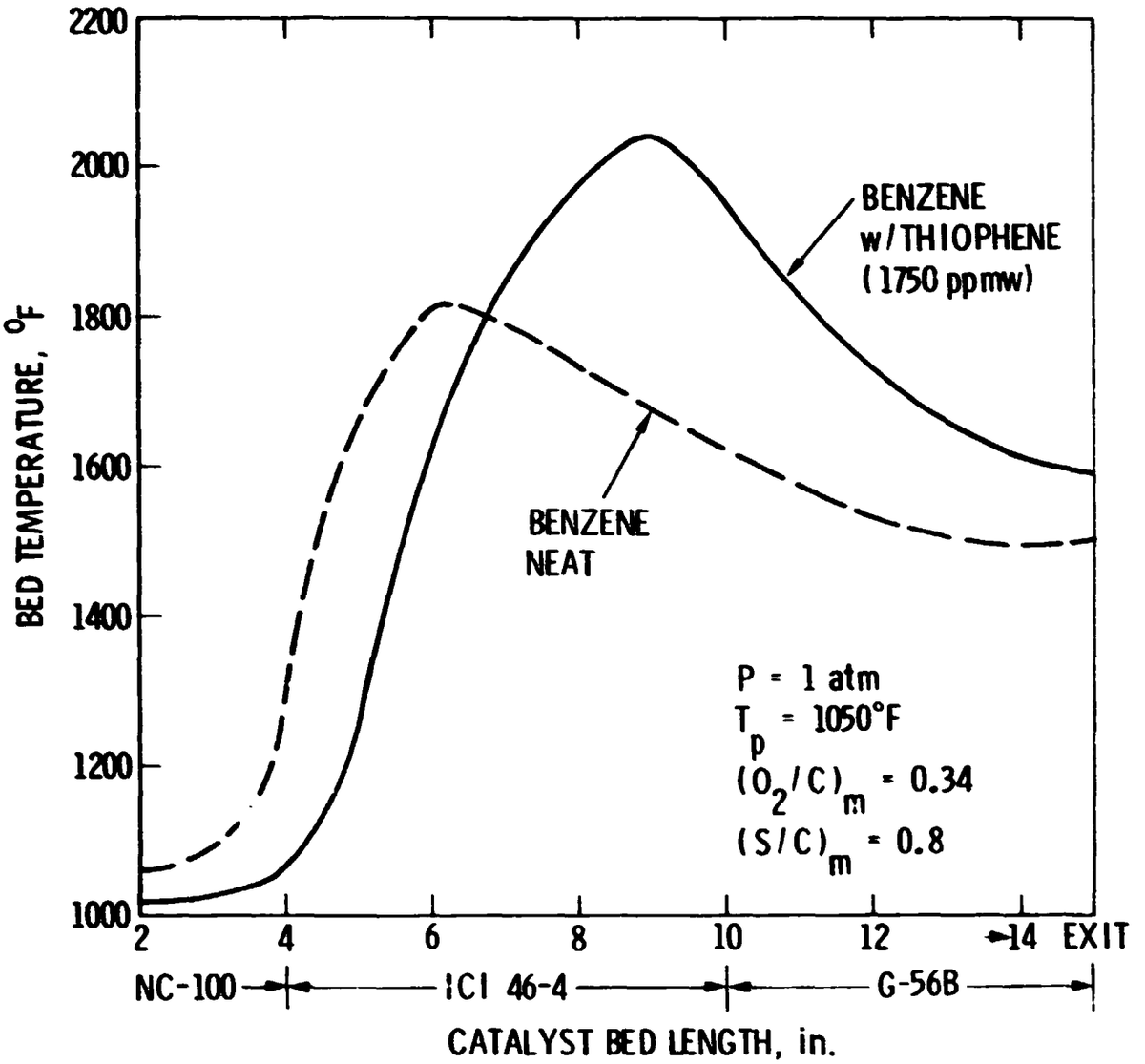

Figure 16. Autothermal Reforming of Benzene, neat and with 1750 ppmw Thiophene.
Axial Bed Temperature Profiles.

ing of the front-end catalyst was rapid, pushing the temperature peak down the bed in later runs (Table VII).

Analysis of gas samples from various bed locations is given in Table VII, and axial profiles for CH_4, C_2H_4, C_3H_6, and C_6H_6 are shown in Figure 17 for the conditions of Figure 16. Higher amounts of olefins and methane were produced throughout the catalyst bed, and more unconverted benzene was detected in the exhaust gases with the benzene/thiophene mixture than with benzene alone. Carbon was formed when the mixture was used at these conditions, which were carbon-free for neat benzene (test CP-203). Because of the higher amount of unconverted benzene and higher temperatures around the temperature peak region, the rate of carbon formation there might have been enhanced, perhaps via dehydrogenation of the benzene molecule.

Gas phase sulfur products, H_2S and COS, appeared early in the bed during the ATR of benzene/thiophene. Qualitative plots of the axial bed profiles of these two compounds are shown in Figure 18. A flat profile is observed for H_2S, while COS peaks close to the location of the temperature peak (similar to the plots of Figure 14). Thiophene could not be detected by the G.C. (FPD) in these tests because it was masked by benzene which had the same retention time as thiophene in the Poropak QS column of the G.C.

Another set of conditions with benzene/thiophene were tested in tests CP-240, 242 and 244, with $(O_2/C)_m$ = 0.29, $(S/C)_m$ = 1.0 (Table VII). By comparing this data to test CP-61 (neat benzene) similar reactivity can be seen concerning the effect of sulfur on conversion efficiency and propensity for carbon formation in the ATR of aromatic hydrocarbons.

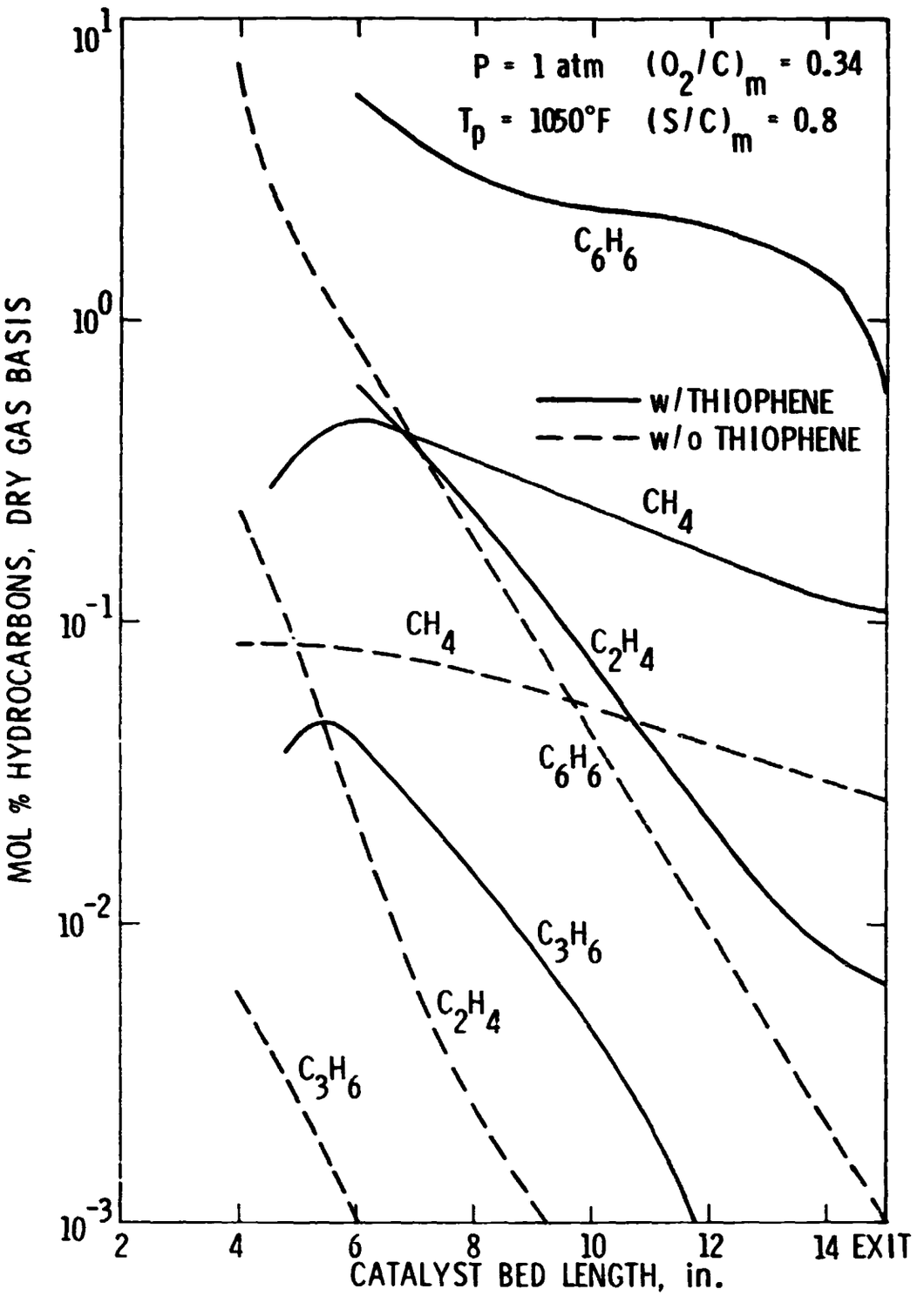

Figure 17. Autothermal Reforming of Benzene, neat and with 1750 ppmw Thiophene Axial Bed Composition Profiles.

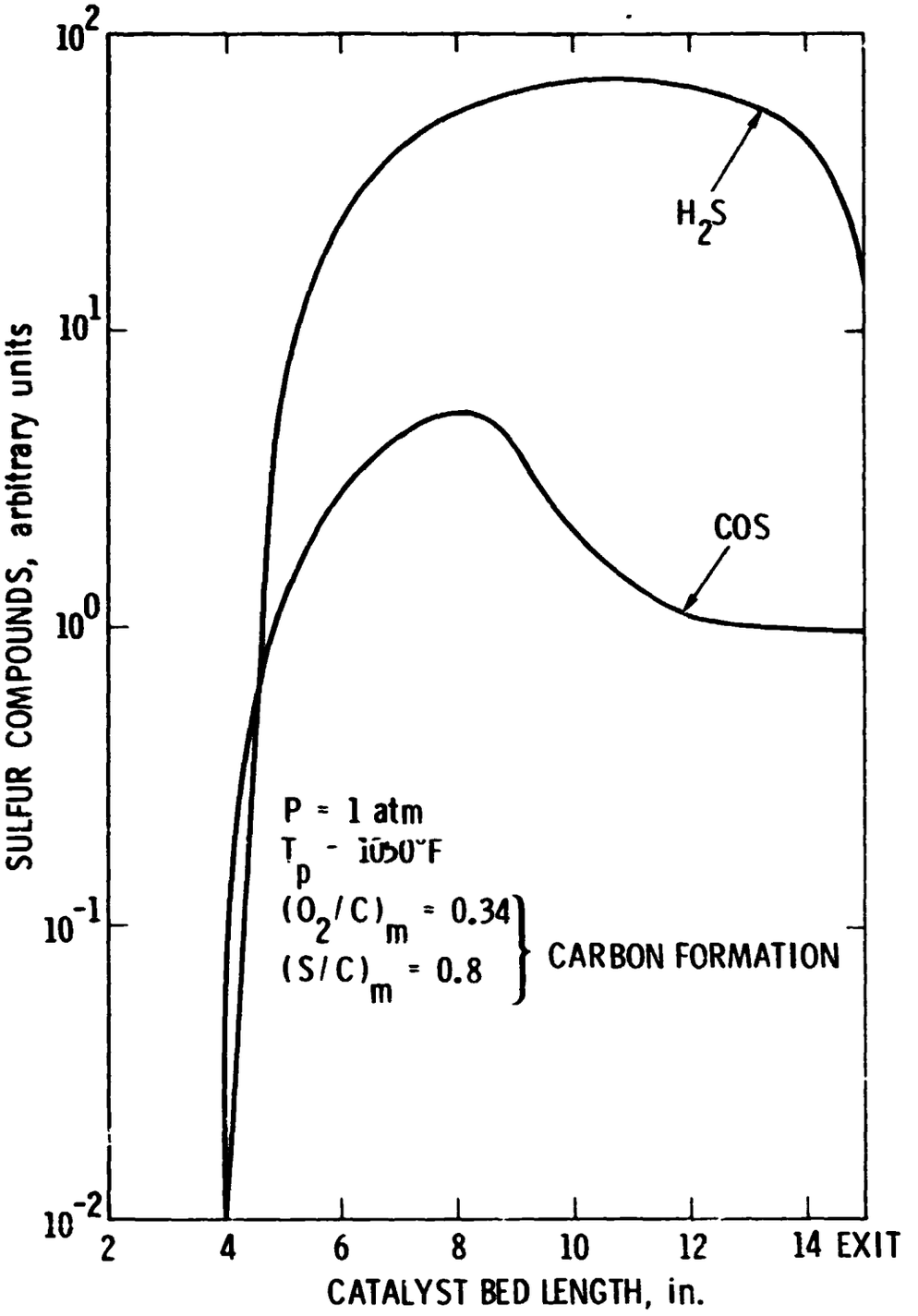

Figure 18. Autothermal Reforming of Benzene with 1750 ppmw Thiophene.
Gas Phase Axial Profiles of Sulfur Compounds.

Post-examination of the catalysts used at the conditions of Figures 16-18 was performed by SEM/EDAX. All catalyst samples had changed color from gray to green during operation. Sulfur was found on the surface of all three catalyst types, indicating that sulfur had reacted with the catalyst/support throughout the bed. Presumably a sulfate had been formed on the catalyst surface in the partial oxidation region. Figure 19 shows a SEM photomicrograph of the top ICI 46-4 catalyst surface on which crystalline material is seen. This "sulfated" catalyst was less active in ATR than the uncontaminated catalyst.

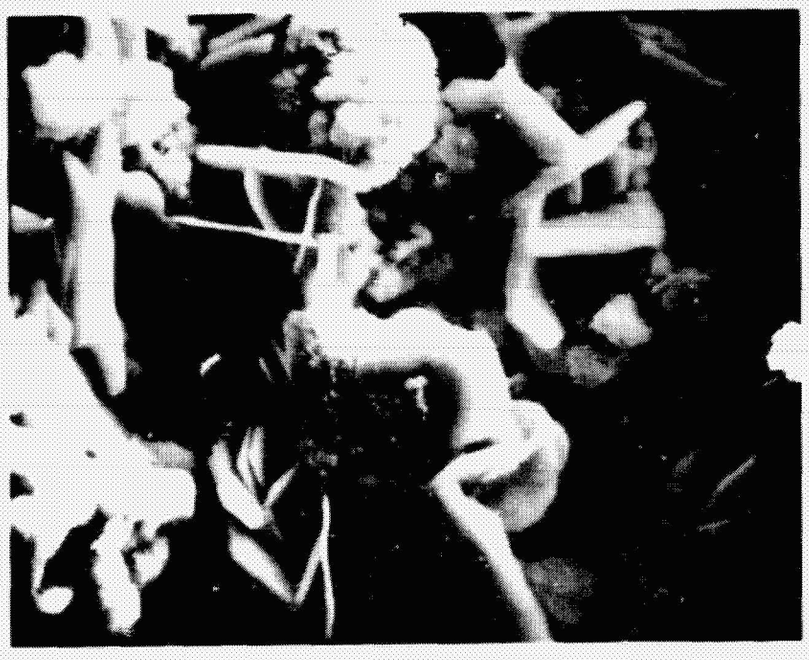

Figure 19. SEM photomicrograph of the surface of the top ICI 46-4 catalyst used in ATR of the benzene/thiophene mixture at P = 1 atm, T_p = 1030°F, $(O_2/C)_m$ = 0.34, $(S/C)_m$ = 0.8, and S.V. = 9440 hr^{-1}; 2000 X.

CONCLUSIONS

In autothermal reforming work at JPL, a comparative study has been undertaken whereby different types of liquid hydrocarbons, additives, and mixtures thereof have been examined from the aspect of chemical reactivity and carbon formation characteristics in ATR. Effects of changing several of the operating parameters on the propensity for carbon formation have been studied with each hydrocarbon type.

In experiments with sulfur-free hydrocarbon liquids, paraffins and aromatics have been tested extensively in ATR to identify possible reactive differences or similarities that could explain (at least in part) the behavior of heavy fuels, e.g., No.2 fuel oil, which is mainly comprised of paraffins and aromatics. In an earlier experimental study of No.2 fuel oil in ATR (6), this had been found to form carbon at oxygen/steam ratios much higher than those predicted by thermodynamic equilibrium. In the work discussed here, the same catalyst types and configuration have been used as in the fuel oil tests to facilitate comparisons.

Reactive differences between paraffins and aromatics have been found in ATR. These were indicated by very different bed temperature profiles obtained from each fuel type under similar operating conditions. Also, very different experimental carbon formation lines (in the $(O_2/C)_m$-$(S/C)_m$ plane) were determined for each hydrocarbon. Thus, at low $(S/C)_m$ ratios, paraffins were more prone to form carbon if the $(O_2/C)_m$ ratios were low, while high $(O_2/C)_m$ ratios were unfavorable (carbon-forming) for the aromatics at the same operating conditions.

Gaseous reaction products obtained from different locations throughout the length of the catalyst bed have been analyzed and compared for n-tetradecane (a paraffin) and benzene (an aromatic). Intermediate species (hydrocarbons) identified from each fuel type were different in amounts, not in types. However, the conversion profiles of these intermediates along the bed and the respective bed temperatures profiles are indicative of different carbon formation mechanisms operative for each hydrocarbon type in ATR. In the case of n-tetradecane, considerable cracking to mainly olefinic compounds takes place at the inlet and throughout the partial oxidation region of the bed. These olefins can easily degrade to carbon either in the gas phase (at the higher temperatures, >1500°F, close to the temperature peak location), or on the catalyst/support surfaces at high and intermediate temperatures. In the case of benzene, however, no inlet cracking, and very low amounts of olefinic intermediates are produced in the front end of the bed; the predominant species is unconverted benzene throughout the bed. Benzene can degrade to carbon by dehydrogenation in the gas phase at the higher temperatures prevailing in the vicinity of the temperature peak, which is 200°F higher than for n-tetradecane due to the absence of cracking. Benzene-nickel interaction resulting in surface-bound carbon is also possible throughout the steam reforming region of the reactor.

Carbon types and locations of carbon formation were identified for each sulfur-free fuel used in ATR. In all cases, carbon was a mixture of seemingly gas phase generated as well as surface-bound forms. The former was powder-like, filling catalyst voids and not adhering to the surface. The latter was filamentous carbon (whiskers growths) of the kind that has been observed in the steam reforming, CO disproportionation, and methanation literature. As was found by XRD analyses, both types of carbon were (at least in part) graphitic.

With aromatics, gas phase carbon appeared to be the predominant type of carbon in the ICI catalyst zone, which exhibited limited erosion. With paraffins, however, considerable catalyst erosion was typically observed in the ICI zone. Carbon from this part of the bed clearly consisted of a mixture of fines and surface grown whiskers. On the last catalyst zone, G-56B, surface grown carbon was detected regardless of the hydrocarbon type, but considerable catalyst disintegration (fines) was also observed in this zone.

The described characteristics of n-tetradecane and benzene in ATR were the same for their homologs, n-hexane and naphthalene, respectively. The main conclusion here is that the higher the molecular weight, the higher the propensity for carbon formation in ATR. The use of benzene/naphthalene mixtures caused a more pronounced departure from the equilibrium carbon line even at low (<0.36) $(O_2/C)_m$ ratios, indicative of a higher carbon-forming tendency of the polynuclear aromatic molecule (naphthalene).

Intermediate species from either aromatics or paraffins in ATR have been found to vary in amounts only, not in type, when comparing carbon-forming to carbon-free conditions. This probably indicates that a "critical" amount of each carbon precursor (olefinic, aromatic) must be reached in the bed before the local $(S/C)_m$ ratios become too low for carbon-free operation. It was previously (11) shown that the propensity for carbon formation in the steam reforming region of the bed was more sensitive to changes in the local $(S/C)_m$ ratios than to temperature for the same other operating parameters.

Effects of olefin (propylene) addition on the ATR performance of benzene have been described in this report. The "tolerance" of the system (i.e., resistance

to carbon formation) to propylene addition at the inlet is higher than to injections at locations within the steam reforming region of the bed. Propylene addition inhibits the conversion of benzene and enhances methane production in the lower part of the bed. After a "critical" amount of propylene is injected in this region, a reduction in the overall $(S/C)_m$ ratio is effected such that the carbon formation rate becomes faster than that of carbon removal. From these tests, however, it cannot be deduced that propylene itself is the carbon precursor. Higher amounts of unconverted benzene are now present in the bed which may degrade to carbon. To elucidate the mechanism of carbon formation in this case would require well controlled, small scale experiments (e.g., labeling experiments using carbon isotopes).

When mixtures of paraffins and aromatics (n-tetradecane and benzene) were tested in the autothermal reformer under similar conditions as for the pure hydrocarbon components, synergistic effects were identified. Thus, bed temperatures, extent of cracking rections, and propensity for carbon formation for the mixtures were intermediate between those of the component fuels, n-tetradecane and benzene.

Comparisons of the whole body of experimental ATR results of sulfur-free pure hydrocarbons with No.2 fuel oil (Figure 11) indicate that the deviation of the carbon formation line of the latter from those of the pure hydrocarbon iquids cannot be explained by molecular weight and chemical character (e.g., aromaticity) effects alone. It appears that the sulfur content of No.2 fuel oil (3000-5000 ppmw) may be the limiting factor for an efficient (low O_2/C and preheat temperature) ATR operation. Exploratory tests were thus undertaken in which the effect of sulfur on the conversion characteristics of paraffins

and aromatics in ATR was examined by using mixtures of n-tetradecane and thiophene (2000 ppmw), and benzene and thiophene (1,50 ppmw), respectively. Thiophene was chosen as the sulfur additive in these tests, because most of the fuel-bound sulfur in No.2 fuel oil is thiophenic.

Data from the thiophene-containing hydrocarbons were similar for both hydrocarbon types (paraffins, aromatics). Thus, the front part of the bed rapidly became poisoned, and temperature profile peaks were shifted down the bed, while reaction rates were inhibited, as indicated by lower bed temperatures. Upon post-examination of catalyst surfaces from this part of the bed, crystalline material, possibly inorganic sulfates, was detected by SEM, and sulfur was identified by EDAX. The steam reforming region of the bed operated under higher temperatures (since the temperature peak was shifted down the bed). Gas analysis throughout the bed length showed enhanced cracking rates of n-tetradecane, and limited conversion of benzene in the presence of thiophene. These results indicate that carbon formation would take place easier for the sulfur-contaminated than for the sulfur-free fuels, as was actually the case in one set of operating conditions with the benzene/thiophene mixture. Catalyst from the steam reforming region of the bed also contained sulfur, but it was not possible to quantitatively determine if the sulfur-catalyst interaction was lower there than in the partial oxidation region of the bed.

Sulfur species identified by G.C. (FPD) in the gas phase include H_2S (predominantly) and COS apart from unconverted thiophene. However, thiophene was the only sulfur species in the gas phase down to the vicinity of the maximum temperature, where H_2S and COS were first detected. It appears that stable

surface compound(s) formed from the thiophene-catalyst interaction in the upper part of the bed where oxygen is present, since thiophene was being depleted and no other sulfur compound could be detected in the gas phase. On the other hand, the H_2S - nickel interaction in the lower part of the bed appears to be limited, since the H_2S profile is flat through this part. The reason for this may be that higher bed temperatures and sufficient hydrogen pressure there do not favor stable nickel sulfide(s). The sulfur detected (by EDAX) on catalyst samples taken from the lower part of the bed may be due to transients in operation.

These preliminary experimental results from the ATR of sulfur-containing paraffins and aromatics appear to indicate the necessity for higher preheat temperatures in order to alter the thermodynamic equilibrium of the reactions in the front part of the bed and avoid deactivation. This, however, may require increased amounts of steam at the inlet to control potential carbon formation, which can occur from precombustion (in the gas phase) of the fuel at very high inlet temperatures ($\sim$1400°F). Future experiments should focus on examining the effects of these parameters (preheat, steam) on the ATR of sulfur-containing hydrocarbons with respect to conversion efficiency and propensity for carbon formation. Based on the outcome of this research, a realistic model can be constructed for the autothermal reforming of fuels of any composition. Moreover, by carefully monitoring all reaction species and apparent catalyst activities in complementary catalyst screening experiments, it will be possible to determine the optimal catalyst types and configurations needed for carbon-free ATR operation under high thermal and conversion efficiencies.

D2

PART II

STEAM REFORMING OF n-HEXANE ON PELLET AND MONOLITHIC CATALYST BEDS

A Comparative Study on Improvements due to Heat Transfer

INTRODUCTION

Steam reforming of desulfurized heavy hydrocarbon fuels for fuel cell applications of interest to electric utilities requires high catalyst temperatures (1500-1700°F) and high steam-to-carbon rati Since steam reforming is endothermic, the heat must be transferred through the reactor walls and throughout the catalyst bed. The temperature required on the outside walls of the reactor, therefore, is in excess of the temperature within the catalyst bed. Preheat of the fuel and steam prior to entry into the catalyst bed can provide a certain amount of the energy required, but is limited to the point at which steam-cracking of the fuel (which can produce soot) occurs. Most of the reaction energy required, therefore, is supplied through the reactor walls. Steam reforming of heavier fuels, which normally contain as much as 0.3-0.5 wt.% sulfur, without removing the sulfur, would require even higher wall temperatures than for clean fuels to inhibit the poisoning of base metal catalysts. However, as higher temperatures are reached, the reactor materials become more expensive and less durable. In addition, the high temperature operation is less efficient because of the higher heat loss in the exhaust gas. Thermal gradients through the catalyst bed from wall to centerline contribute to sintering or poisoning of the catalyst, particularly during a load-following transient that might be anticipated in actual fuel cell use in utilities.

Honeycomb monolithic supports for steam reforming catalysts appear promising in that they have the potential of improving radial heat transfer necessary to reduce thermal gradients in the catalyst bed. The connecting walls of the monolith provide a continuum for superior heat transfer relative to the poor heat transfer through edge and point contact present in a pellet bed. With the more uniform bed temperature of a monolith, the possibility of hot spots and areas of nonreactive holes due to poor packing can be eliminated. The more uniform temperature also results in a more uniform reaction zone that is easier to control. This is of particular importance in avoiding soot formation in the catalyst bed. Another important factor is that because of better heat transfer properties, monoliths are expected to "respond" faster during transients in fuel cell load following. As a result of better heat transfer through the catalyst bed, less expensive wall material with longer lifetime can be implemented. Successful application of monolithic catalysts to steam reformers could thus offer substantial energy savings in both steady state and transient operation.

We have recently reported (11) on steam reforming tests of n-hexane on monolithic catalyst beds. A 20-inch long bed was loaded first with a commercial pellet steam reforming catalyst (G-90C), and then with two different honeycomb monoliths. In one case, the total length of the bed was made up of ceramic monoliths (Cordierite) supporting nickel catalyst, while in a second case, a hybrid configuration was used having 8 inches of a metal monolith support (Kanthal), also impregnated with nickel, followed by 12 inches of the same ceramic monolith catalyst as in the first case. A washcoat of γ-alumina was used on both types of monoliths to provide a high surface area for the nickel catalyst.

Comparative tests between the pellet and monolithic beds were run at similar operating conditions (steam-to-carbon ratios, external heat flux, inlet temperatures and space velocities). Results from tests with the ceramic monolith have shown that the Cordierite support with its γ-alumina washcoat was not stable when used throughout the length of the bed; a rapid disintegration of the solid was observed at conditions common to steam reformers. This instability was probably due to breaking of the washcoat (through phase changes and carbon formation), and subsequent extraction of the support silica by steam at the high temperatures of operation.

In following tests, the combination of a metal honeycomb monolith (at the top of the bed) and a ceramic monolith (at the bottom) was tested in the steam reformer. With this configuration, the shortcomings of using the Cordierite monolith exclusively throughout the total length of the bed were expected to be alleviated because the metal monolith at the top would have better heat transfer characteristics and, thus, be less prone to carbon formation. The Cordierite monolith at the end of the bed would complete the steam reforming reaction with lower probability of hydrothermal disintegration due to lower amounts of steam present there. This "hybrid" monolith was found to have better radial heat transfer properties than the pellets, and a similar conversion efficiency to that of the pellets, initially. In later tests, however, which followed carbon formation in the bed (and irreversible plugging of many monolith cells), the conversion characteristics of the hybrid monolith were changed. Intermediate hydrocarbons (ethylene, propylene) were produced in higher amounts, and temperatures dropped because of higher effective flowrates through unplugged cells. Carbon formation in the Cordierite monolith followed by long desooting periods caused the complete physical breakdown of portions of

this monolith. The metal monolith pieces, however, were retrieved in good condition, even though many of their cells had been plugged with carbon.

In the work reported here, we have used only metal monolithic supports, which appear to have better radial heat transfer characteristics in the steam reformer than conventional pellet beds, and which were also found to be stable in our previous tests. Reaction temperatures and products, and the propensity for carbon formation have been compared between a commercial catalyst pellet (G-90C) bed and two different metal monolithic catalysts under similar operating conditions.

EXPERIMENTAL

Apparatus

The steam reforming system used in this work is simply a tubular packed bed reactor positioned inside a three-zoned furnace. Figure 20 shows a schematic of this steam reforming system. Fuel is vaporized in an electrical heater and mixed with steam that is also vaporized and preheated by electric heaters. The hot mixture is then fed down through the catalyst bed.

A 2.5 inch I.D. by 31.5 inch long Inconel reactor was used in all tests. Both end pieces are constructed with two multiport accesses for thermocouple inlets to the catalyst bed. The reactor is mounted vertically inside a hinged type 35 kW Mellen furnace. Three-zone heating is provided by three individually controlled zones in the furnace. The furnace is 29.5 inches long but the design of the furnace is such that the top 2 inches and the bottom 2.5 inches are unheated and contain insulating material. Thus, approximately the top 4 inches of the reactor are at lower temperature than the main body of the furnace. For this reason, this area is not filled with catalyst. In this phase of the work, the inlet to the reactor was made of refractory material with a conical shape to avoid stagnation areas and to provide uniform inlet conditions. Pieces of multi-channel alumina sponge were used to fill the reactor inlet. All feed lines, heaters, etc., were insulated to minimize heat losses.

Bed temperatures were monitored by Inconel sheathed chromel-alumel thermocouples. In the tests described here the catalyst bed was 8 inches long, so only sixteen thermocouple ports in the top flange were used. Figure 21 shows a schematic of the catalyst bed and the position of the imbedded thermocouples.

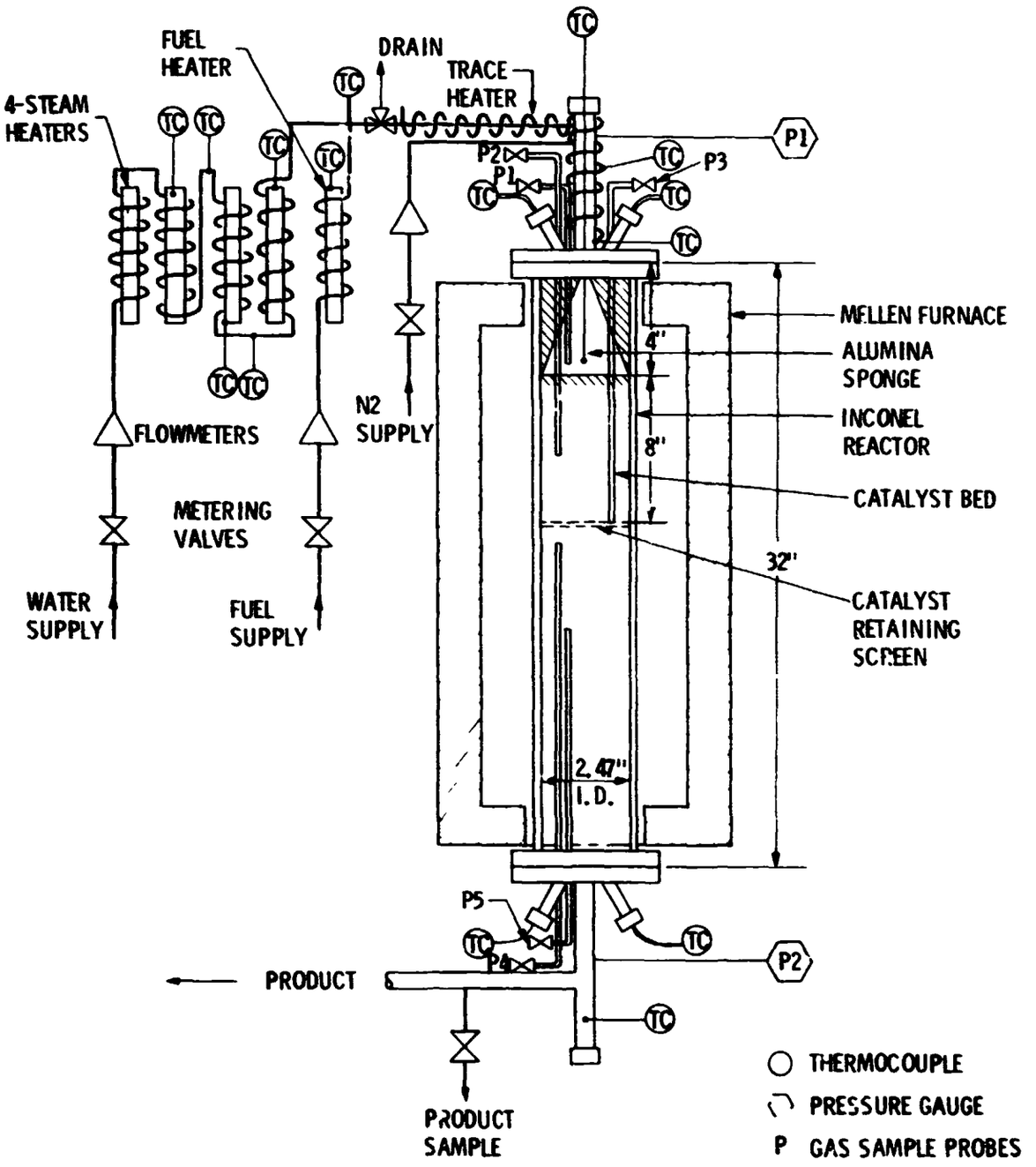

Figure 20. Schematic of the Steam Reforming System.

Additional thermocouples were used externally to monitor the reactor wall temperatures. Three gas probes (1/8 inch I.D.) were also installed through the top flange to sample gases from different bed locations. Gas samples were continuously analyzed for hydrogen, carbon monoxide, carbon dioxide and total hydrocarbons with analyzers specific for each gas. A HP-5830 gas chromatograph (FID) was also used for individual hydrocarbons identification and analyses.

Materials

(a) Fuel

n-Hexane was the choice of hydrocarbon for steam reforming, in part because whatever is unconverted can be measured by the gas chromatograph. Technical grade was used for economy reasons. The chemical composition of the technical grade n-hexane purchased from Phillips Petroleum is as follows:

Normal Hexane:	97.7% (Min = 95.0%)
Methylcyclopentane:	2.1%
3-methylpentane:	0.2%
2-methylpentane:	trace

(b) Catalysts

Steam reforming tests in this phase of the work were performed on catalysts supported by metal monolith and ceramic pellets. The monolithic bed used was comprised of four, 2-inch long pieces, as shown in Figure 21. These had a honeycomb geometry (hexagonal channels) with a cell density of 250 cells/in^2. The monolithic catalyst substrate was made

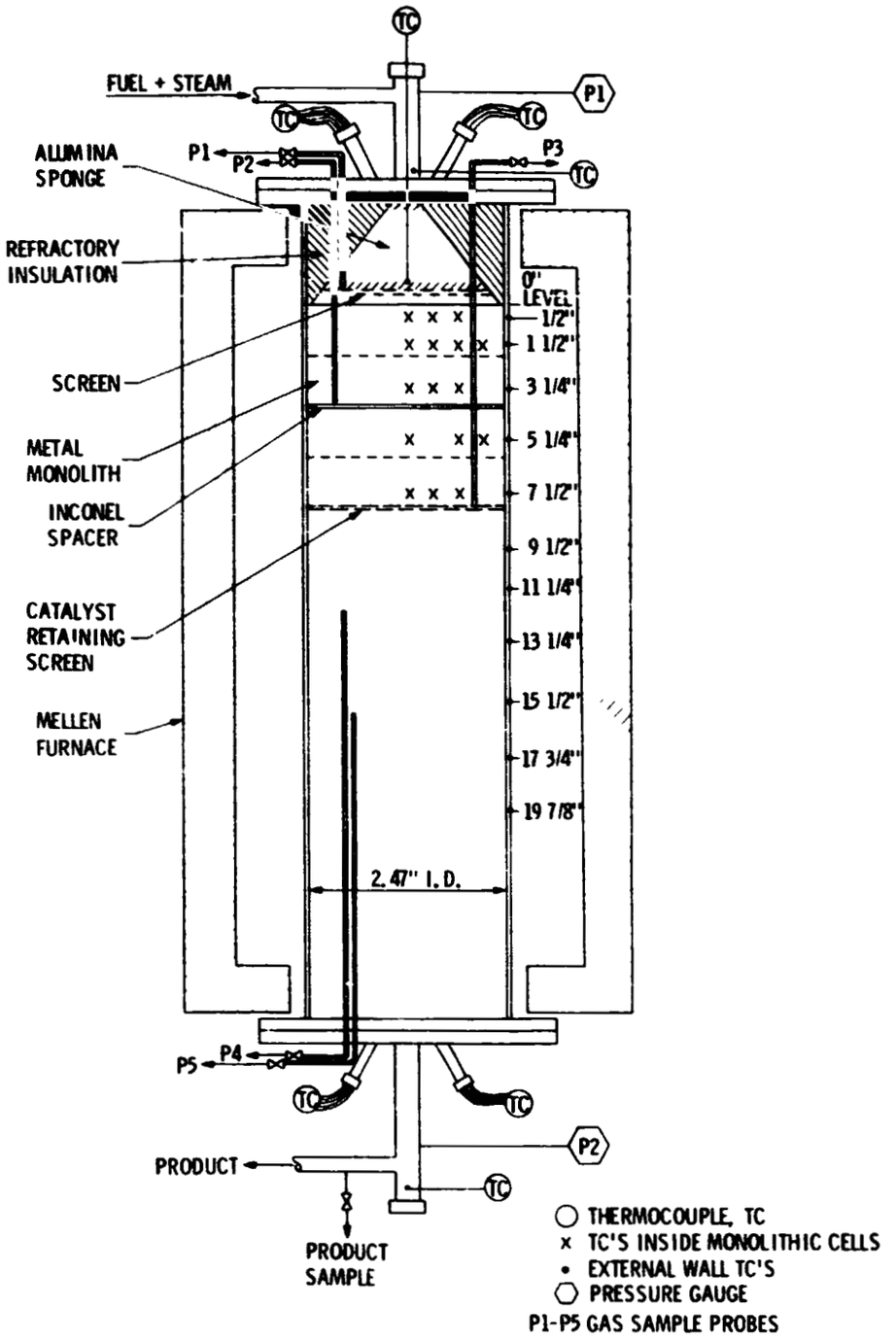

Figure 21. Schematic of the Steam Reformer. Locations of the thermocouples and gas sampling probes are indicated for the honeycomb metal monolith.

from Kanthal (Fe-Cr-Al alloy) which was washcoated with γ-alumina, then impregnated with nickel. The first metal monolith (I) used was the same as the one used in earlier tests (11) in series with the ceramic (Cordierite) monolith. The composition of the four monolithic pieces as received is shown in Table VIII.

Following the series of tests on metal monolith I, new steam reforming tests were run using a conventional pellet catalyst. The commercial Girdler G-90C catalyst was used in the form of cylindrical tablets (1/4 in x 1/4 in). This is composed of nickel impregnated on a ceramic support (calcium aluminate). The physical and chemical characteristics of this catalyst are given in Table VIII.

Upon completion of the tests with the pellet catalyst bed, a new metal supported monolithic catalyst (II) was tested in the steam reformer. The same substrate was used as before (Kanthal), washcoated with γ-alumina, but its impregnation with nickel catalyst was done in-house. After the four monolithic segments had been cut to fit tightly inside the reactor tube, they were impregnated with nickel. The final composition of each segment of the metal monolith II is shown in Table VIII.

TABLE VIII

PHYSICAL AND CHEMICAL CHARACTERISTICS OF STEAM REFORMING TEST CATALYSTS

A. METAL MONOLITH I (4 pieces, 2 inches long each), as purchased:

250 cells/in^2 Kanthal support/γ-Al_2O_3 washcoat/NiO catalyst

Weight, g (before cutting)	#1	#2	#3	#4
Bare Metal (Kanthal)	177.4	171.8	171.9	172.4
γ-Al_2O_3 washcoat	9.76	10.31	9.63	10.50
NiO	6.21	5.33	5.33	5.69
γ-Al_2O_3/Kanthal, %	5.50	6.00	5.60	6.09
NiO/Al_2O_3, %	63.63	51.70	55.35	54.19

B. GIRDLER G-90C (1/4" x 1/4" cylindrical tables), 8-inch long bed

Chemical Analysis, Wt. %

NiO	19.2
γ-Al_2O_3	78.6
CaO	2.0
SiO_2	0.2

C. METAL MONOLITH II (4 pieces, 2 inches long each) impregnated in-house

250 cells/in Kanthal support/γ-Al_2O_3 washcoat/NiO catalyst

Weight, g (after cutting)	#1	#2	#3	#4
Bare metal (Kanthal)	123.08	131.95	137.47	129.33
γ-Al_2O_3 washcoat	8.24	7.92	7.83	8.53
NiO	7.08	6.38	6.20	5.97
γ-Al_2O_3/Kanthal, %	6.69	6.00	5.70	6.60
NiO/Al O , %	85.92	80.56	79.18	69.99

Procedure

For start-up of the steam reforming system, each zone of the Mellen furnace was heated to a specified temperature so that a uniform temperature would be reached along the outside reactor wall. Hydrogen was introduced into the reactor and the nitrogen flow, used as inert protection, was shut off. The hydrogen flow was maintained during this heating period to reduce the nickel catalyst. The steam heaters were turned on, and a specified water flow was heated and dumped before entering the reactor as shown in Figure 20. When the temperature of the steam coming out of the last steam heater was 1200°F, the steam was diverted into the heated reactor. After the reactor inlet temperature reached 1000°F, the trace heater at the reactor inlet, and the fuel heater were turned on. Heated fuel was gradually added to the steam, until the specified flow was reached. The fuel temperature was maintained between 400°F and 550°F. The steam heaters were adjusted to maintain the reactor inlet at 1000°F.

During each test, reactant flowrates, product compositions, catalyst bed temperatures, and bed pressure drop were monitored. In all tests, after steady state was established, temperatures were recorded and gas samples from the reactor exit as well as from each of the bed locations shown in Figure 21 were analyzed. Dry volume percentages of H_2, CO, CO_2 and total hydrocarbons were calculated from gas analyzer data. The detailed volume percentages and analyses of hydrocarbons were calculated from G.C. (FID) data.

A pressure rise during a run was an indication that solid carbon was forming. In addition, carbon fines were sometimes detected in the probe condenser or in the exhaust filter. To desoot the bed, the reactor inlet temperature was

raised to 1200°F, and the steam flowrate was increased while the fuel was turned down to around 0.5 lb/hr, resulting in a $(S/C)_m$ ratio of about 5. The system was left at these conditions until the CO_2 and H_2 levels in the exhaust were stabilized, and the pressure drop through the bed was less than 5 psig for approximately 1 hour. Following desooting, new test parameters were set for continued operation. At the end of operation, the system was shut down under nitrogen with steam shut-off being preceded by the fuel.

RESULTS AND DISCUSSION

(A) Tests With The Metal Monolith I

Initially, steam reforming tests were performed on the metal monolith catalyst I that had been used in the hybrid monolith experiments (in series with the ceramic monolith segments). The composition of the monoliths used are shown in Table VIII.

Tests SR-208 through 226 were run with n-hexane using this 8-inch long metal monolith bed at P = 1 atm, T_{inlet} = 1000°F, and for $(S/C)_m$ ratios of 2.5, 3.0 and 3.5. External reactor wall temperatures of 1500°F and 1700°F were used with nominal reactants' space velocities equal to 2000 and 4000 hr^{-1}. The nominal space velocity is defined here by:

$$S.V. = \frac{[\text{vol. Flowrate of Reactants, } ft^3/hr]_{\ 60°F,\ 14.7\ psia}}{\text{Reactor Volume, } ft^3}$$

C-2

The reactor volume rather than the monolithic catalyst volume is used in this expression. In all tests, the bed temperatures, product yields, and carbon-forming tendency were examined and compared with data from previous tests in which the 20-inch long hybrid monolith or pellet bed were used. The data from these tests are summarized in Table IX. In order to keep nominal space velocities the same as with the longer beds used in earlier tests (2.5 times longer), the flowrates (and, hence, the flow velocities) used in the present study were 2.5 times lower.

In Figures 22 and 23, the dry gas volume percentages of the various gaseous species are plotted as a function of the catalyst bed length for the short metal monolith, and the longer hybrid monolith and pellet bed. Higher amounts of total hydrocarbons and lower amounts of hydrogen and carbon monoxide were found at the level of probe 3 when the short metal monolith was used than for the other two catalyst beds. The amount of unconverted hexane at this level was lower with the metal monolith, while higher amounts of intermediates (ethylene, propylene, etc.) and methane were produced in this case. This finding indicates that cracking reactions in the gas phase rather than steam reforming on the catalyst surface were taking place throughout the length of the monolith cells under these conditions. Since the conversion of the fuel at the exit of the 8-inch long monolith is lower than that at the corresponding point of the longer monolith or the pellet bed (location of gas probe 3), this means that external mass transfer limitation exists (diffusion of the reacting species from the gas phase to the catalyst surface). All operating conditions examined here were found to be mass transfer limited.

TABLE IX

STEAM REFORMING OF N-HEXANE ON THE METAL MONOLITH I

TEST	$(S/C)_m$	(1) $\dot{m}_w$	(1) $\dot{m}_f$	(2) SPACE VELOCITY	(3) T_{WALL}	CARBON	(4) GAS PROBE	DRY GAS COMPOSITION, MOL %												
		LB/HR	LB/HR	HR^{-1}	°F		AT INCHES	H_2	CO_2	CO	HC_T	CH_4	C_2H_4	C_2H_6	C_3H_6	C_3H_8	C_4	C_5	C_6H_{14}
208	3.0	2.0	0.53	2000	1500	NO	EXIT	62.77	15.61	12.60	9.28	3.60	3.27	0.77	0.81	0.01	0.19	0.05	0.58
209	3.0	2.0	0.53	2000	1500	NO	4-1/8	59.93	15.67	11.62	13.01	2.34	1.88	0.47	0.37	-	0.10	0.03	7.82
	"	"	"	"	"	"	8-1/4	64.44	14.87	14.45	6.35	2.12	1.88	0.42	0.51	-	0.16	0.06	1.20
	"	"	"	"	"	"	EXIT	62.52	14.44	13.44	11.93	4.65	4.36	1.05	1.01	0.01	0.23	0.04	0.58
210	2.5	2.0	0.64	2000	1500	NO	EXIT	60.17	12.62	14.44	16.46	5.92	5.77	1.36	1.58	0.01	0.44	0.08	1.30
211	2.5	2.0	0.64	2000	1500	NO	4-1/8	54.77	13.45	12.53	13.61	2.50	2.14	0.53	0.51	-	0.16	0.04	7.73
	"	"	"	"	"	"	8-1/4	61.17	12.92	15.70	6.70	2.05	1.94	0.42	0.60	-	0.21	0.06	1.42
	"	"	"	"	"	"	EXIT	59.44	12.20	14.65	11.77	4.36	4.17	0.99	1.09	0.01	0.28	0.06	0.81
212	2.5	2.0	0.64	2000	1700	NO	4-1/8	58.63	11.61	15.11	10.38	2.20	2.01	0.35	0.40	-	0.20	0.06	5.16
	"	"	"	"	"	"	8-1/4	64.27	9.88	19.64	4.75	2.03	1.89	0.31	0.26	0.01	0.07	0.02	0.17
	"	"	"	"	"	"	EXIT	61.94	10.84	17.44	7.21	5.62	-	0.95	0.21	0.02	0.08	0.02	0.31
214	2.5	2.0	0.64	2000	1700	NO	4-1/8	58.69	11.58	15.13									
	"	"	"	"	"	"	8-1/4	63.90	10.53	18.96	4.99	2.11	1.99	0.33	0.27	0.01	0.07	0.05	0.16
215	3.0	2.0	0.53	2000	1700	NO	4-1/8	58.69	11.71	14.87	10.48	2.29	2.35	0.34	0.65	-	0.32	0.09	4.44
	"	"	"	"	"	"	8-1/4	64.14	10.98	18.24	4.98	2.16	2.03	0.31	0.25	0.01	0.07	0.01	0.14
	"	"	"	"	"	"	EXIT	62.51	11.14	16.67	8.76	4.16	3.67	0.67	0.08	0.01	0.2	0.01	0.12
216	2.5	2.0	0.64	2000	1700	NO	4-1/8	57.97	11.40	15.05	11.07	2.31	2.24	0.37	0.53	-	0.26	0.08	5.28
	"	"	"	"	"	"	8/1/4	63.98	10.47	18.86	4.84	2.05	1.95	0.33	0.27	0.01	0.07	0.01	0.15
	"	"	"	"	"	"	EXIT	62.28	11.23	17.37	8.74	4.22	3.52	0.71	0.13	0.01	0.04	0.01	0.10

TABLE IX (Cont'd)

TEST	$(S/C)_m$	(1) $\dot{m}_w$	(1) $\dot{m}_f$	(2) SPACE VELOCITY	(3) T_{WALL}	CARBON	(4) GAS PROBE	DRY GAS COMPOSITION, MOL %											
		LB/HR	LB/HR	HR^{-1}	°F		AT INCHES	H_2	CO_2	CO	HC_T	CH_4	C_2H_4	C_2H_6	C_3H_6	C_3H_8	C_4	C_5	C_6H_{14}
218	3.5	2.0	0.46	2000	1500	NO	4-1/8	58.02	15.43	10.42	10.85	2.23	1.79	0.44	0.37	-	0.13	0.05	5.84
	"	"	"	"	"	"	8-1/4	63.28	15.71	12.13	6.23	2.22	1.99	0.40	0.53	-	0.16	0.05	0.88
	"	"	"	"	"	"	EXIT	61.68	15.50	11.94	9.92	4.24	3.49	0.85	0.74	-	0.14	0.03	0.43
219	3.5	2.0	0.46	2000	1700	NO	4-1/8	63.47	15.91	12.20	5.56	1.58	0.74	0.13	0.30	-	0.14	0.05	2.62
	"	"	"	"	"	"	8-1/4	66.04	15.25	14.81	2.62	1.61	0.69	0.16	0.07	-	0.01	-	0.08
	"	"	"	"	"	"	EXIT	66.36	17.16	11.98	3.31	2.57	0.39	0.23	0.01	-	-	0.01	0.10
220	3.5	4.0	0.92	4000	1700	NO	4-1/8	48.74	10.94	12.06	29.88	5.00	5.86	7.32	1.13	0.24	0.50	0.13	9.70
	"	"	"	"	"	"	8-1/4	58.87	12.03	15.23	12.30	4.17	4.90	0.58	1.05	0.02	0.38	0.08	1.12
	"	"	"	"	"	"	EXIT	54.90	11.47	13.46	20.46	7.17	4.90	0.58	1.05	0.02	0.38	0.08	1.12
222	3.0	4.0	1.06	4000	1700	NO	EXIT	52.84	10.84	13.42	20.68	7.62	8.95	1.17	1.44	0.04	0.49	0.09	0.88
223	3.0	4.0	1.06	4000	1700	NO	4-1/8	43.06	12.18	12.09	19.75	3.87	4.10	0.63	0.81	0.02	0.31	0.08	9.21
	"	"	"	"	"	"	8-1/4	50.16	12.14	15.19	10.83	3.53	3.78	0.56	0.90	0.02	0.33	0.07	1.64
	"	"	"	"	"	"	EXIT	47.67	12.13	12.80	18.83	7.11	7.63	1.15	1.37	0.03	0.46	0.08	1.00
224	2.5	2.0	0.64	2000	1700	NO	4-1/8	56.38	11.41	14.73	13.43	3.03	2.89	0.47	0.63	0.01	0.29	0.09	6.02
	"	"	"	"	"	"	8/1/4	62.73	10.89	18.73	7.26	3.18	2.90	0.48	0.37	0.01	0.10	0.02	0.30
	"	"	"	"	"	"	EXIT	58.96	10.54	16.43	12.22	5.68	5.15	0.96	0.22	0.01	0.08	0.02	0.10
225	2.5	2.0	0.64	2000	1700	NO	4-1/8	56.12	11.12	14.91	13.82	3.[illegible]	3.19	0.50	0.78	0.01	0.35	0.09	5.71
	"	"	"	"	"	"	8-1/4	62.93	10.75	18.87	6.79	2.77	2.42	0.42	0.29	0.01	0.73	0.01	0.14
	"	"	"	"	"	"	EXIT	60.02	10.66	16.90	11.30	5.57	4.52	0.91	0.15	0.01	0.06	0.01	0.07
226	2.5	2.0	0.64	2000	1500	NO	4-1/8	51.27	12.58	11.94	19.92	3.75	3.48	0.76	0.95	0.01	0.36	0.09	10.52
	"	"	"	"	"	"	8-1/4	57.93	12.36	14.91	13.22	4.18	4.35	0.84	1.22	0.01	0.41	0.09	2.12
	"	"	"	"	"	"	EXIT	54.63	12.69	12.60	20.83	7.76	8.07	1.66	1.79	0.02	0.28	0.09	1.16

(1) Mass flowrates of water, fuel
(2) Space velocity based on reactants' flowrates (NTP)
(3) Nominal external wall temperature based on steam + CO_2 (no reaction) data.
(4) Gas sample probe location with reference to the top of catalyst bed (Fig. 21)

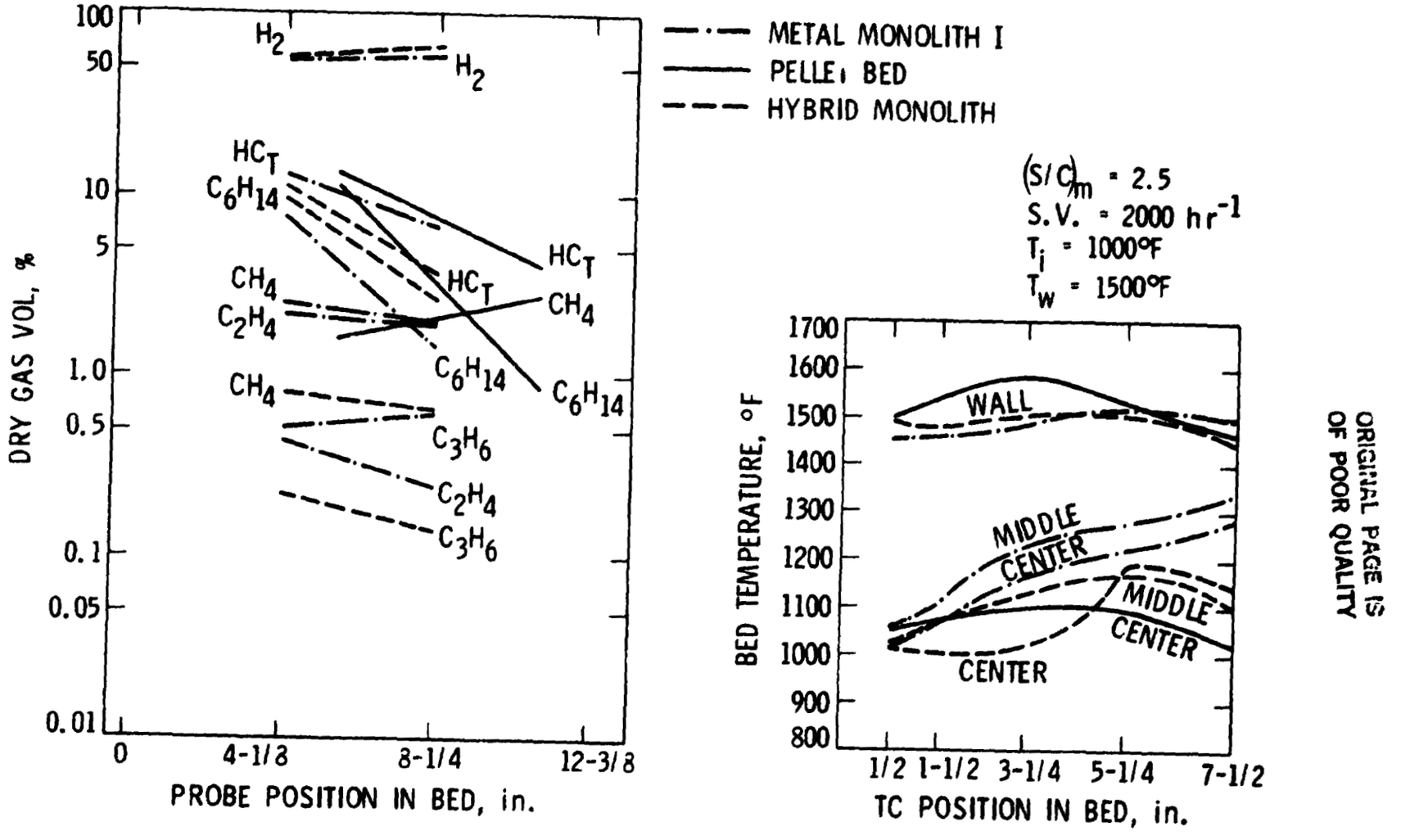

Figure 22. Steam Reforming of n-Hexane. Axial bed temperature and composition profiles for the metal monolith I, the hybrid monolith (20 in. long, ref. 11) and the G-90C pellet bed (20 in. long, ref. 11) at T_W = 1500°F.

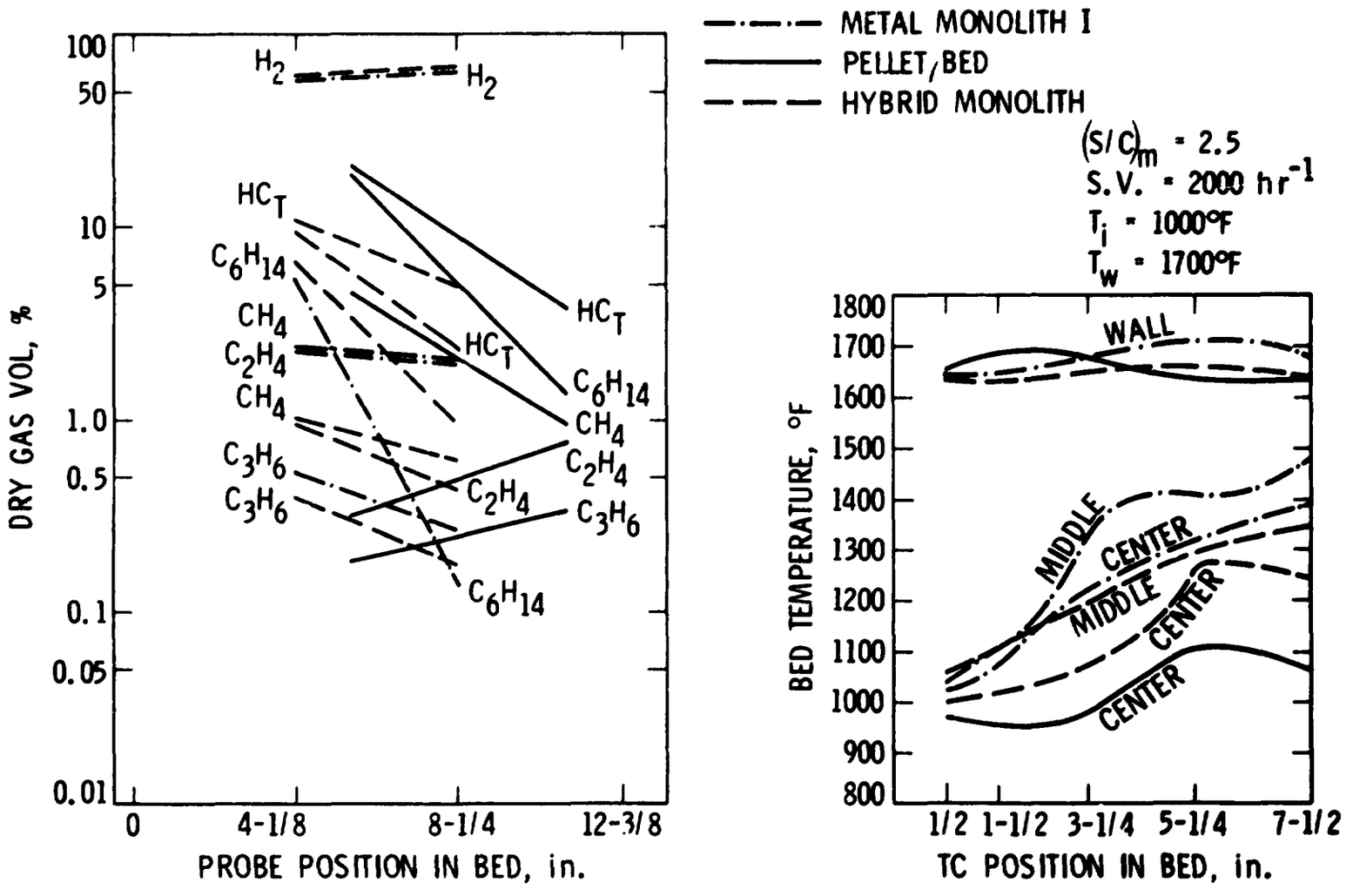

Figure 23. Steam Reforming of n-Hexane. Operating conditions are the same as in Figure 22 except that T_w = 1700°F.

Additional gas phase cracking took place downstream of the monolith catalyst in all test runs. This can be seen in Table IX from the different gas composition between gas probe 3 and product samples. This gas phase cracking is caused by the high temperatures prevailing in the lower end of the reformer, which is also inside the clam-shell furnace. Since cracking products (low molecular weight olefins) are soot precursors, carbon was expected to form and deposit on the screen and the inner tube walls close to the exit of the reactor. Indeed, upon post-inspection of the monolith and the reactor tube at the end of these tests, a large amount of flaky carbon was found at the exit of the reactor. Since the monolith cells were not plugged with carbon, these soot deposits must have been produced in the gas phase downstream of the monolith.

As can be seen from the temperature plots of Figures 22 and 23, improved radial heat transfer (from reactor wall to centerline) was observed with the 8-inch long metal monolith. For the same length of catalyst bed and same space velocities, the temperature differential from wall to centerline is minimal for the short metal monolith throughout the length of the bed. The observed temperature differences between pellet and metal monolith catalyst are easily understood. However, the difference between the metal and the hybrid monolith with identical front sections must be attributed to the lower gas flow velocity in the former rather than in the latter monolith.

Operating at higher space velocities (e.g., tests SR-219 vs. SR-220) with the short metal monolith severely limited fuel conversion to hydrogen. Higher amounts of olefinic and paraffinic intermediates were produced,

indicating that gas phase cracking reactions rather than steam reforming on the catalyst surface were more predominant in this case than at low space velocities. However, at higher space velocity, the mass diffusion limitation should be reduced, thereby enhancing surface reaction and, hence, steam reforming. If, on the other hand, the surface catalyst is not active enough, then the acidic alumina washcoat would initiate cracking, particularly when good heat transfer is possible.

In tests SR-224 (or 225) and 226, which were run at identical operating conditions as the earlier tests SR-216 and 211 respectively, a lower catalyst activity was observed by lower conversion to hydrogen and carbon monoxide. This may be due to gradual losses of washcoat (and nickel) from the monolith surface. The reactor was then opened for inspection of the catalyst. The multi-channel alumina in the conical reactor inlet was found intact, and the majority of cells in each of the four monolith segments appeared clean (open to free reactant flow). Small pieces from the center of each monolithic segment were cut for SEM examination. Cracks were found on the surface of these pieces and in several locations the washcoat was observed as islands on the bare support (Kanthal) surface. In these cases it was possible to detect the bare support by a strong signal of iron obtained by the EDAX (Energy Dispersive Analysis of X-rays) accessory of the electron microscope. Thus, the low activity observed when high space velocity operations were conducted was due to loss in catalyst activity, not reduced heat transfer.

(B) Tests With The G-90C Pellet Catalyst

Following tests with the used metal monolith, a fresh pellet catalyst bed was loaded and tested in the steam reformer. This was comprised of an 8-inch long bed of Girdler G-90C pellets (1/4 in x 1/4 in cylinders), the same catalyst as described in Table VIII. Tests were run at identical conditions as for the 8-inch long metal monolith I, keeping the inlet configuration and the thermocouple and gas probe locations the same as before (see Figure 21). Table X summarizes the data collected from tests on the pellet bed. From these and the corresponding data of Table IX for the metal monolith I, comparisons of bed temperatures and gas composition and product yields can be made between the pellet and monolithic catalysts.

Figures 24-26 show axial bed temperature profiles [centerline, middle line (half-way between centerline and the wall) and external wall temperatures] for the two catalysts under the same operating conditions. In all cases, the temperature differential between wall and either centerline or middle line was lower for the monolith in the first half of the bed. This indicates a potential improvement of the reformer performance with a monolith catalyst at the inlet where temperatures of the steam reforming catalyst are the lowest due to the endothermicity of the reaction.

The left hand side of Figures 24-26 shows dry gas analyses (as obtained by gas chromatography) for mid-bed and exit (product) gas samples. The operating conditions listed in these figures apply to both plots. Higher

TABLE X

STEAM REFORMING OF N-HEXANE ON G-90C PELLETS

TEST	$(S/C)_m$	(1) $\dot{m}_w$	(1) $\dot{m}_f$	(2) SPACE VELOCITY	(3) T_{WALL}	CARBON	(4) GAS PROBE	DRY GAS COMPOSITION, MOL %											
		LB/HR	LB/HR	HR^{-1}	°F		AT INCHES	H_2	CO_2	CO	HC_T	CH_4	C_2H_4	C_2H_6	C_3H_6	C_3H_8	C_4	C_5	C_6H_{14}
227	3.0	2.0	0.53	2000	1700	NO	4-1/8	66.84	16.24	11.15	1.87	1.84	0.01	-	-	-	-	-	0.03
	"	"	"	"	"	"	8-1/4	67.38	9.11	16.63	0.05	0.05	-	-	-	-	-	-	-
	"	"	"	"	"	"	EXIT	67.48	8.54	17.08	0.11	0.11	-	-	-	-	-	-	-
228	2.5	2.0	0.64	2000	1700	NO	4-1/8	65.76	11.63	13.59	2.51	2.21	-	-	-	-	-	-	0.30
	"	"	"	"	"	"	8-1/4	66.94	6.67	19.50	0.22	0.07	-	-	-	-	-	-	0.15
	"	"	"	"	"	"	EXIT	67.27	8.17	17.73	0.06	0.05	-	-	-	-	-	-	0.01
229	2.0	2.0	0.80	2000	1700	NO	4-1/8	63.59	11.78	13.08	5.06	2.99	0.04	0.01	0.02	-	0.01	-	1.99
	"	"	"	"	"	"	8-1/4	67.10	6.33	20.23	0.73	0.70	-	-	-	-	-	-	0.03
	"	"	"	"	"	"	EXIT	67.16	5.80	21.01	1.21	1.17	-	-	-	-	-	-	0.04
230	3.0	2.0	0.53	2000	1500	NO	4-1/8	65.54	17.47	10.37	5.25								
	"	"	"	"	"	"	8-1/4	67.48	9.77	15.40	0.29	0.12	-	-	-	-	-	-	0.17
	"	"	"	"	"	"	EXIT	67.16	8.91	16.63	0.10	0.09	-	-	-	-	-	-	0.01
231	3.0	2.0	0.53	2000	1500	NO	4-1/8	64.62	18.58	8.66	6.02	5.53	-	-	-	-	-	-	0.49
	"	"	"	"	"	"	8/1/4	67.70	11.86	14.00	0.84	0.72	-	-	-	-	-	0.01	0.11
	"	"	"	"	"	"	EXIT	68.02	11.42	14.42	0.80	0.68	-	-	-	-	-	-	0.12
232	2.5	2.0	0.64	2000	1500	NO	4-1/8	62.65	18.32	9.32	7.98	7.02	0.01	-	-	-	-	-	0.95
	"	"	"	"	"	"	8-1/4	66.40	9.93	15.76	2.50	1.96	-	-	-	-	-	-	0.54
	"	"	"	"	"	"	EXIT	66.84	9.16	16.38	0.02	-	-	-	-	-	-	-	0.02

TABLE X (Cont'd)

TEST	$(S/C)_m$	(1) $\dot{m}_w$	(1) $\dot{m}_f$	(2) SPACE VELOCITY	(3) T_{WALL}	CARBON	(4) GAS PROBE	DRY GAS COMPOSITION, MOL %											
		LB/HR	LB/HR	HR^{-1}	°F		AT INCHES	H_2	CO_2	CO	HC_T	CH_4	C_2H_4	C_2H_6	C_3H_6	C_3H_8	C_4	C_5	C_6H_{14}
233	2.0	2.0	0.80	2000	1500	NO	4-1/8	61.05	15.21	10.62	9.75	7.13	0.03	0.01	0.02	-	0.01	-	2.55
	"	"	"	"	"	"	8-1/4	63.87	10.17	15.18	6.81	6.76	0.01	-	-	-	-	0.01	0.03
	"	"	"	"	"	"	EXIT	64.62	9.18	16.11	6.16	6.09	0.02	0.01	0.01	-	-	-	0.03
234	3.5	2.0	0.46	2000	1500	NO	4-1/8	67.27	18.43	9.21	1.71	1.51	-	-		-	-	-	0.20
	"	"	"	"	"	"	8-1/4	67.59	14.24	12.21	0.37	0.12	-	-		-	-	-	0.25
	"	"	"	"	"	"	EXIT	67.70	15.17	12.33	0.42	0.24	-	-	-	-	-	0.01	0.17
235	3.5	2.0	0.46	2000	1700	NO	4-1/8	66.02	14.01	12.32	0.29	0.24	-	-	-	-	-	-	0.05
	"	"	"	"	"	"	8-1/4	66.02	10.98	14.83	0.02	0.01	-	-	-	-	-	-	0.01
	"	"	"	"	"	"	EXIT	68.35	10.40	15.34	0.02	0.01	-	-	-	-	-		0.01
236	3.0	2.0	0.53	2000	1700	NO	4-1/8	67.05	12.07	13.15	1.18	1.04	-	-	-	-	-	-	0.14
	"	"	"	"	"	"	8-1/4	67.48	8.12	16.86	0.04	0.03	-	-	-	-	-	-	0.01

(1) - (4) See Table IX

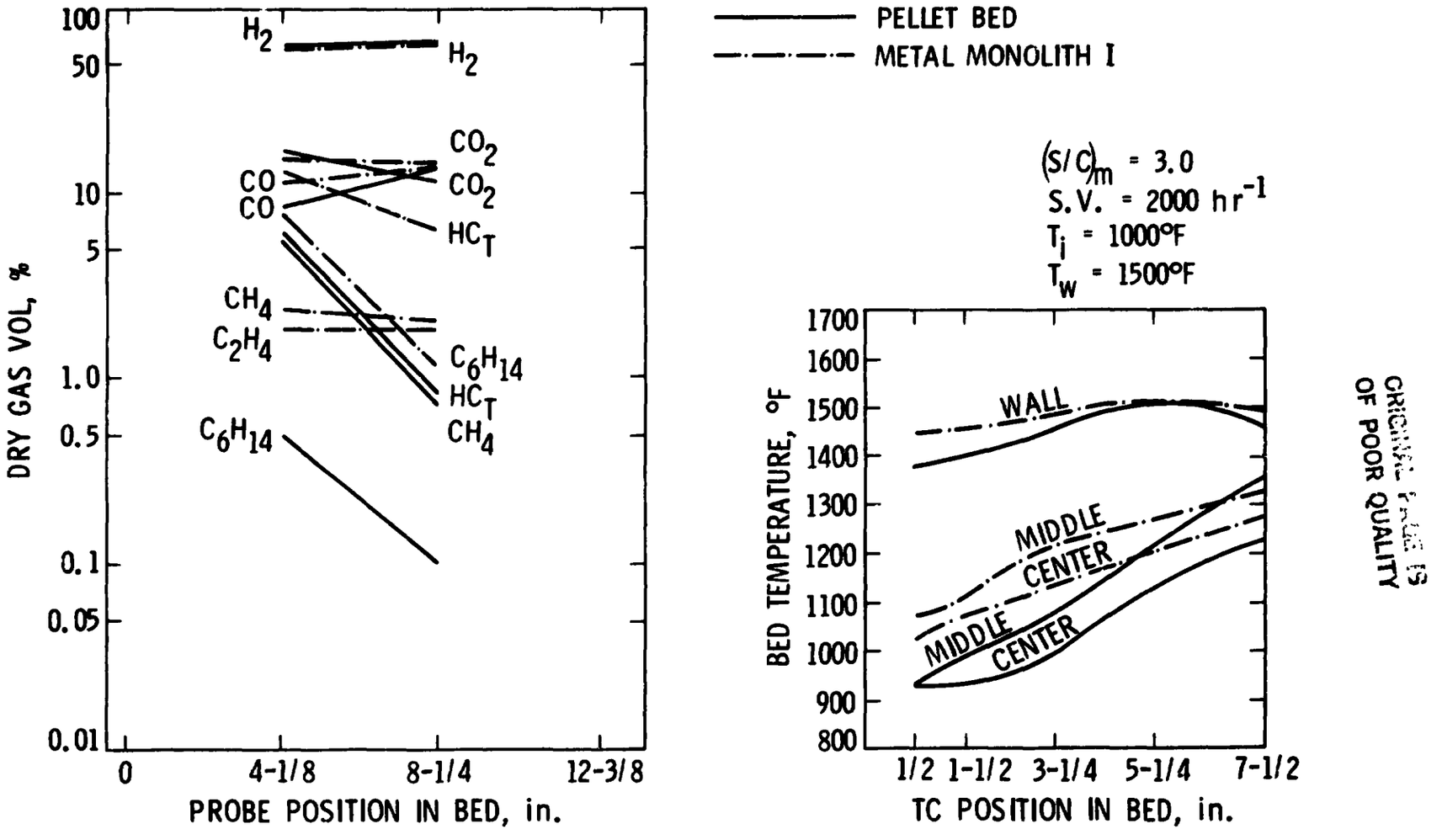

Figure 24. Steam Reforming of n-Hexane. Axial bed temperature and composition profiles for the metal monolith I and the 8-in. long G-90C pellet bed.

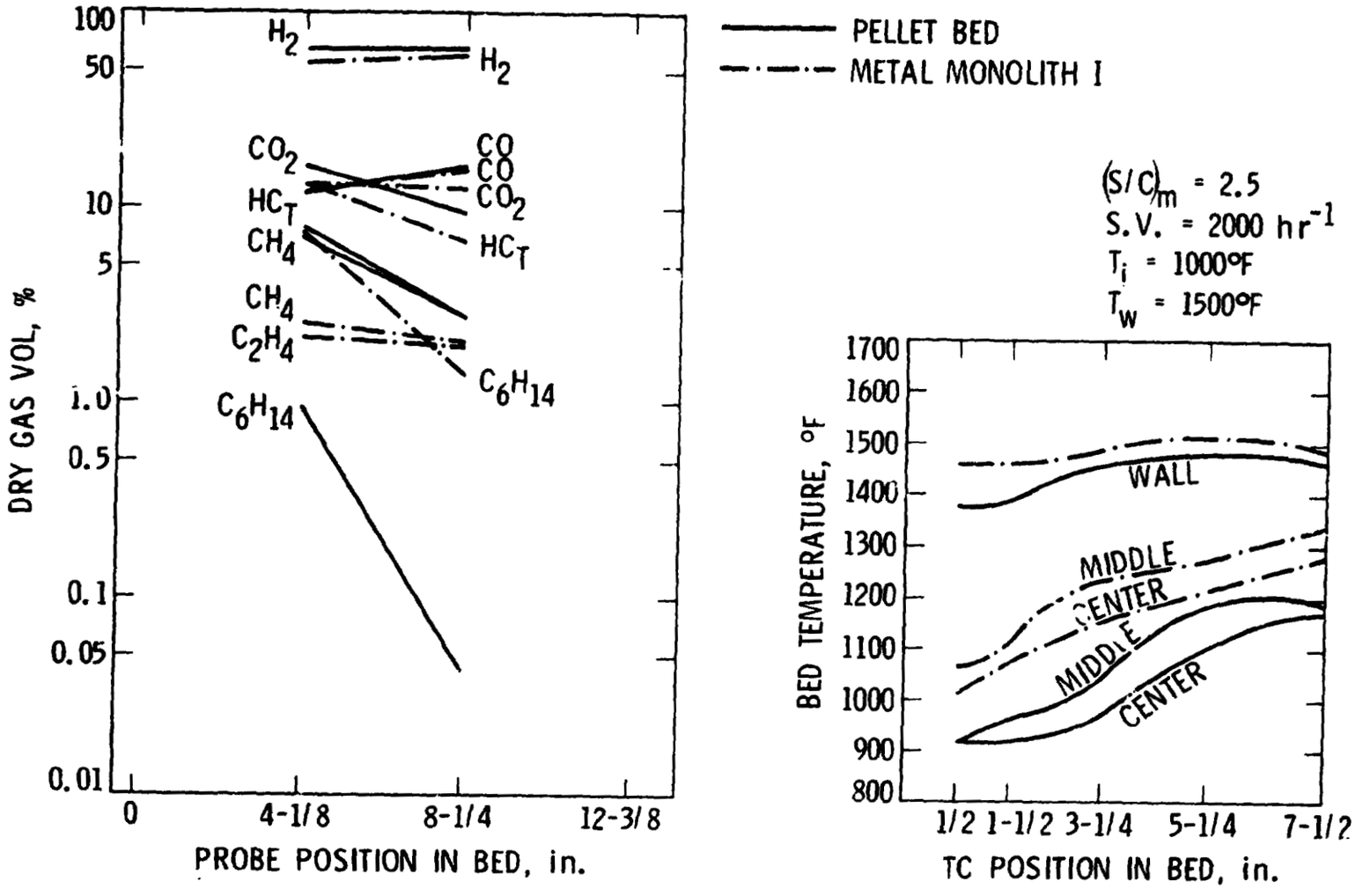

Figure 25. Steam Reforming of n-Hexane. Operating conditions are the same as in Fig. 24, except that $(S/C)_m$ = 2.5.

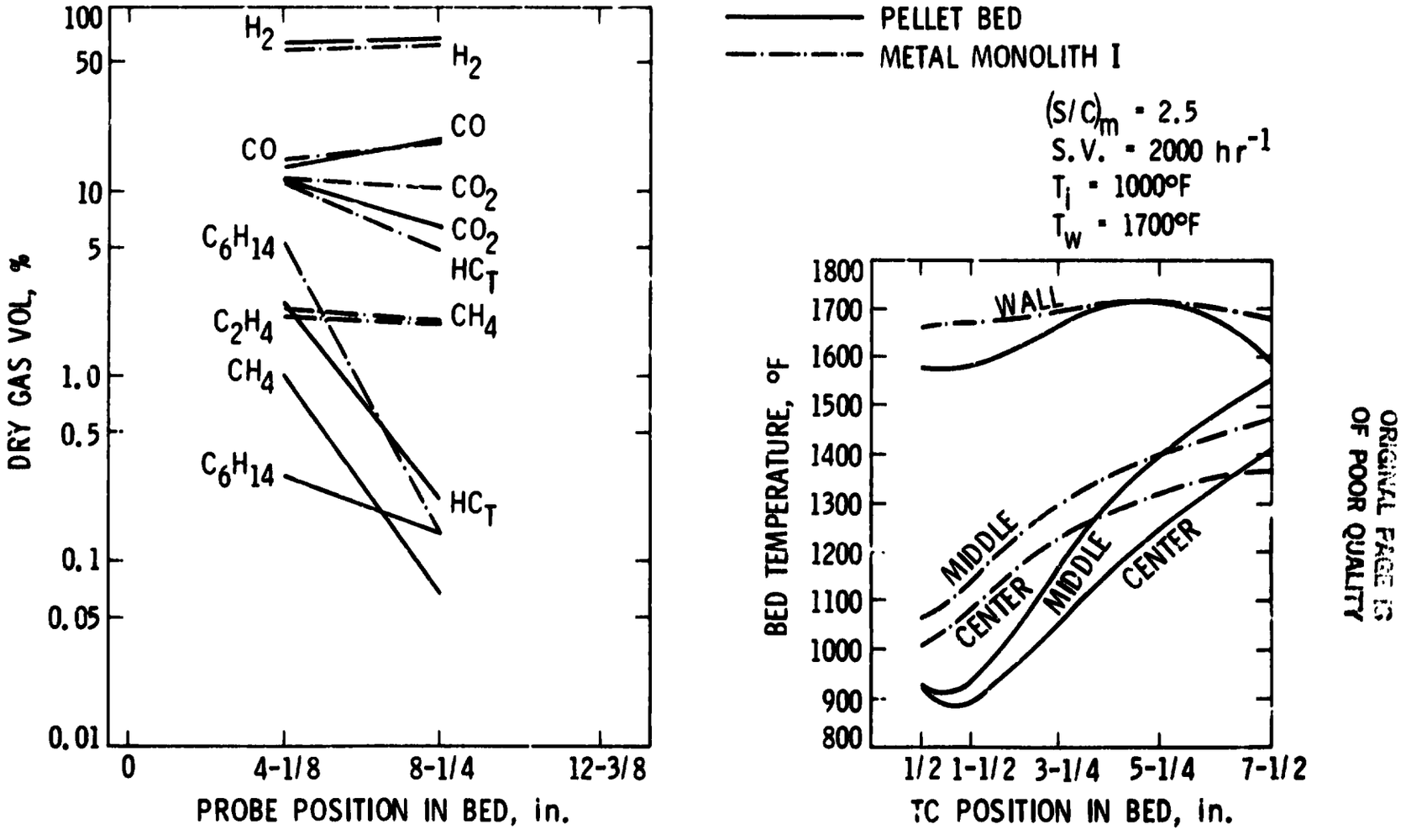

Figure 26. Steam Reforming of n-Hexane. Operating conditions are the same as in Fig. 25, except that T_W = 1700°F.

hydrogen yields were obtained and the amounts of hydrocarbon intermediates and methane at the exit of the pellet bed were extremely low.

In comparison, these results indicate that the metal monolith I had a lower overall conversion efficiency than the pellet bed of equal size. However, a one-to-one comparison between the two catalysts cannot be made, because of their non-compatible nickel loading, dispersion, and surface areas and the fluid dynamics involved. In order for identical comparisons of catalysts with respect to heat transfer, catalyst loading, surface area, gas flows and related conditions, a more detailed characterization of monolithic catalysts is necessary.

(C) Tests With The Metal Monolith II

Following the pellet tests, reactive characteristics were determined for the metal monolith II, which had been impregnated with nickel in-house to a loading higher than that of metal monolith I (Table VIII). Tests SR-280 through 294 were run with n-hexane on this new metal monolith at P = 1 atm, T_{inlet} = 1000°F, and for $(S/C)_m$ ratios of 3.5, 3.0, 2.5, 2.0, and 1.5. Reactor wall temperatures T_w of 1500°F and 1700°F, and nominal space velocities of 2000 and 4000 hr^{-1} were used. The data from tests with the metal monolith II are summarized in Table XI.

Initial tests were run at T_w = 1700°F. Improved heat transfer between reactor wall and catalyst bed was observed with the metal monolith as compared to the pellets, particularly at the top of the bed. This is

TABLE XI

STEAM REFORMING OF N-HEXANE ON THE METAL MONOLITH II

TEST SR -	$(S/C)_m$	(1) $\dot{m}_w$ LB/HR	(1) $\dot{m}_f$ LB/HR	(2) SPACE VELOCITY HR^{-1}	(3) T_{WALL} °F	CARBON	(4) GAS PROBE AT INCHES	DRY GAS COMPOSITION, MOL %											
								H_2	CO_2	CO	HC_T	CH_4	C_2H_4	C_2H_6	C_3H_6	C_3H_8	C_4	C_5	C_6H_{14}
280	3.0	2.0	0.53	2000	1700	NO	4-1/8	66.92	13.63	12.82	0.80	0.46	-	0.05	-	-	-	-	0.29
"	"	"	"	"	"	"	8-1/4	67.31	9.04	16.49	0.01	0.01	-	-	-	-	-	-	-
281	2.5	2.0	0.64	2000	1700	NO	4-1/8	66.93	9.94	15.84	0.80	0.60	0.02	0.01	0.01	-	-	-	0.17
"	"	"	"	"	"	"	8-1/4	67.46	6.29	19.67	0.05	0.03	-	-	-	-	-	-	0.02
282	2.0	2.0	0.80	2000	1700	NO	4-1/8	64.31	9.43	14.88	3.41	1.07	0.14	0.03	0.08	-	0.04	0.01	2.04
"	"	"	"	"	"	"	8-1/4	67.22	4.67	22.48	0.52	0.52	-	-	-	-	-	-	-
283	1.5	2.0	1.06	2000	1700	?	4-1/8	57.28	7.91	14.71	11.60	1.60	0.60	0.14	0.29	-	1.27	0.04	7.65
"	"	"	"	"	"	"	8-1/4	66.30	3.26	24.57	1.70	1.59	0.03	0.02	0.01	-	-	-	0.05
284	3.0	2.0	0.53	2000	1500	NO	4-1/8	65.54	16.30	10.11	2.93	0.87	0.02	0.01	0.01	-	0.01	-	2.01
"	"	"	"	"	"	"	8-1/4	67.54	10.42	15.62	0.19	0.19	-	-	-	-	-	-	-
285	2.5	2.0	0.64	2000	1500	NO	4-1/8	61.39	15.02	9.58	6.58	1.14	0.10	0.04	0.05	-	0.02	0.01	5.22
"	"	"	"	"	"	"	8-1/4	67.11	9.59	15.60	1.12	0.92	0.02	0.02	-	-	-	-	0.16
286	2.0	2.0	0.80	2000	1500	NO	4-1/8	53.88	11.51	10.81	13.03	1.84	0.83	0.34	0.27	-	0.08	0.02	9.65
"	"	"	"	"	"	"	8-1/4	62.65	9.95	15.85	3.44	1.85	0.40	0.16	0.15	-	0.04	0.01	0.85
287	1.5	2.0	1.06	2000	1500	NO	4-1/8	62.48	6.75	10.86	15.77	3.34	0.77	0.31	0.25	-	0.07	0.01	11.02
"	"	"	"	"	"	"	8-1/4	50.79	6.44	17.09	5.42	3.16	0.80	0.31	0.27	-	0.07	0.02	0.79

TABLE XI (Cont'd)

TEST SR -	$(S/C)_m$	(1) $\dot{m}_w$ LB/HR	(1) $\dot{m}_f$ LB/HR	(2) SPACE VELOCITY HR^{-1}	(3) T_{WALL} °F	CARBON	(4) GAS PROBE AT INCHES	DRY GAS COMPOSITION, MOL %											
								H_2	CO_2	CO	HC_T	CH_4	C_2H_4	C_2H_6	C_3H_6	C_3H_8	C_4	C_5	C_6H_{14}
288	3.5	2.0	0.46	2000	1500	NO	4-1/8	65.58	18.59	8.20	2.98	0.82	0.01	0.01	0.01	-	-	-	2.14
	"	"	"	"	"	"	8-1/4	67.59	17.52	10.73	0.71	0.33	-	-	-	-	-	-	0.38
289	3.0	4.0	1.06	4000	1500	NO	4-1/8	52.53	15.96	7.35	14.63	1.79	1.30	0.35	0.33	-	0.09	0.01	10.76
	"	"	"	"	"	"	8-1/4	60.96	15.36	10.48	6.02	1.67	1.22	0.31	0.33	-	0.28	0.02	2.19
290	3.5	4.0	0.92	4000	1500	NO	4-1/8	58.42	15.98	8.72	" 34	0.83	0.46	0.14	0.12	-	0.04	0.01	6.74
	"	"	"	"	"	"	8-1/4	65.21	14.97	12.83	1.97	0.72	0.35	0.10	0.09	-	0.05	0.01	0.67
291	3.5	4.0	0.92	4000	1700	NO	4-1/8	59.37	15.07	9.50	7.06	0.65	0.22	0.05	0.07	-	0.04	0.01	6.02
	"	"	"	"	"	"	8-1/4	66.07	11.66	14.24	1.10	0.54	0.16	0.04	0.03	-	0.01	-	0.32
292	3.0	4.0	1.06	4000	1700	NO	4-1/8	57.91	14.06	9.02	14.03	1.03	0.13	-	0.16	-	0.08	0.03	12.60
	"	"	"	"	"	"	8-1/4	65.32	11.42	14.17	1.83	0.85	0.34	0.09	0.05	-	0.02	0.01	0.48
293	3.0	2.0	0.53	2000	1700	NO	4-1/8	6[illegible].95	13.33	12.41	2.24	0.57	0.08	0.02	0.04	-	0.02	0.01	1.11
	"	"	"	"	"	"	8-1/4	6[illegible].38	9.60	16.11	0.32	0.31	-	-	-	-	-	-	0.01
294	2.5	2.0	0.64	2000	1700	NO	4-1/8	63.74	11.68	12.88	3.79	0.86	0.23	0.04	0.11	-	0.06	0.02	2.47
	"	"	"	"	"	"	8-1/4	66.90	6.91	19.71	0.46	0.43	0.01	0.01	-	-	-	-	0.01

(1) - (4) See Table IX

shown by the axial bed temperature profiles plotted in Figures 27 and 28 for the metal monolith II and pellets at T_w = 1700°F, S.V. = 2000 hr^{-1}, and $(S/C)_m$ = 2.5 and 2.0, respectively. Axial bed composition profiles for the same operating conditions are also shown in Figures 27 and 28. Higher conversion of hexane to hydrogen and carbon monoxide was attained with the monolith, and the amounts of methane and unconverted hexane were lower than for the pellets throughout the bed and at the exit. Thus, this monolith bed appears to have a higher steam reforming activity than the pellets, even though the actual space velocity is approximately twice as high for the monolith (void fraction ~ 70%) as for the pellets (void fraction ~ 30%). This activity difference could also be due in part to the higher nickel loading and perhaps the nickel dispersion, because of the high surface alumina washcoat of the metal monolith.

In test SR-283 with $(S/C)_m$ = 1.5, carbon might have been formed in the upper half of the monolith. This was indicated by a gradual decline in activity observed in following tests, but could not be confirmed at that point because there was no rise in the pressure drop through the bed, and no carbon fines were found in the gas samples. Figure 29 shows axial temperature and composition profiles for T_w = 1500°F, $(S/C)_m$ = 3.0, and S.V. = 2000 hr^{-1} (test SR-284). The monolith still has a better conversion efficiency than the pellets, but, as can be seen from the hexane profile, the unconverted hexane coming out of the upper two monolith segments is higher than that corresponding to the same location in the pellet bed.

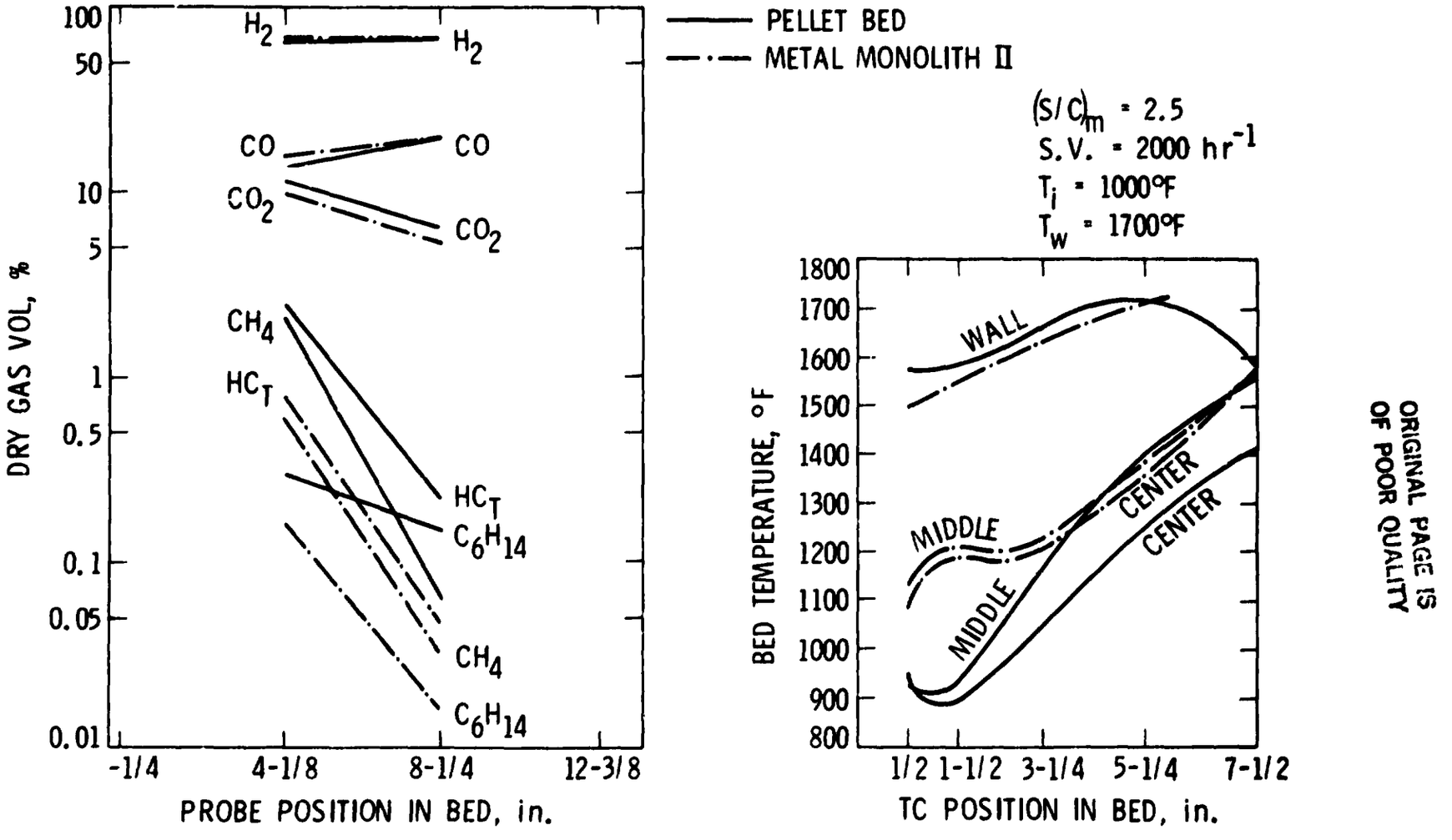

Figure 27. Steam Reforming of n-Hexane. Axial bed temperature and composition profiles for the metal monolith II and G-90C pellets at T_w = 1700°F, S.V. = 2000 hr^{-1}, and $(S/C)_m$ = 2.5.

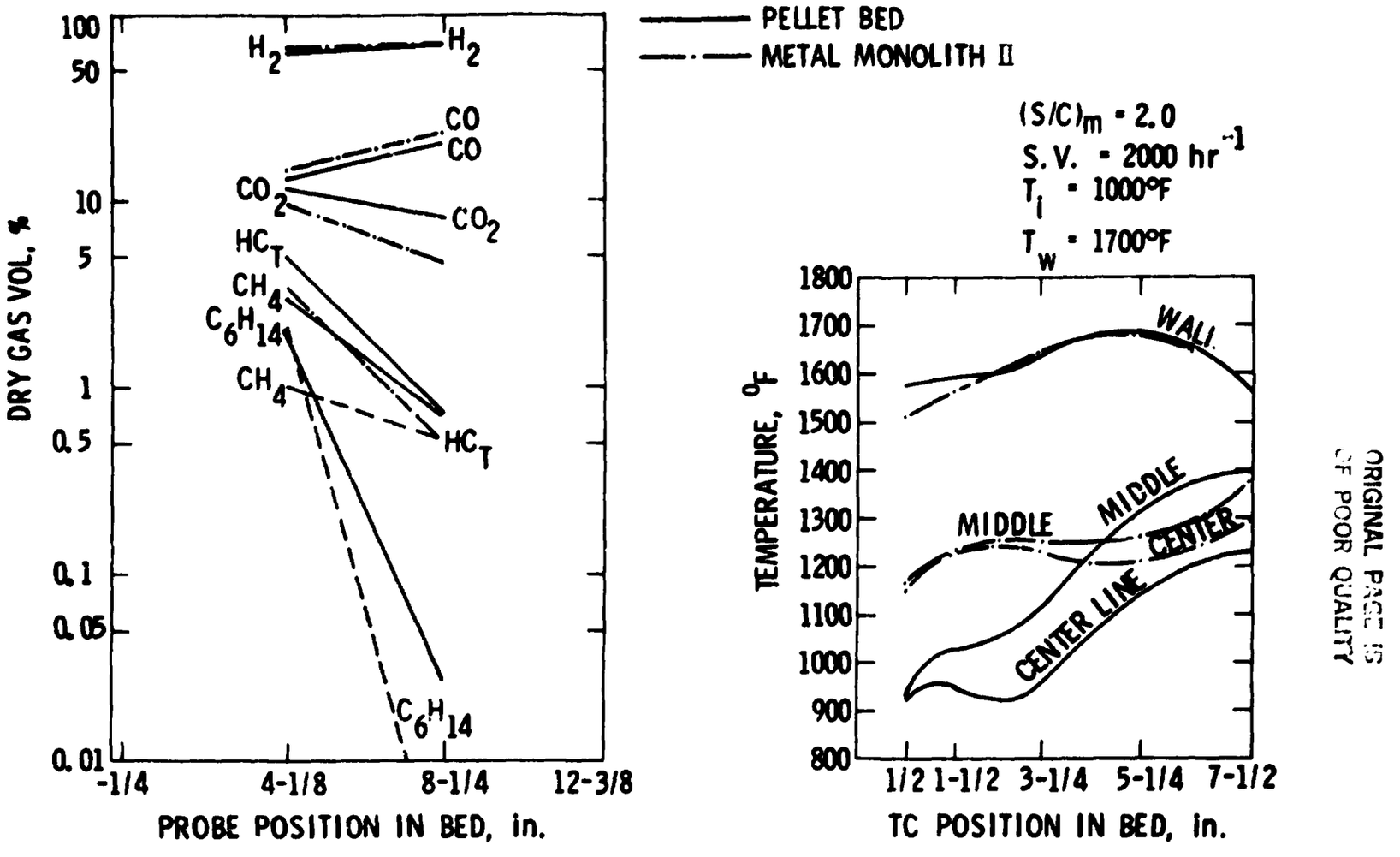

Figure 28. Steam Reforming of n-Hexane. Operating conditions are the same as in Fig. 27, except that $(S/C)_m = 2.0$.

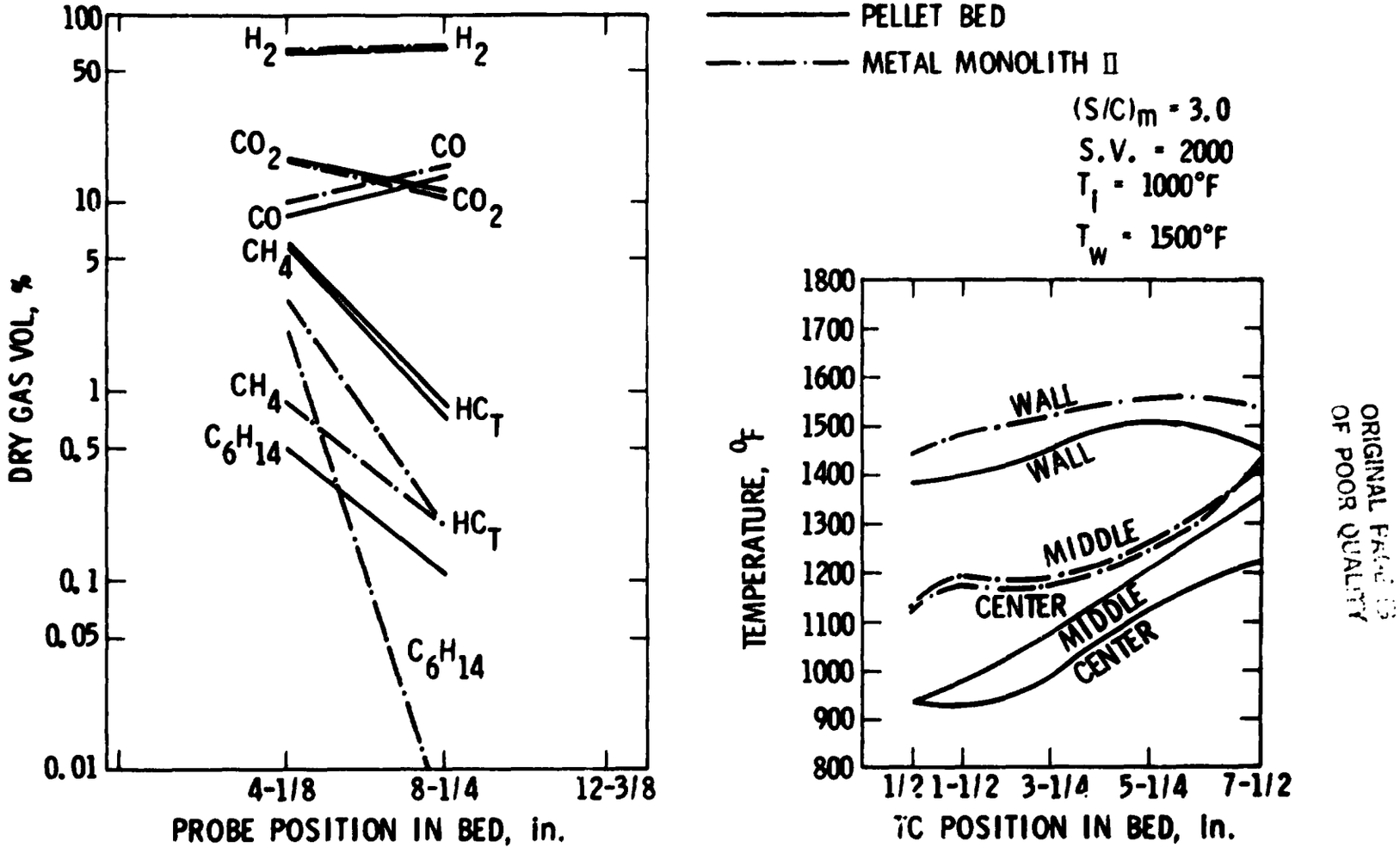

Figure 29. Steam Reforming of n-Hexane. Axial bed temperature and composition profiles for the metal monolith II and G-90C pellets after carbon formation had taken place in the monolith (test SR-284).

Starting with test SR-285, the decline in monolith steam reforming activity became evident. Figure 30 depicts this for the conditions of test SR-286. Higher amounts of unconverted hexane throughout the bed are now observed for the monolith, and olefins (ethylene, propylene) appear in the bed, indicating high gas phase cracking rates. The amount of methane, however, is much lower for the monolith than for the pellets, so that the percentage of total hydrocarbons at the monolith exit is lower. Radial heat transfer rates for the monolith have remained higher at these conditions, and continued to do so in all subsequent tests.

The effects of $(S/C)_m$ ratios and space velocity changes on the monolith performance were similar to those for the G-90C pellet bed. Thus, at higher $(S/C)_m$ ratios, the hexane conversion was higher, and lower methane was produced throughout the bed. Higher space velocities, resulted in lower catalyst temperatures and lower conversion efficiency as can be seen from the data of Table XI. Figure 31 compares the performance of metal monolith II to the pellet bed for a space velocity of 4000 hr^{-1}. The comparative heat transfer characteristics and steam reforming activity of each of these two catalysts follows the same trend as in the case of lower space velocities.

Tests SR-293 and 294 were run at identical conditions as the first tests of the series, SR-280 and 281, respectively, to determine the effect of the presumed carbon deposits in the bed on the monolith activity. Figure 32 shows axial bed temperature and composition profiles for the conditions of tests SR-281 and 294, run with the metal monolith before and (presumably) after carbon formation had taken place. Lower bed tempera-

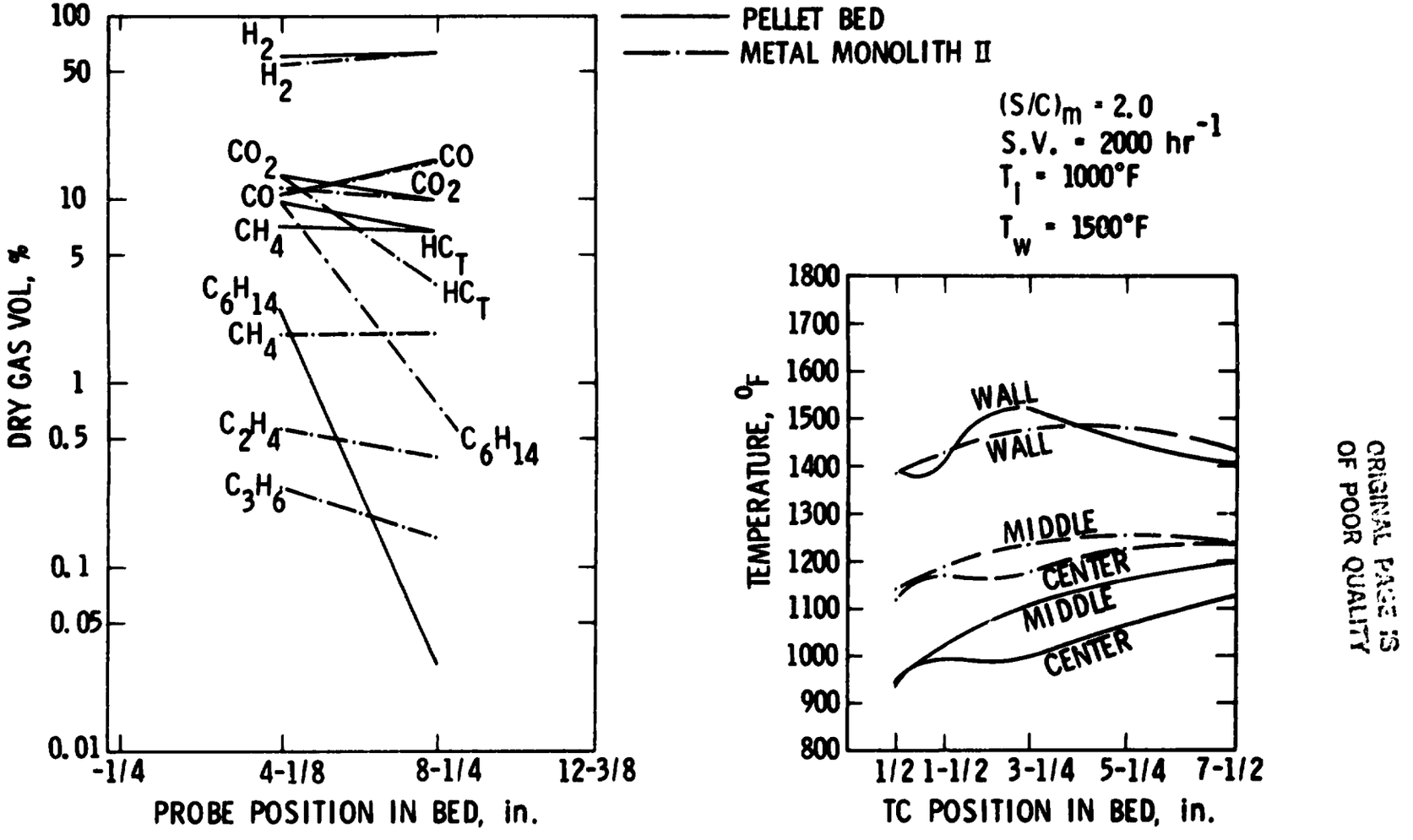

Figure 30. Steam Reforming of n-Hexane. The metal monolith II data (test SR-286), indicate a further decline in monolith activity due to carbon plugging of monolith cells.

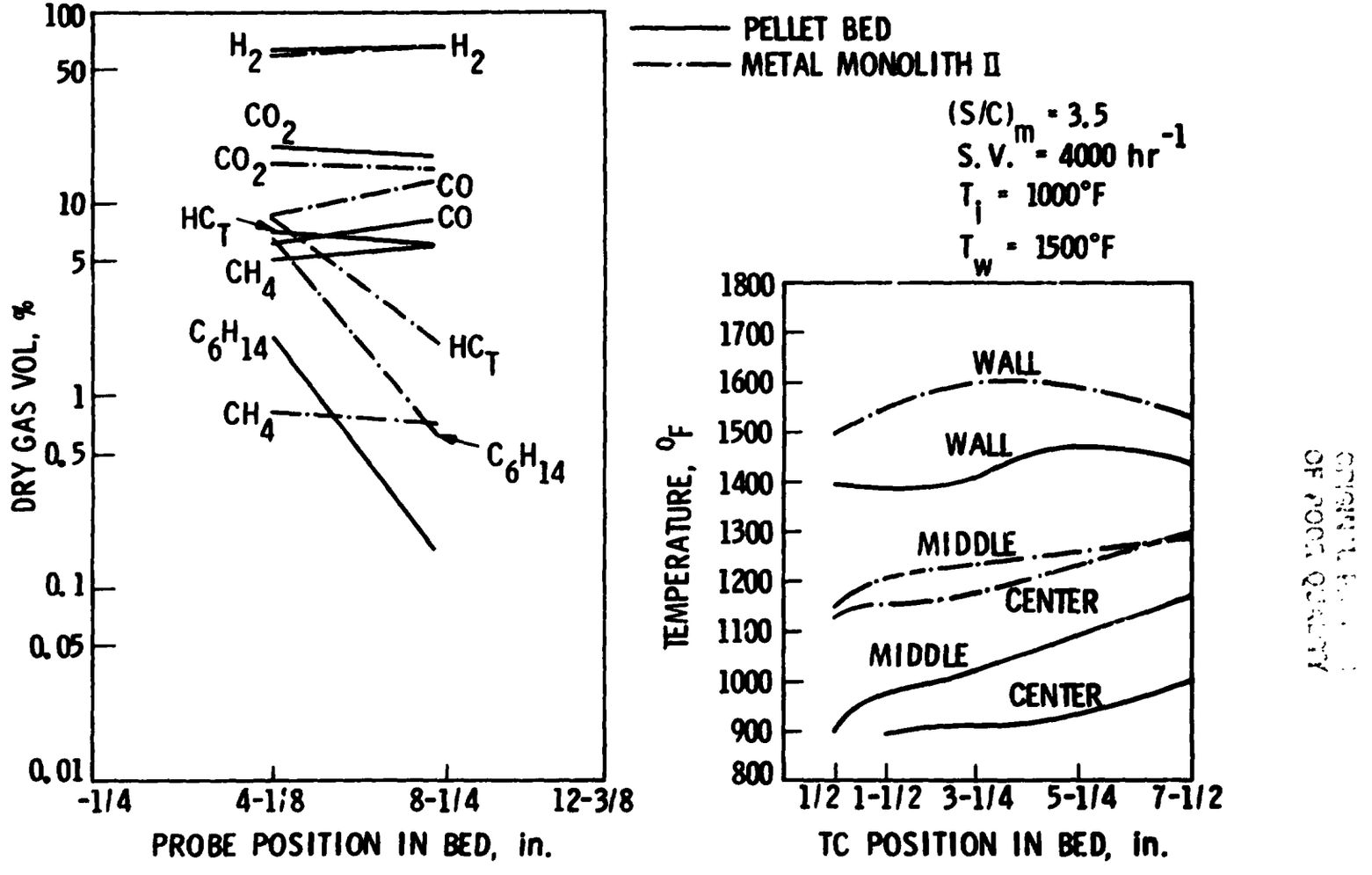

Figure 31. Steam Reforming of n-Hexane. Axial bed temperature and composition profiles for the metal monolith II and the G-90C pellets at the higher space velocity of 4000 hr^{-1}.

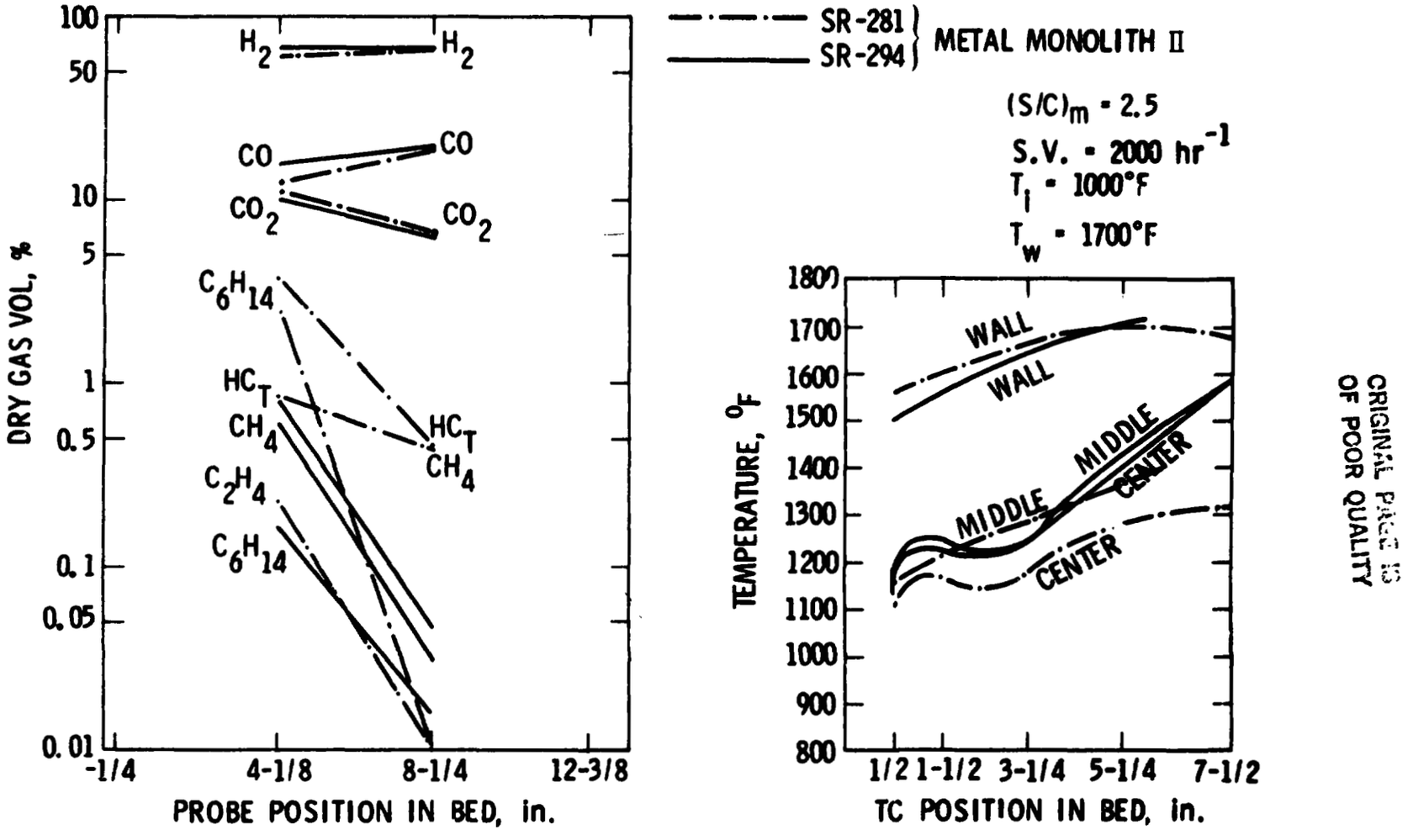

Figure 32. Steam Reforming of n-Hexane. Performance comparison of the metal monolith II before (test SR-281) and after (test SR-294) carbon formation in the bed.

tures were observed for the SR-294 test, which may be attributed to partial carbon plugging of monolithic cells. This would force all gas flow through fewer cells, i.e., a lower volume of the catalyst would be used for reaction, space velocity would be higher, and temperatures lower. For the same reason, more gas phase reactions (cracking) would take place, and the monolith would have a lower conversion efficiency. This is shown in the composition profiles of Figure 32. Ethylene is observed only for test SR-294, in which the methane content is also higher, while lower amounts of hydrogen and carbon monoxide are produced. Unconverted hexane coming out of the second monolith segment is much higher than before, but this rapidly decreases in the lower part of the bed, where initial activity appears to be retained.

Post-inspection of the monolith after test SR-294 verified the existence of carbon deposits in the upper half of the bed only, in agreement with indications from the experimental data discussed above. Figure 33 shows pictures (front and bottom view) of the four monolithic segments after they were taken out of the reactor. The third and fourth monoliths were clean throughout, except that black chunks of carbon were deposited on the top of the third monolith. This carbon had presumably been formed in the gas phase in this region (void) where the thin Inconel spacer allows for gas mixing. The bottom of the fourth segment was clean, but as the pieces were being pushed upwards to take them out of the reactor tube, some soft carbon was filtered to the bottom, leaving the imprint shown in Figure 33.

(a)

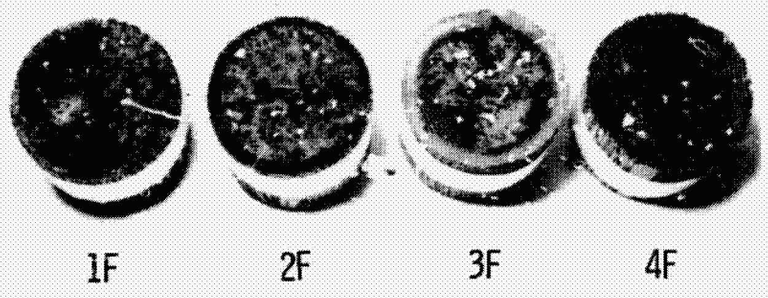

(b)

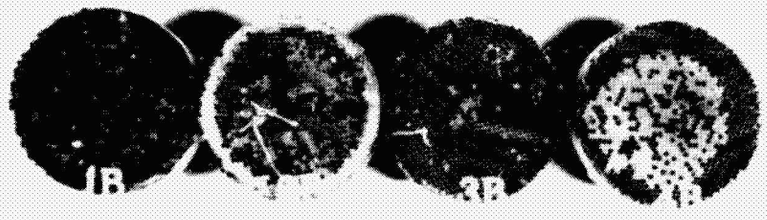

Figure 33. Pictures of the four metal monolith segments as retrieved after test SR-294 showing carbon deposition patterns. (a) Front view, (b) Bottom view.

The bottom of the cells just above the spacer between the second and third monoliths was filled with soft grey carbon fines to 1/4 in., while the top of the second monolith was partially plugged with hard black carbon. This carbon had a chunky appearance and was found to extend down inside the cells to 1/8 in. Catalyst samples from the top of the second monolith were examined by SEM. As shown in the photomicrograph of Figure 34, some of the observed carbon was surface grown (whisker growths on the surface). This presents evidence of gas/surface interaction, i.e., carbon was not formed in the gas phase (homogeneous) only. The top area of the first monolith segment was nearly all plugged with very hard black carbon. (Most of the cells that were open were found around the outer edges of the monolith.) This carbon must have originated from gas phase reactions upstream of the monolith, because carbon chunks mixed with the multi-channel alumina were also found in the conically shaped inlet. Since the inlet temperature (1000°F) is not high enough for extensive hexane thermocracking to take place, it appears that non-uniform flow and mixing conditions might have existed in the inlet region which enhanced the coking rate of hexane. To prevent this, the inlet design of the reformer may be modified to decrease the void and improve the mixing and flow distribution of the reactants.

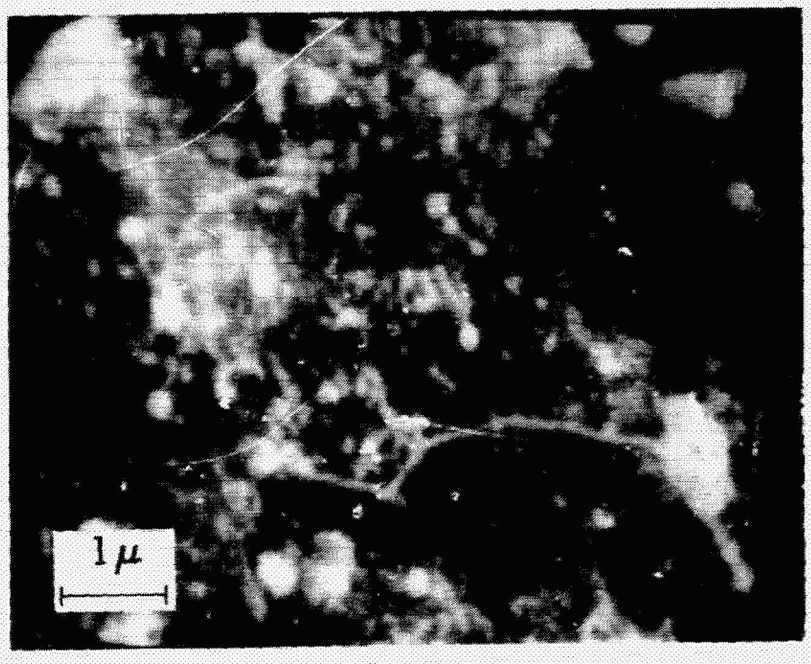

Figure 34. SEM photomicrograph of the top surface of the second piece of metal monolith II showing surface grown carbon (whisker growths).

SUMMARY

Steam reforming of hydrocarbons is an endothermic reaction whose thermal and conversion efficiencies are limited by heat transfer from the reactor wall into and throughout the catalyst bed. The heat transfer limitation is believed to be due, in part, to conduction which is affected by edge and point contact of the catalyst in a typical packed bed and also by the insulating property of the catalyst support material. Catalyst geometry is normally that of pellets or Raschig rings with dimensions compatible with a given reactor size (diameter, length) to provide optimal void-to-catalyst surface ratio. Optimization of this ratio, for the flows used, leads to control of gas phase and surface reactions and heat transfer via convection and conduction during tortuous path flow through the packed bed.

Heat conductivity improvements by ceramic monolithic supported catalysts in combustion and methanation reactions have been demonstrated. In these exothermic reactions, heat is conducted out more efficiently by monoliths than by packed beds. Application of these types of catalysts to steam reforming, therefore, appeared to be advantageous for transferring heat in the opposite direction, i.e., into the catalyst bed. The initial purpose for the experimental steam reforming work conducted in this contract was to examine the effect of this novel approach to transferring heat into the catalyst bed.

With catalyst supports that have a honeycomb structure, heat transfer by conduction directly from the walls through the bed is possible. The restriction due to edge and point contact is removed. Monolith support material may be ceramic, which is relatively inexpensive yet insulating in nature, as compared

to a metal support. The contact between a monolithic support and the reactor wall can not be direct when the monolith material is ceramic but can be direct when the material is metal. In both cases, however, uniformity throughout the catalyst bed is maintained via the integral support configuration.

A further consideration in comparing a honeycomb structure monolith to pellets is in regard to the flow pattern. Passage of gases through the pellets results in a tortuous multi-directional flow, with a typical 30% void fraction within a given reactor bed volume. Flow through a honeycomb monolith catalyst, on the other hand, is a stream line flow, each channel serving as a "mini-reactor tube". The availability of catalyst surface is, therefore, different in these two catalyst bed geometries.

The catalyst support used in the initial tests was ceramic (Cordierite) possessing a coating of γ-alumina. This "washcoat" provided a surface with uniform porosity and high area onto which the catalyst was supported. Nickel catalyst on this support was found not to be an acceptable catalyst system because of high carbon production and subsequent erosion of ceramic support, particularly at the inlet section. The silica content of the Cordierite may also have contributed to the structural deterioration by hydrothermal leaching. When heat transfer through the bed is high and the activity or availability of the catalyst is low, gas phase as well as surface carbon formation could readily take place when the void-to-surface ratio is high. The specific cause of carbon formation was not ascertained in the ceramic tests.

The key experiments during this work were directed toward determining the relationships between (1) location of carbon formation within the catalyst bed

and ceramic support deterioration, (2) metal monolith and pellet performance, and (3) catalyst loadings on metal monoliths.

In order to define whether the inlet area of the catalyst bed was responsible for the previously observed destruction of the Cordierite-supported nickel catalyst, the inlet section was replaced with metal-supported nickel catalyst. The nickel loading and void fraction (~70%) were nearly the same. Results indicated that Cordierite honeycomb monoliths were not suitable for steam reforming under the conditions tested, as evidenced by their observed deterioration when located in the bottom half of the reactor. Changes in nickel loading (activity), cell density (void fraction), and washcoat acidity may have altered this condition, but these parameters were not investigated.

Performances of metal monoliths with two different loadings of nickel were compared to pellets. Temperature and product profiles of metal monoliths with two different catalyst loadings were necessary to determine whether catalyst loading (surface reaction) or void fraction (gas phase reaction) was responsible for conversion.

The conclusions based on comparing data, Table XII, from the two metal monolith catalysts are (1) higher catalyst loading increases conversion, (2) lower catalyst loading increases methane production, and (3) changes in temperature and $(S/C)_m$ ratio are reflected in conversion more apparently in the higher loaded catalyst. Since no carbon formed at $(S/C)_m > 2.0$, even when high temperatures were maintained due to high heat transfer (and low conversion in the case of the low activity catalyst), it appears that gas phase carbon formation is not the major contributor to carbon formation in the Cordierite and hybrid bed

TABLE XII

GAS COMPOSITION COMPARISONS FROM STEAM REFORMING
OF N-HEXANE ON PELLETS AND TWO METAL MONOLITHS

$(S/C)_m$ = 2.5, S.V. = 2000 hr^{-1} T_i = 1000°F							
Gas Species	Gas Probe	Pellets		Metal Monolith I		Metal Monolith II	
		T_w=1500°F	1700°F	1500°F	1700°F	1500°F	1700°F
CH_4	#2	7.02	2.21	2.50	2.20	1.14	0.60
	#3	2.78	0.07	2.05	2.03	0.92	0.03
C_6H_{14}	#2	0.95	0.30	7.73	5.16	5.22	0.17
	#3	0.42	0.15	1.42	0.17	0.16	0.02
$(S/C)_m$ = 3.0, S.V. = 2000 hr^{-1} T_i = 1000°F							
Gas Species	Gas Probe	Pellets		Metal Monolith I		Metal Monolith II	
		T_w=1500°F	1700°F	1500°F	1700°F	1500°F	1700°F
CH_4	#2	5.53	1.84	2.34	2.29	0.87	0.46
	#3	0.72	0.05	2.12	2.16	0.19	0.01
C_6H_{14}	#2	0.49	0.03	7.82	4.44	2.01	0.29
	#3	0.11	-	1.20	0.14	-	-

under similar conditions.

The heat transfer improvement in metal monoliths over pellets can specifically be attributed to the metal monolith support when the relative conversions, at constant wall temperatures, of metal monolith II and pellets are compared, Table XII. Under the same S/C, S.V. and T_i conditions, the higher catalyst loaded monolith can be seen to provide higher conversion than pellets. The comparison of their respective product and thermal profiles, Figures 27 and 29, illustrates that bed temperatures remain higher in the early section of the metal monolith bed while also maintaining higher activity than the pelleted catalyst. Thus, enhancement of heat transfer with the metal monolithic support has been demonstrated. However, information regarding the role of fluid dynamics, availability of catalyst to reactants, and void fraction is still inadequate and must be obtained to completely define the range of advantages offered by metal monolithic supported catalysts to steam reforming.

REFERENCES

1. Houseman, J. and Cerini, D.J., "On-board Hydrogen Generator for Automobiles", 11th IECEC Paper 769001, 1976.

2. Houseman, J., "Autothermal and Steam Reforming of Distillate Fuel Oils", National Fuel Cell Seminar, San Francisco, California, July 1978.

3. Bett, J.A.S., Lesieur, R.R., McVay, D.R. and Setzer, H.J., "Adiabatic Reforming of Distillate Fuels", ibid.

4. Gordon, S. and McBride, B.J., "Computer Program for Calculation of Complex Chemicals Equilibrium Compositions, Rocket Performance, Incident and Reflected Shocks and Chapman-Jouguet Detonations", NASA 1971.

5. Jellinek, K. and Zakowski, J., Z. Anorg. Chem. 142, 1 (1925).

6. Shah, R., Voecks, G.E. and Houseman, J., "Autothermal Reforming of No. 2 Fuel Oil", Final Report to EPRI, RP 1041-2, July 1979.

7. Bett, J.A.S., Bushnell, C.L., Buswell, R.F., Gruver, G.A., King J.M. and Kunz, H.R., "Advanced Technology Fuel Cell Program", Annual Report to EPRI, EM-1328, January 1980.

8. Houghtby, W.E., Buswell, R.F., Bett, J.A.S., Lesieur, R.R., Meyer, A.P., Preston, J.L. and Setzer, H.J., "Development of the Adiabatic Reformer to Process No. 2 Fuel Oil and Coal-Derived Liquid Fuels", Interim Report to EPRI, EM-1701, February 1981.

9. Hwang, H.S., Yarrington, R.M. and Kaufman, A., "Hydrogen Production from No. 2 Fuel Oil by Autothermal Reforming", Seventh Steam Reforming Working Group Meeting, Engelhard Industries, Menlo Park, N.J., November 1981.

10. Flytzani-Stephanopoulos, M. and Voecks, G.E., "Autothermal Reforming of n-Hexane, Benzene and n-Tetradecane", Final Report to DOE, ET-78-A-03-2042, October 1979.

11. Flytzani-Stephanopoulos, M. and Voecks, G.E., "Autothermal Reforming of n-Tetradecane and Benzene Solutions of Naphthalene on Pellet Catalysts, and Steam Reforming of n-Hexane on Pellet and Monolithic Catalyst Beds", Final Report to DOE, DE-AI03-78ET-11326, October 1980 (in press).

12. Flytzani-Stephanopoulos, M. and Voecks, G.E., "Catalytic Autothermal Reforming Increases Fuel Cell Flexibility", Energy Progress 1, 52 (1981).

13. ICI Catalysts Information Bulletin, ICI Ltd., Agricultural Division, Billingham, Cleveland, England.

14. Rostrup-Nielsen, J.R., in "Steam Reforming Catalysts. An Investigation of Catalysts for Tubular Steam Reforming of Hydrocarbons", Teknisk Forlag A-3, Copenhagen, 1975.

15. Maat, H., "The Sulfur Problem: HDS of Heavy Feed to Low S Levels", Fuel Processing for Fuel Cell Power Generation Meeting, Palo Alto, California, April 1977.